UNIVERSITÀ DEGLI STUDI DI MILANO

Scuola di Dottorato in Scienze e Tecnologie Chimiche
Dipartimento di Chimica
XXVI Ciclo Dottorato in Chimica Industriale

Biomass to Liquid Process: new kind of cobalt and iron based catalysts for the Fischer-Tropsch Synthesis

(Settori Scientifico Disciplinari: ING-IND/25; CHIM/04)

Antonieta Di Fronzo
(Matricola R09037)

Tutor: Prof. Claudia L. Bianchi
Co-Tutor: Prof. Carlo Pirola

Coordinatore del Dottorato: Prof. Dominique Roberto

A.A. 2012/2013

TABLE OF CONTENTS

General abstract 5
Chapter 1. General Introduction 27
Chapter 2 Chemistry of Fischer-Tropsch Synthesis 57
2.1 FT Thermodynamics 58
2.2 FT Reaction Mechanism 59
2.3 FT Products Selectivity 65
2.4 FT kinetics 68
2.5 Influence of FT process conditions 71
Chapter 3. Catalysts for Fischer Tropsch Synthesis 76
3.1 Iron and Cobalt industrial FT catalysts 80
i) Iron catalysts: 80
ii) Cobalt catalysts: 81
3.2 Chemical State of active phase 82
3.3 Size of active phase 83
Chapter 4. Experimental: FT plant and analytical methods 86
4.1 FT Laboratory plant 88
a) First FTS unit (Unit 1): 88
4.1a Main parts of the plant 90
4.2a Analytical instruments 94
4.3a Analytical instruments calibration 98
4.4a Experimental procedure 109
b) Second FTS unit (Unit 2): 114
4.1b Main parts of the plant 116
4.2b Analytical instruments 119
4.3b Experimental procedure 121
4.2 Experimental data elaboration 124
a)First FTS unit (Unit 1) 124
4.2.5 Hydrogen 137
4.2.7 Oxygen Balance 139
b)Seconf FTS unit (Unit 2) 140
4.3 Novelties on the FT plant made in this PhD work 142
Chapter 5. Catalysts preparation and characterization 143
5.1 Catalysts preparation 146
5.1.1 Catalyst preparation procedure 146
5.2 Catalysts characterization: 155
5.2.1 Catalysis characterization: introduction and theory 155

5.2.1.1 BET analysis 157
5.2.2 Catalysts characterization: results 174
Chapter 6. High Fe Loaded Supported Catalysts for Biosyngas Fischer – Tropsch Conversion: experimental and simulation results 197
6. Development of the kinetic model 197
6.1 Regression of kinetic constants 197
6.2 Mass Balance 199
6.3 Energy Balance 200
6.4 Pressure variation 201
6.5 Catalyst Efficiency 202
Chapter 7. Fischer Tropsch runs results and discussion 204
Chapter 8. Final remarks and Conclusions 216
List of publications 219
Publications in Conference Proceedings (peer reviewed) 219
Communications at congress 220

General abstract

1. Introduction

Nowadays it is imperative to develop economical and energy-efficient processes for the sustainable production of fuels and chemicals alternative to the ones deriving from petroleum. Climate change and air quality are major environmental concerns because they directly affect the way we live and breath. In order to meet the present and future threats generated by emissions to the atmosphere, environmental agencies around the world have issued more stringent regulations. One of them is the control of residual sulfur in diesel fuel and emission standards for particulates from diesel vehicles. All these facts have recently aroused renewed interest in the Fischer–Tropsch Synthesis because it can produce super clean diesel oil fraction with high cetane number (typically above 70) without any sulfur and aromatic compounds, using syngas (mixture of H_2, CO, CO_2) from natural gas, CH_4, coal or, as a new tendency, from biomass. [1, 2]. The essential target of FTS is to produce paraffins and olefins with different molecular weight and to limit the maximum formation of methane and CO_2 [3].

The main reactions involved in FTS are reported in the following scheme [4-8]:

Irreversible reactions:

1) $n\ CO + 2n\ H_2 \rightarrow C_nH_{2n} + n\ H_2O$ for olefins

2) $n\ CO + (1+2n)\ H_2 \rightarrow C_nH_{(2n+2)} + n\ H_2O$ for paraffins

3) $2n\ CO + n\ H_2 \rightarrow C_nH_{2n} + n\ CO_2$ for olefins

4) $n\ CO + 2n\ H_2 \rightarrow C_nH_{(2n+1)}OH + (n-1)\ H_2O$ for alcohols

Equilibrium:

5) $CO + H_2O \leftrightarrow CO_2 + H_2$ Water-gas-shift reaction (WGS)

6) $CO + H_2 \leftrightarrow C + H_2O$ Carbon deposition

7) $2\ CO \leftrightarrow C + CO_2$ Boudouard equilibrium

The whole reaction gives an energetic contribution strongly exothermic (about 150 kJ/mol CO reacted). FTS is a particularly complex system, in which a number of different reactions are combined to a unique mechanism: irreversible Fischer Tropsch (FT) reactions produce hydrocarbons and some equilibrium reactions between CO, CO_2, CH_4 and C, such as the WGS reaction and the Boudouard equilibrium, are present too. Nevertheless, it is possible to suppose that FTS can be simplified as a combination of the FT reactions and the WGS reaction [7]. According this hypothesis, hydrocarbons are primary products of FT reaction, and CO_2 can only be produced by WGS reaction, a reversible parallel-consecutive reaction with respect to CO [9].

FTS usually requires catalysts based on cobalt or iron. Co-based catalysts have been more largely used due to their high selectivity to heavy hydrocarbons and low activity in the water-gas shift reaction, so limiting the CO_2 formation. Moreover Co-based catalysts have shown longer life-time and higher CO conversion compared to the Fe-based ones [10]. Iron based catalysts are, recently, highly investigated for FTS. Compared to cobalt systems, iron-based catalysts are cheaper but less resistant to deactivation due to the oxidizing effect of water, despite activating Water Gas Shift reaction ($CO + H_2O \leftrightarrow CO_2 + H_2$) well [5, 9]. Moreover they are flexible to changes in temperature, pressure and they can work at different H_2/CO feed ratios (for iron based catalysts this ratio can be between 0.5 and 2.5) [11, 12].

2. Aims of the work

Considering very recent research results [13-15] the aim of the PhD's research was addressed toward the development of three particular kind of catalysts:

The first group of catalysts tested were the ***Co-based hydrotalcites (HTlc)*** with different amount of Co in two different pilot plants. HTlc-based materials have been recently reported as good catalysts for several processes in the energy field [16], [17] and [18]. Up to now the only study reported in literature on the use of synthetic HTlc as FTS catalysts concerns their use as inert supports for the catalytically active metal. According to this study, hydrotalcite-supported catalysts result in higher activity than Co/Al_2O_3, even in absence of reduction promoters [19].

The second group of catalysts tested were the ***Co-based catalysts and bimetallic Co-Ru based catalyst synthesized with the help of ultrasound***, because the ultrasound are presented in literature as an innovative way to synthesize new kind of materials.

Finally, were synthesized and tested samples of ***Fe-based catalysts*** supported on silica with different methods of synthesis (traditional impregnation method with the help of ultrasound or microwave) and changing the H_2/CO ratio, with the aim to evaluate the performance of biomass. Almost, the development of a kinetic model (modeling, parameter regression and simulation) in collaboration with the *Politecnico di Milano*.

3. Experimental Details

a. Preparation of catalysts

i) Cobalt based catalysts – Hydrotalcites: a series of ternary hydrotalcites, with general formula $[Co_xZn_{(1-x-y)}Al_y(OH)_2](NO_3)_y \cdot 0.5H_2O$, by a modified-urea method [20]. Different volumes of the solutions of the metals nitrates, all at a concentration of 0.5 M, were mixed to obtain either a Al/(Co+Al) or Al/(Co+Al+Zn) molar ratio of 0.3, as indicated in Table 1.

Solid urea was added to the solution, in a molar ratio of 4 vs. Al. The obtained solution was maintained at the reflux temperature in an open flask for 48 hours. The precipitate was separated by centrifugation, washed with water, and then dried at 80°C.

Table 1: Details of the synthesis, composition and specific surface area (SA) of samples, general formula $[Co_xZn_{(1-x-y)}Al_y(OH)_2](NO_3)_y \cdot 0.5H_2O$. % M sol. = molar percentage of metals in the precipitation solution.

Sample	%wt Co	% M sol.			*x*	*y*	SSA (m^2g^{-1})
		Zn	Co	Al			
Co5	5.1	55	15	30	0.10	0.33	17.5
Co10	10.8	45	25	30	0.21	0.34	11.5
Co15	16.6	35	35	30	0.32	0.29	7.2
Co35	35.3	-	70	30	0.67	0.33	5.8

ii) <u>Cobalt based catalysts and bimetallic Co-Ru based catalysts synthesized with the help of ultrasound:</u> All the catalysts were prepared by a modified impregnation method. The metal precursors (cobalt and ruthenium carbonyl) were dissolved in n-decane together with the different support (SiO_2, Al_2O_3 or TiO_2). The solution was irradiated by an ultrasound generator with a horn type of 750 W, a frequency of 20 kHz, a diameter tip of 13 mm and an amplitude of 40-50% for 3 h, and then put into a rotating vacuum oven at 40°C at 36 rpm for 24 h (impregnation step). Samples have been calcinated at 350 °C for 4 h. The ultrasound horn used have a cooling jacket where the coolant has a low viscosity at low temperature and is a dielectric liquid [21].

iii) <u>Iron catalysts:</u> there were prepared the iron based catalysts using different method of synthesis: traditional impregnation (TR), impregnation with the help of the microwave (MW), impregnation with the help of ultrasound (US) and co-precipitation method. MW and US techniques seem to be promising that offer many advantages in the catalyst preparation as reported in [22-23] and their effect was also evaluated.

There were prepared according to the traditional impregnation method by incipient wetness (TR) with 30wt% of iron supported on a commercial, high surface area SiO_2 (Fluka, BET surface area 520 m^2g^{-1}, pore volume: 1.22 ml g^{-1} and pore diameter: 8.7 nm). The catalysts are promoted by K (2.0wt %) and Cu (3.75wt %). The percentages are regarding a previous research [13] where those compositions result as the most suitable catalyst. In this work all the percentages concerning the catalysts composition are on weight basis, while the percentages about the process conversion and selectivity are on molar basis. The catalysts will be named as $Fe_{30}K_{2.0}Cu_{3.75}$ referring the wt % of Fe, K and Cu on catalyst. The support, after heating treatment at 120°C for 12 h, was impregnated with an aqueous solution of $Fe(NO_3)_3{\cdot}9H_2O$ (Riedel de Haen product), KNO_3 (Merk product) and $Cu(CH_3COO)_2{\cdot}H_2O$ (Fluka product), and then put into a vacuum oven at 40 °C at 36 rpm for 24 h. The samples were heated at 100 °C for 12 h and at 500°C for 4 h in air. The results were also modeled with a collaboration with the *Politecnico di Milano* and presented in this PhD's work.

The synthesis of the catalyst with the aid of microwave is quite similar to the TR. The difference is the addition of a final step where the powder of catalyst, already calcined, is subjected to a MW irradiation. Two different methods for the MW irradiation were used. In the first one (MW1), it was taken a sample of catalyst, put it into a beaker and then put into a kitchen microwave oven

(Moulinex. Micro-Chef 1305E. 600W) for 30 min. In the second method (MW2), the catalyst (2 g) was suspended in hexane (400 ml), put it into a microwave chemical reactor (ordinary 400 mL round bottom glass flask, filled with the liquid to be heated and activated) and treated for 1 h at 60W. MW were produced by a MW generator, and sent to the MW applicator by an insulated coaxial antenna. Details of the MW applicator and of the associated experimental techniques can be found in [24].

The US treatment have been used between the impregnation and the evaporation step, by irradiating the silica-precursors solution using a Sonicator (W-385 Heat Systems Ultrasonics) with an effective input power of 60 W and a tip diameter of 13 mm. Silica solution, promoters and water have been sonicated by the US horn for 0.5 h in air atmosphere (US1). The same sample of US1 was successively sonicated in a suspension of hexane in argon atmosphere (instead of air) for 3h (US2).

b. <u>Catalysis Characterization</u>

The obtained materials were characterized by X-ray powder diffraction (XRD: PANalytical X'Pert Pro, CuKα radiation) operating at 40kV and 40mA, step size 0.0170 2θ degree and step scan 20s.

The metal content of samples was determined by inductively coupled plasma optical emission spectrometry (ICP-OES), using a Varian Liberty Series instrument.

Field emission scanning electron microscopy (SEM) images were obtained using a LEO1525 instrument after depositing the samples depositing the catalysts onto the sample holder and sputter coating with chromium.

The elemental mapping of metals was obtained by using energy dispersive X-ray spectroscopy (EDS) with a Bruker Quantax EDS instrument.

Transmission electron microscopy (TEM) images were obtained using a Philips 208 instrument.

FT-IR spectra of different samples, dispersed in KBr pellets, were recorded at room temperature using a Bruker IFS113V spectrometer. Typically, each spectrum was obtained at a resolution of 1 cm^{-1} in the spectral region 400-5000 cm^{-1}.

Specific surface area (S.S.A.) of all catalysts was determined by conventional N_2 absorption using a Micromeritics ASAP2010 instrument. Before the analysis, the samples were pre-treated at 200°C in a He flow.

Conventional temperature-programmed reduction experiments (TPR) were performed using a Thermoquest Mod. TPR/D/O 1100 instrument. The samples were initially pre-treated in a flow of argon at 200°C for 0.5 h. After being cooled down to 50°C, the H_2/Ar (5.1% v/v) reducing mixture was flushed through the sample at 30 mL min^{-1} and the temperature increased from 50 to 900°C at a constant rate of 10°C min^{-1}.

Water and nitrate content of the solids was determined by thermogravimetric (TG) analysis with a Netzsch STA 449C apparatus, in air flow, and 10°C/min heating rate.

c. <u>Kinetics Run</u>

FT synthesis was performed into a fixed bed reactor, using 1 g of fresh catalyst mixed with 1 g of diluting material (α-Al_2O_3). This diluting material must be inert for FTS and acts as a good thermal conductor to control the process temperature [25]. The calcined catalysts were initially activated in situ with the standard conditions of 46.8 Nml min^{-1} flow of syngas (H_2/CO = 2/1) at 350°C, 3 bar for 4 h. Then, they were tested with the standard conditions of 46.8 Nml min^{-1} flow of syngas (H_2/CO = 2/1) plus 5.0 Nml min^{-1} of N_2 as internal standard, at 20 bar at T = 250°C. Others reducing activating

gases, feeding compositions, pressures, temperatures have been tested in the work. Analyses of the gas-phase products (C_1–C_7) were performed with an on-line micro gas-chromatograph (Agilent 3000). Liquid products were collected in a trap at 5 °C and 20 bar and analyzed by a gas-chromatograph (Fisons Mod. 8000 Series) equipped with a Poparak-Q column after the total time of reaction. The aqueous phases collected in the cold trap were analyzed by a TOC (Schimadzu Mod. 5000A) to quantify the amount of carbonaceous species dissolved in water.

In the case of hydrotalcites, FTS was performed in two different laboratory plants with the same flow sheet. The first one, recently described and located at the *Università degli Studi di Milano*, and the second one at the *Universidad Central de Venezuela* during a complementary stage in Venezuela. In this case, the FTS was performed in a continuous flow system with a fixed bed stainless-steel reactor (di =32mm, l = 30 cm). The reactor was loaded with 0.3 g of fresh catalyst mixed with 0.3 g of see sand as a diluting material [26]. The calcined catalysts were initially reduced in situ by flowing hydrogen for 4 hours at 90.0 $Nml^{\cdot}min^{-1}$, 350°C and 0.8 MPa. After the reduction step, the temperature was lowered to 220°C under H_2. They were then tested in the standard conditions by flowing syngas (H_2: CO: N_2, 63:32:5, v/v, N_2 as internal standard) at 15.6 $Nml^{\cdot}min^{-1}$, increasing the system pressure slowly up to 2.0 MPa and 220-260°C. Once the reaction temperature was achieved, the reaction was led to proceed during a period of 280 h.

During reaction, the reactor effluent passed through a hot trap kept at 150ºC and 0.2 MPa to collect waxes, and the products leaving this trap were passed through a second trap kept at 0ºC and 0.2MPa to collect the lighter products (water, alcohols and hydrocarbons). The analyses were performed

in various chromatographs according to the nature of the sample to be analyzed. Permanent gases and light hydrocarbons were analyzed on-line in a PerkinElmer 3000GC Autosystem fitted with TCD detectors using a Carbosieve SII Supelco column. The liquid products (collected at 150ºC and 0ºC) were weighted and analyzed in a PerkinElmer chromatograph fitted with a 50m long Alumina RT capillary column connected to a FID.

A mass molar balance was performed for each FT run, resulting in a maximum error of ± 5% on molar basis.

4. Results and discussion

a) Catalysts activation:

i) Cobalt catalysts: The catalytic activity of the samples depends on the presence of metallic Co centres on the surface and the particle size. Many works have been done on the reducibility by TPR of CoO_x mixed oxides. The reduction profile of Co_3O_4 consists of a low-temperature peak and a high-temperature peak, which correspond to the reduction of Co^{+3} to Co^{+2} and Co^{+2} to Co^0 [27-30]

Two kinds of Co based catalysts were tested.

The HTlc materials contain Co (II) ions randomly dispersed inside the brucitic layers, then the active phase in the FTS is the metallic cobalt. Therefore, in order to have an active catalyst, a reduction procedure is requires to maintain the cobalt dispersion. TPR analyses were performed to study the reduction process and to select the best conditions for the catalyst activation. Fig. 1 reports the TPR profile of the sample Co5, Co10, Co15, Co35. All the profiles exhibit two regions of reduction; the first at lower temperatures (below 400°C), which is due to the reduction of Co while the second peak, above 700°C, indicates the presence of hardly reducible species. These species are probably spinel-type mixed oxides formed during the thermal treatment. According to

Alvarez et al [31], these two peaks are well separated for samples with a small particle size, while an intermediate particle size causes the overlapping of the two reduction steps resulting in a complete reduction with only one maximum at an intermediate temperature (328°C). The TPR profiles of our HTlc (Fig. 1) are consistent with the latter case.

Basing on the TPR results, the tested catalysts were activated before FTS at 350°C for 4 hours under hydrogen atmosphere, in order to reduce the Co ions to metallic Co.

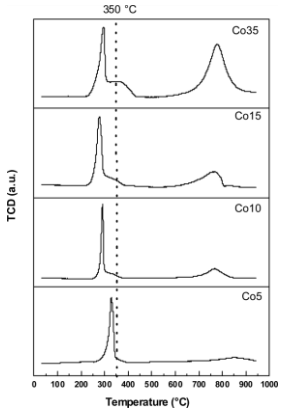

Fig. 1: TPR analysis of the samples Co5, Co10, Co15, Co35. Activation temperature is indicated with the dashed line.

After this treatment, XRD analysis detected only mixed metal oxides and no metallic Co phases, so highlighting the presence of active metal atoms homogeneously dispersed at the nanometer or sub-nanometer level [14,32].

The same thing happens with the cobalt catalysts synthesized with ultrasound. The results of TPR confirm the data found in literature [27-30] where the Co based catalysts need to be activated at 350°C for 4 hours under hydrogen atmosphere. It is important to note in Fig 2, how small amount of Ru decreases the peak of the reduction temperature.

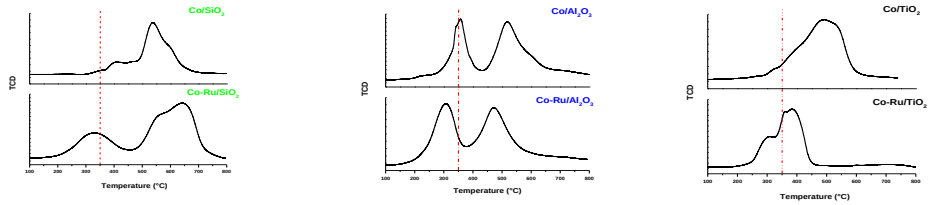

Fig. 2: TPR analysis of the samples Co/SiO_2 and $Co\text{-}Ru/SiO_2$, Co/Al_2O_3 and $Co\text{-}Ru/Al_2O_3$, Co/TiO_2 and $Co\text{-}Ru/TiO_2$. Activation temperature is indicated with the dashed line.

Basing on the TPR results, the tested catalysts were activated before FTS at 350°C for 4 hours under hydrogen atmosphere, in order to reduce the Co ions to metallic Co

ii) Iron catalysts:

As regard the method of synthesis of the iron based catalysts, the main results of catalysts characterization are reported in Table 2. All the surface areas (S.A.) of the prepared catalysts are significantly lower than the S.A. of the corresponding support (SiO_2). This important decrease can be explained considering the dilution effect, due to the presence of iron on the support. The dilution effect can be easily assessed by considering the surface area of bare silica support and assuming a negligible contribution of the iron phases to the surface area. The samples treated with MW and US have higher values of S.A. than the traditional ones; the effect of MW and US on S.A. is proportional with the US or MW emitting power.

The TPR analysis of these samples treated with MW gave results consistent with those prepared by TR, showing that the method of preparation does not influence the step of reduction (Fe_2O_3-> Fe_3O_4 ->α-Fe) of the catalyst but only the peak temperature.

Table 2: Characterization results of iron based catalysts using different method of synthesis.

Sample	Prep. Method	BET		TPR		TPD
		Surface Area (m^2g^{-1})		Temp. of first red. peak (°C)	Temp. of second red. peak (°C)	Temp. of the peak (°C)
		Bare support	Catalyst			
$Fe_{30}K_2Cu_{3.75}/SiO_2$	TR	430.3	160.1	240	600	170
$Fe_{30}K_2Cu_{3.75}/SiO_2$	MW1	430.3	180.0	-	-	-
	MW2		224.0	240	580	162
$Fe_{30}K_2Cu_{3.75}/SiO_2$	US1	430.3	201.1	236	572	171
	US2		210.1	-	-	-

TR= Traditional Impregnation*, MW1= Catalyst put it into a kitchen MW and processed in powder, MW2= Catalyst put it into MW and suspended in hexane, US1= Catalyst suspended in aqueous solution in air atmosphere for 0.5 h, US2= Catalyst sonicated and suspended in hexane in Argon atmosphere for 3h*

In agreement with the literature [33], all the curves show a single TPD's peak in the same range (150-170°C) that confirms the fact that only one type of adsorbing species can exists up on the catalyst (see table 2) for all the catalysts. Before FT runs, the catalysts must be activated reducing the hematite phase (not active for FTS) in iron carbides (in particular $Fe_{2.2}C$ and $Fe_{2.5}C$) and magnetite (Fe_3O_4) [34]. In literature there is not a uniform procedure for this operation. Many tests were performed by [34] and show that the best FT results in term of CO conversion have been obtained using the activating mixture H_2/CO (2/1) or pure CO starting from oxidized catalysts and making this operation at T=350°C. The process selectivity is not particularly modified using the mixture H_2/CO (2/1) or pure CO and changing the activation temperature.

b) FT results:

i) Co based hydrotalcites as catalysts for Fischer-Tropsch synthesis.

The activated samples were tested at different temperatures in the FTS plant, following the procedure reported in the experimental section. In Fig. 3 the CO conversion vs. the reaction temperature is reported for all the catalysts, while the products selectivity is displayed in Table 3.

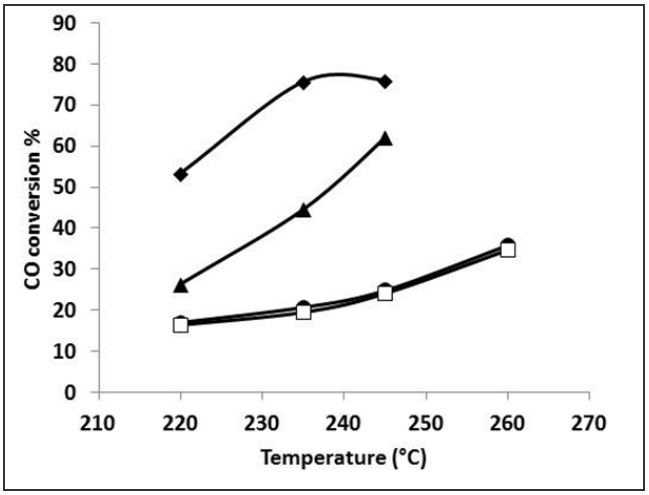

Fig. 3: %molar CO conversion to Co5 (●), Co10 (□), Co15 (♦), Co35 (▲), obtained at different reactor temperatures after 24 hours of reaction.

As expected, for each catalyst the activity is strongly influenced by the reaction temperature: the higher the temperature, the higher the CO conversion, but also the selectivity towards CO_2, CH_4 and light hydrocarbons is favored by a higher temperature. The CO conversion is similar for Co5 and Co10, while it is higher for the two samples with a larger amount of cobalt, i.e. Co15 and Co35. In particular, Co15 exhibits the highest CO conversion at all the selected temperatures. In FTS it is fundamental to obtain low quantities of CH_4 and CO_2 (undesired products) to favor the formation of higher hydrocarbons. For this reason, temperatures in the 220-235°C range are more suitable than the higher ones.

Moreover, Table 3 shows that Co15 exhibits the highest CO conversion and the highest C_2+ total yield (without considering CH_4 and CO_2, see note in Table 3) also at the lowest temperature (220°C). This result confirms that Co15 is the best performing catalyst obtained in this study.

The obtained data suggest the possibility of using synthetic hydrotalcites as Co-based catalysts for FTS and pursuing subsequent studies on the same subject.

Table 3: FTS products selectivity at different reactor temperatures.

Sample	Temperature (°C)	Products Selectivity %				C_2+ Yield
		CO_2	CH_4	≤C_7	>C_7	
Co5	220	0.3	2.9	3.3	93.4	16.5
	235	0.3	5.9	10.4	83.4	19.4
	245	1.1	8.5	12.7	77.6	22.4
	260	1.9	14.1	16.0	67.9	30.0
Co10	220	3.2	2.6	9.8	84.4	15.5
	235	3.8	4.9	14.3	76.9	17.8
	245	3.3	6.0	15.4	75.3	21.8
	260	8.1	16.3	41.3	34.3	26.2
Co15	220	1.4	10.1	17	70.5	46.7
	235	8.1	26.2	47.3	18.5	49.8
	250	17.8	17.7	44.3	20.2	49.1
Co35	220	1.4	3.9	10.3	84.4	25.0
	235	1.8	9.6	23.4	65.1	39.5
	245	5.1	25.7	65.6	10.5	47.3

≤C_7: all the hydrocarbons in the range C_2-C_7

>C_7: all the hydrocarbons greater than C_7

Product ‘‘i” selectivity = (moles C in product i) / (converted moles C) x 100.

C_2+ yield = CO conversion x (selectivity ≤C_7 + selectivity >C_7) $x10^{-2}$

iii) Sonochemical synthesis of Co and Co-Ru based catalysts for Fischer-Tropsch synthesis.

The use of ultrasound might be very efficient to optimize the dispersion of a so high metal charge, as already verified in our laboratory in the past [35-36]. This special type of synthesis should give at the catalyst a particular structure with a high surface area and a high metal dispersion that improves its activity towards the synthesis of Fischer-Tropsch. In the case of cobalt supported catalysts a simple US step has been added in the catalyst preparation. The precursors (cobalt and ruthenium carbonyl) were dissolved in n-decane together with the different support (SiO_2, Al_2O_3 or TiO_2), the solution was irradiated with ultrasound at a frequency of 20 kHz and an output power of 300 W for 3 hours. As seen in table 4, the catalysts show a low selectivity to methane and carbon dioxide and formation of higher hydrocarbons. The more interesting results are the highest CO conversion, at lower temperatures measured with a catalysts promoted with a Ru.

Table 4: CO Conversion; C_{2+}total yield; CH_4, CO_2, light hydrocarbon and heavy hydrocarbon selectivity of Co/Co-Ru based catalyst.

Catalyst	CO Conversion (%)	C_{2+} total yield	Selectivity (%)			
			CH_4	CO_2	$<C_7$	$> C_7$
Co/TiO_2	28	23	5	14	10	71
Co/SiO_2	6	5	19	6	23	52
Co/Al_2O_3	8	6	13	7	19	61
$Co\text{-}Ru/TiO_2$	98	73	18	8	14	60
$Co\text{-}Ru/SiO_2$	94	82	9	4	8	79
$Co\text{-}Ru/Al_2O_3$	84	73	11	2	12	75

As we have seen from the BET and TPR analysis, the support and the promoter play a key role in the performance of the catalyst because they are responsible

for the modification of some key parameters such as surface area and the metal dispersion.

ii)High Fe Loaded Supported Catalysts for Biosyngas Fischer – Tropsch Conversion: experimental results and detailed simulation

With regard to the treatment with the help of US (see table 5), it can be concluded that the sonication of an aqueous mixture, salts and precursors of support (US1), is preferable instead of to the calcined catalyst suspended in non-polar solvent, such as hexane (US2). With regard to treatment with MW (see table 3) there were obtained better results in term of CO conversion, with the powder catalyst treated directly in the MW (MW1), while the test conducted by suspending the catalysts in hexane and then treated in a MW reactor (MW2) for an hour did not give valid results. The best FTS results in term of C_{2+} yield (41%) has been obtained using MW1, while in tem of CO conversion (58%), using US1. All of them gave FTS results better than the traditional one. It's evident that the use of US or MW optimizes the catalytic performance in accord with previous similar results [36].

In agreement with [37] the FTS results show that TEOS as silica source is favorable for the enhancement of the FTS activity.

A very important property of iron based catalysts is their possibility to operate using feeding gas having a ratio H_2/CO not stoichiometric (i.e. $\neq$2). In the present work there were made some tests with $Fe_{30}K_{2.0}Cu_{3.75}$ catalyst, by feeding mixtures with a ratio H_2/CO between 0.5 and 2.0 in order to optimize the activity, selectivity and the lifetime of this kind of FT catalyst in work conditions of biosyngas feeding.

Table 5: Catalytic Results of $Fe_{30}K_{2.0}Cu_{3.75}$. Different preparation techniques. Support: SiO_2, Diluting Material: α-Al_2O_3. T=220°C

Preparation	CO Conversion (%)	C_{2+} Total yield	Selectivity (%)			
			CO_2	CH_4	$< C_7$	$> C_7$
TR	49	32	27	7	22	44
MW1	52	41	17	5	18	60
MW2	32	24	17	8	27	48
US1	58	38	29	6	22	43
US2	36	25	22	9	30	39
Co-precipitation*	38	32	2	13	28	57

$\leq C_7$: all the hydrocarbons in the range C_2-C_7
$>C_7$: all the hydrocarbons greater than C_7
Product ''i" selectivity = (moles C in product i) / (converted moles C) x 100.
C_2+ yield = CO conversion x (selectivity $\leq C_7$ + selectivity $>C_7$) $x10^{-2}$
* *The co-precipitation test was made at T=250°C and TEOS as a support*

On the basis of the collected data, a rigorous simulation of the FT synthesis reactor has been developed for different purposes: (i) to support the experimentations and their planning; (ii) to predict the reactor yield and conversion; (iii) to optimize the performance of the reactor system with different operating conditions; and (iv) to calculate novel reliable kinetic parameters based on the experimental data fitting by means of model-based nonlinear regression techniques. To do so, the FT reactor is modeled as a catalytic plug-flow reactor using mass and energy balances and reaction kinetics for Fe-based catalyst defined by Zimmerman and Bukur [38] leading to an ordinary differential equation system with structured Jacobian. Lumping techniques have been used to model heavy hydrocarbons. The system is solved by means of dedicated solvers to handle stiffness and nonlinearities of heterogeneous reactive systems [39].

Typical H_2/CO ratio of syngas manufactured from coal or biomass are between 0.7-1.2 and the Fig. 4 show that the activity of catalyst is good enough using also feeding ratio between 1.0 and 2.0.

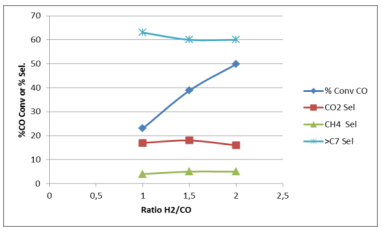

Fig.4. % CO conversion or % selectivity vs H_2/CO feeding ratio for $Fe_{30}K_{2.0}Cu_{3.75}$ catalyst at T=250°C

In Table 6 there is the data concerning the carbon monoxide conversion (%), and the selectivity towards undesired products (CO_2 and CH_4) and lighter and heavy hydrocarbons of Fe-based catalyst. The data collected using this catalyst were modeled in collaboration with *Politecnico di Milano*.

The selected model was based on the hypothesis that both FT and WGS reaction were active on this catalyst. The kinetic parameters were calculated and compared with the experimental data.

Table 6: FTS products selectivities at different H_2/CO ratio and reactor temperatures of $Fe_{30}K_{2.0}Cu_{3.75}$.

				Selectivity (%)			
H_2/CO	T(°C)	CO Conversion (%)	C_{2+} total yield	CO_2	CH_4	<C7	>C7
2/1	220	8,5	6,9	11	8	22	59
2/1	235	21,1	17,5	11	6	20	63
2/1	250	49,8	39,3	16	5	19	60
2/1	260	56,7	42,5	19	6	20	55
1.5/1	250	38,8	29,9	18	5	17	60
1.5/1	260	46,3	33,8	22	5	17	56
1/1	250	23	18,2	17	4	16	63
1/1	260	38,9	27,2	26	4	16	54

$\leq C_7$: all the hydrocarbons in the range C_2-C_7
$>C_7$: all the hydrocarbons greater than C_7
Product ''i" selectivity = (moles C in product i) / (converted moles C) x 100.
C_2+ yield = CO conversion x (selectivity $\leq C_7$ + selectivity $>C_7$) $x10^{-2}$

In Fig. 5 is presented a comparison between the experimental data obtained in the laboratory and the data obtained using the kinetic model. The first two columns represent the conversion of hydrogen and carbon monoxide, while in the other columns are represented the molar fraction of hydrogen, carbon monoxide, water, methane, and lump C_2, $C_{3\text{-}4}$, $C_{5\text{-}10}$, C_{11+}. It can be seen that the kinetic model present a good fitness regard to the experimental data.

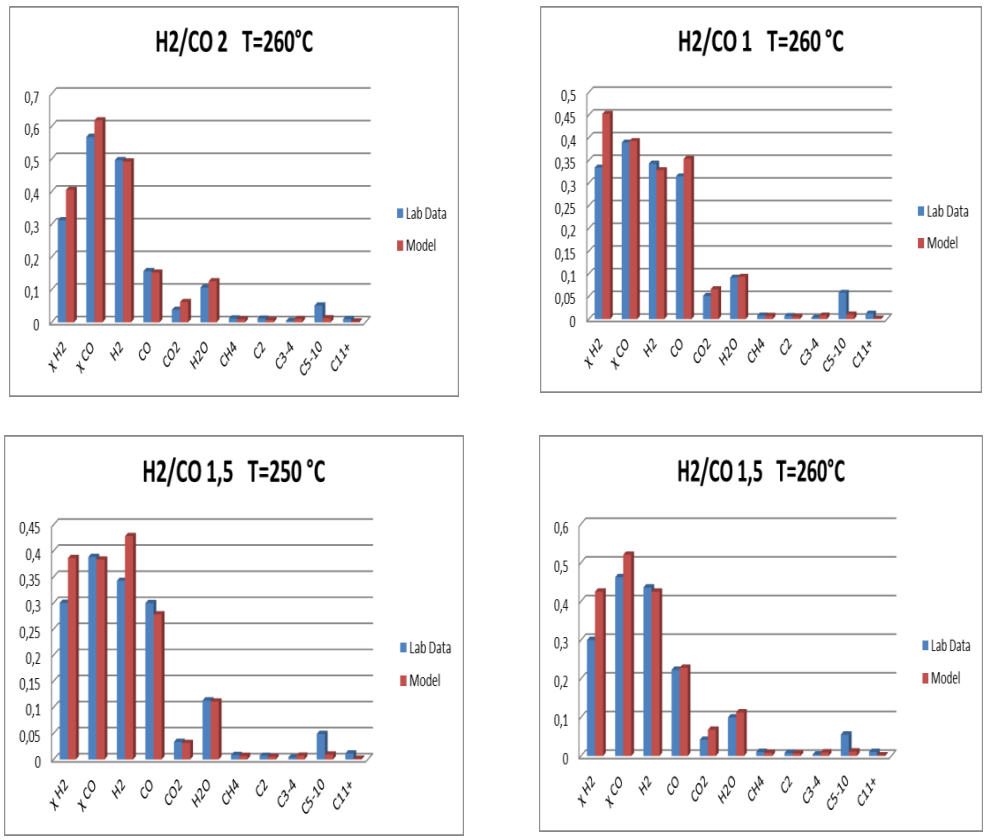

Fig. 5. Comparison between experimental data and kinetic model.

5. Conclusions

Concerning the results obtained in this PhD's research work, it is clear that all the samples tested have given good results. The Co-based catalysts, synthesized using the traditional impregnation method, with an additional step of ultrasound have given good results in comparison with the results in the current literature. The hydrotalcites have given lower results, if compared with the Co-based catalysts synthesized with the help of ultrasound, but they have opened an alternative and innovative way, that has never been tried before. Iron based catalysts allow a direct conversion of the biosyngas, and the results have shown how our catalysts are active with an H_2/CO ratio ≤2. Furthermore, trends have been modeled with success. In conclusion, the PhD's research work, has given a serious contribution to the current state of the art on catalysis in the Fischer-Tropsch synthesis either with cobalt and iron based catalysts. With cobalt has been optimized a traditional synthesis procedure with the introduction of ultrasound, furthermore has been created a completely new kind of catalyst. With iron has continued an optimization's work of iron supported with high loading metals, so to develop a suitable kinetic model able to work not only with syngas, but also with biosyngas.

References:

[1] M. S. Hadnadev-Kostic, J. Tatjana, T. Vulic, R. Marinkovic-Neducin, A. D. Nikolic, B. Jovic, Journal of the Serbian Chemical Society 76 (12) (2011) 1661–1671
[2] E. Lira, C. López, F. Oropeza, M. Bartolini, J. Alvarez, M. Goldwasser, F. López, J, Lamonier, J. Pérez, Journal of Molecular Catalysis A: Chemical 281 (2008) 146–153
[3] Q. Zhang, J. Kang, Y. Wang, ChemCatChem Catalysis 2 (2010) 1030
[4] F. Fischer and H. Tropsch, Brennst.Chem. 4, (1923) 276
[5] M. E. Dry, Enciclopedia of Catalysis, New York (2003) 247
[6] Fischer-Tropsch Technology, Studies in Surface Science and Catalysis, Elsevier, (2004)

[7] G. P. Vaan Deer Laan, A. A. C. M. Beenackers, Catalysis Reviews: Science and Engineering, 41(3&4) (1999) 255
[8] H. Schulz, Applied Catalysis A 186 (1999) 3
[9] G.P. van der Laan, A.A.C.M.Beenackers, Applied Catalysis A 193 (2000) 39
[10] A. Martinez, C. Lopez, F. Marquez, I.J. Diaz, Catalysis 220 (2003) 486.
[11] A.Y. Khodakov, W.Chu, P. Fongarland, Chemical Reviews 107 (2007), 1692
[12] B.H.Davis, Catal. Today 84 (2003) 83
[13] Pirola C, Bianchi CL, Di Michele A, Diodati P, Vitali S, Ragaini V. Catal Lett 2009; 131:294–304.
[14] A. Di Fronzo, C. Pirola, A. Comazzi, F. Galli, C.L. Bianchi, A. Di Michele, R. Vivani, M. Nocchetti, M. Bastianini, D.C. Boffito, Fuel 119 (2014) 62-69
[15] C. Pirola, C.L. Bianchi, A. Di Michele, S. Vitali, V. Ragaini, Catal. Comm. 10 (2009) 823–827
[16] T. Montanari, M. Sisani, M. Nocchetti, R. Vivani, M. C. H. Delgado, G. Ramis, G. Busca, U. Costantino, Catalysis Today 152 (2010) 104.
[17] C. Resini, T. Montanari, L. Barattini, G. Ramis, G. Busca, S. Presto, P. Riani, R. Marazza, M. Sisani, F. Marmottini, U. Costantino, Applied Catalysis A 355 (2009) 83
[18] Y. Lee, J. H. Choi, H. J. Jeon, K. M. Choi, J. W. Lee, J. K. Kang, Energy Environment Science 4 (2011) 914.
[19] Y. Tsai, X. Mo, A. Campos, J. G. Goodwin Jr., J. Spivey, Applied Catalysis A: General 396 (2011) 91–100
[20] M. Bastianini, D. Costenaro, C. Bisio, L. Marchese, U. Costantino, R. Vivani, M. Nocchetti, Inorg. Chem. 51 (2012) 2560-2567
[21] Suslick S.K. "Applications of ultrasound to materials chemistry", MRS Bulletin, 1995
[22] S. Qi, B. Yang, Methane aromatization using Mo-based catalysts prepared by microwave heating, Catal. Today 98 (2004) 639-645.
[23] Y. Liu, Y. Lu, S. Liu, Y. Yin, The effect of microwaves on the catalysts preparation and the oxidation of o-xilene over a V_2O_5/SiO_2 system, Catal. Today 51 (1999) 147-151.]
[24] G. Biffi Gentili, M. Linari, I. Longo, A. Ricci, IEEE Transactions on microwave theory and techniques, Vol. 57, (2009) 9
[25] C. Bianchi, C. Pirola, V. Ragaini, Catalysis Communications 7 (2006) 669-672
[26] M.L. Cubeiro. López, A. Colmenares, L. Texeira, M. Goldwasser, M. J. Pérez, F. Machado, F. González, Applied Catalysis A: General 167 (1998) 183-193
[27] C. L. Bianchi, Catalysis Letters Vol. 76, No. 3–4 (2001)155-159.
[28] H.-Y. Lin, Y.-W. Chen, C. Li, Thermochim. Acta 400 (2003) 61–67.
[29] H.-Y. Lin, Y.-W. Chen, Materials Chemistry and Physics 85 (2004) 171–175.

[30] B.A. Sexton, A.E. Hughes, T.W. Turney, Journal of Catalysis 97 (1986) 390–406.
[31] A. Alvarez, S. Ivanova, M.A. Centeno, J.A. Odriozola, Applied Catalysis A: General (2012) 431– 432
[32] C. L. Bianchi, C. Pirola, D.C. Boffito, A. Di Fronzo, A. Di Michele, R. Vivani, M. Nocchetti, M. Bastianini, S. Gatto, *DGMK Tagungsbericht* Volume2011-2 IssuePreprints of the DGMK-Conference "Catalysis: Innovative Applications in Petrochemistry and Refining", 2011 Pages 93-98 Journal 2011 CODEN: DGTAF7 ISSN:1433-9013
[33] 7. H. Wan, B. Wu, C. Zhang, H. Xiang, Y. Li, Promotional effects of Cu and K on precipitated iron-based catalysts for Fischer – Tropsch synthesis, J. molecular Catalysis 283 (2008) 33-42
[34] J. Xu, C.H.Bartholomew, J. Phys. Chem. B 109 (2005) 2392
[35] C.L.Bianchi, V.Ragaini, Catalysis Letters 95 (2004) 61-65
[36] C. Pirola, C. L. Bianchi, A. Di Michele, P. Diodati, D. C. Boffito, V. Ragaini, Ultrasonic Sonochem. 17, (2010) 610.
[37] Suo, Haiyun; Zhang, Chenghua; Wu, Baoshan; Xu, Jian; Yang, Yong; Xiang, Hongwei; Li, Yongwang; A comparative study of Fe/SiO2 Fischer–Tropsch synthesis catalysts using tetraethoxysilane and acidic silica sol as silica sources. Catalysis Today Volume 183, Issue 1, 20 March 2012, Pages 88–95
[38] W.H. Zimmerman, D.B. Bukur Can. J. Chem. Eng., 68, (1990) 292-301
[39] F. Manenti, I. Dones, G. Buzzi-Ferraris, H.A. Preisig, Ind. Eng. Chem. Res. 48, (2009) 9979-9984

Chapter 1. General Introduction

The National Renewable Energy Laboratory (NREL) and the Pacific Northwest National Laboratory (PNNL) [1] are undertaking studies of biomass conversion technologies to hydrocarbon fuels.

Process designs and preliminary economic estimates for each of these pathway cases were developed using rigorous modeling tools. This technology pathway case investigates the upgrading of woody biomass derived synthesis gas (syngas) to hydrocarbon biofuels. While this specific discussion focuses on the conversion of syngas via a methanol intermediate to hydrocarbon blend stocks, there are a number of alternative conversion routes for production of hydrocarbons through a wide array of intermediates from syngas (Fig. 1.1). Technical barriers and key research needs have been identified that should be pursued for the syngas-to-hydrocarbon pathway to be competitive with petroleum-derived gasoline-, diesel- and jet-range hydrocarbon blend stocks

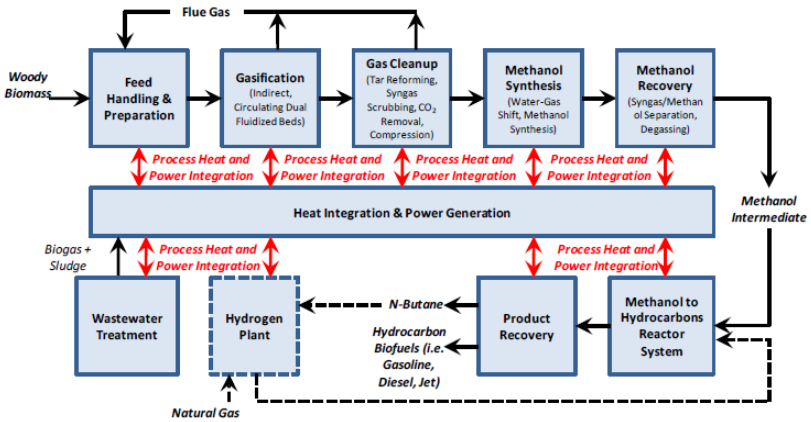

Fig. 1.1. Process Block Diagram [1]

At present, the development of economical and energy-efficient processes for the sustainable production of alternative fuels and chemicals is a global

demand and FTS is a crucial technology for this purpose [2]. On the one side, the observed climate change, particularly global warming, is widely held as a consequence of the increase of atmospheric CO_2 concentration due to fossil fuel combustion. On the other side, people are increasingly aware that fossil fuels reserves are huge but not unlimited and the air quality are major environmental concerns because they directly affect the way we live and breathe.

In order to meet the present and future threats generated by emissions to the atmosphere, environmental agencies around the world have issued more stringent regulations. One of them is the control of residual sulfur in diesel fuel and emission standards for particulates from diesel vehicles. All these facts have recently aroused renewed interest in the Fischer–Tropsch Synthesis because it can produce super clean diesel oil fraction with high cetane number (typically above 70) without any sulfur and aromatic compounds, using syngas (mixture of H_2, CO, CO_2) from natural gas, CH_4, coal landfill gas, coal or biomass, through steam reforming, partial or auto thermal oxidation, gasification processes or as a new tendency, from biomass [3-5]. Mineral diesel basically results from refining and fractional distillation of crude oil between 160 and 380°C at atmospheric pressure and is mostly formed by mixtures of paraffins containing between 12 and 20 carbon atoms per molecule. In these mixtures, linear paraffins are particularly appreciated due to their high cetane number, i.e. their excellent ignition performances. Expansion and social progress is however boosting a further increase of energy demand, particularly in the transportation sector which, in developed countries, accounts for most of this increase. This is the reason why carbon-neutral biofuels are largely considered a possible way to satisfy the energy demand without dramatically increasing the CO_2 content of the atmosphere [6].

In this context the production of hydrocarbons starting from syngas (CO + H_2) is a crucial topic, because syngas can be manufactured from natural gas (GTL: Gas to liquid), coal (CTL: coal to liquids) or biomass (BTL: Biomass to liquid) [7]. In Fig. 1.2 the industrial way to utilize syngas are reported; the fuels produced from syngas include hydrogen by the water-gas-shift (WGS) reaction, methanol by methanol synthesis, alkenes by Fischer Tropsch synthesis (FTS), isobutene by isosynthesis, ethanol by fermentation, or with homogeneous catalysts and aldehydes or alcohols by oxosynthesis.

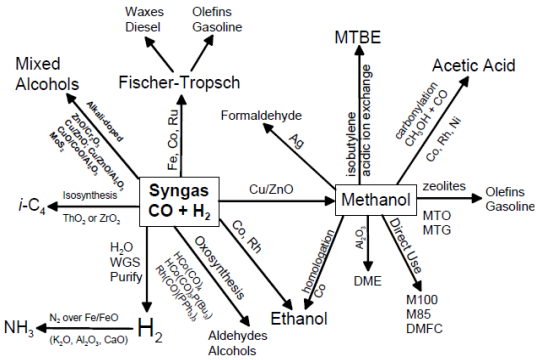

Fig. 1.2 Diagram of Syngas Conversion Processes [8]

Fischer-Tropsch Synthesis (FTS) is a well-known industrial process discovered by Franz Fischer and Hans Tropsch in Germany in 1923 [9]; starting from syngas (H_2 + CO) and using iron or cobalt based catalysts, it is possible to produce several hydrocarbons, in the range from 1 to 100 carbon atoms. Co-based catalysts have been more largely used due to their high selectivity to heavy hydrocarbons and low activity in the water-gas shift reaction, so limiting the CO_2 formation. Moreover Co-based catalysts have shown longer life-time and higher CO conversion compared to the Fe-based ones [10-11]. The essential target of FTS is to produce paraffins and olefins with different molecular weight

and to limit the maximum formation of methane and CO_2 [4, 12-15]. The main reactions involved in FTS are reported in the following scheme:

Irreversible reactions:

1) $n\ CO + 2n\ H_2 \rightarrow C_nH_{2n} + n\ H_2O$ for olefins

2) $n\ CO + (1+2n)\ H_2 \rightarrow C_nH_{(2n+2)} + n\ H_2O$ for paraffins

3) $2n\ CO + n\ H_2 \rightarrow C_nH_{2n} + n\ CO_2$ for olefins

4) $n\ CO + 2n\ H_2 \rightarrow C_nH_{(2n+1)}OH + (n-1)\ H_2O$ for alcohols

Equilibria:

5) $CO + H_2O \leftrightarrow CO_2 + H_2$ Water-gas-shift reaction (WGS)

6) $CO + 3\ H_2 \leftrightarrow CH_4 + H_2O$

7) $2\ CO \leftrightarrow C + CO_2$ Boudouard equilibrium

The whole reaction gives an energetic contribution strongly exothermic (about 150 kJ/mol CO reacted). FTS is a particularly complex system, in which a number of different reactions are combined to a unique mechanism: irreversible FT reactions produce hydrocarbons and some equilibria reactions between CO, CO_2, CH_4 and C, such as the WGS reaction and the Boudouard equilibrium, are present too. Nevertheless, it is possible to suppose that FTS can be simplified as a combination of the FT reactions and the WGS reaction [14]. Hydrocarbons are primary products of FT reaction, and CO_2 can only be produced by WGS reaction, a reversible parallel-consecutive reaction with respect to CO [16].

At present, the marketplace places a premium on FT diesel but not gasoline; thus, the current view is that the most attractive option is to produce high molecular weight FT products and then to hydrocrack them to produce high quality diesel fuel [17]. According to Calderone et al [18] the most important limitation to the industrialization of FT processes is the availability of cheap oil. Industrial interest in FT reactions always peaks during oil crises (Fig. 1.3). The

Kyoto protocol recognizes the importance of developing and deploying new technologies with less impact on the environment.

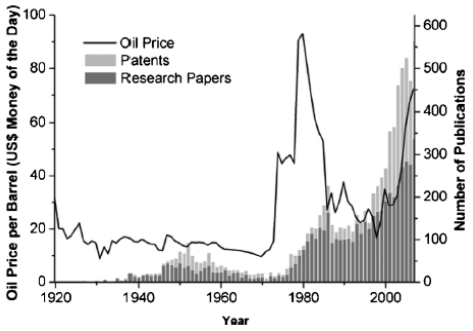

Fig. 1.3. The oil price (line) related to the output of peer reviewed FTS research papers and patents (bars) in 1925–2007 [19]

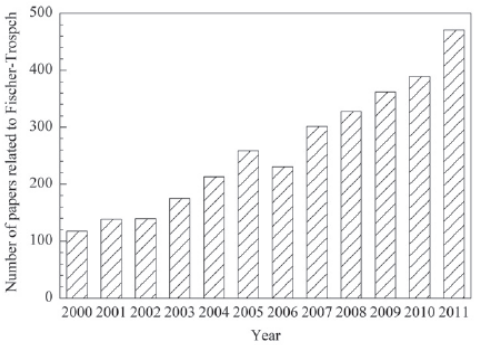

Fig. 1.4. Number of papers related to FT synthesis published in the past decade. From ISI Web of Science using the keyword “Fischer-Tropsch” [20]

Selectivity control remains one of the most important and difficult challenges in the research area of FTS. Development of efficient catalysts with controlled selectivity or tuned product distribution is a highly desirable goal [5].

Compared to cobalt systems, iron-based catalysts are cheaper but less resistant to deactivation due to the oxidizing effect of water, despite activating Water Gas Shift (WGS) reaction ($CO + H_2O \leftrightarrow CO_2 + H_2$) [12, 16]. Moreover they are flexible to changes in temperature, pressure and they can work at different H_2 / CO feed ratios (for iron based catalysts this ratio can be between 0.5 and 2.5) [21-22]. Iron catalysts seem to be more suitable to work with biomass-derived

syngas, as outlined by Corma et al. [23], that are characterized by a low ratio H_2/CO and by the presence of CO_2 (the activation of WGS reaction in fact can produce CO from CO_2). They present lower methane selectivity and they are less deactivated by poisons species [24]. The iron based catalysts have different active site: the Fe-carbides sites are active for the formation of hydrocarbons (FTS) while the magnetite (Fe_3O_4) sites are the most active phase for the WGS reaction [16, 25-26].

1.1 Fischer Tropsch Synthesis. Historical background

A Short Historical Sketch:

Year			Ref
1902	P. Sabatier and J. D. Senderens	Hydrogenated CO over Ni to produce CH_4	[27]
1910	A. M. Mittasch, C. Bosch, and F. Haber	Developed promoted Fe catalysts for the synthesis of NH_3	[28]
1913	Badische Anilin und Soda Fabrik (BASF)	Received patents on the preparation of hydrocarbons and oxygenates by the hydrogenation of CO at high pressure, usually on oxide catalysts	
1936	Eugene Houdry	Developed and installed the first commercial catalytic cracking unit.	[29]
1943-1944	Kòlbel, KWIK and five companies participated	Initiated and directed the comparative tests I and II held at Schwarzheide to select a Fe catalyst to replace Co in existing reactors. Although the results were remarkably good, no replacement catalyst was selected, probably because of the overall disarray of activity that attended the approach of the end of the war.	[30]
1949	Kòlbel and F. Engelhardt	Discovered that H_2O and CO react on FTS catalysts to yield typical FTS products.	
1950		A fluidized-fixed bed process developed by Hydrocarbon Research, Trenton, New Jersey was installed in Brownsville, Texas. This plant, called Carthage Hydrocol, Inc., used reformed natural gas. Severe operating difficulties required designing a new reactor, which was installed in 1953. The new reactor operated properly, but the plant was promptly shut down, sold, and dismantled. By the time the plant was operating correctly, the price of natural gas had more than doubled. Merely selling the gas was more profitable than converting it to gasoline and chemicals. At the same time, in South Africa, the SASOL FTS plant using coal was constructed and opened in 1955. Lurgi gas generators and Rectisol gas-cleaning units were employed. Two types of FTS reactors both with Fe catalysts, were used: a fixed-bed with recycle unit designed by Ruhrchemie in West Germany, having long tubes with an internal diameter of 2 inch, and an entrained-solids reactor by M. W. Kellogg in New Jersey. After a year or more of start-up problems, these units have operated successfully up to the present.	[31]
1953	R. B. Anderson and J. F. Shultz	Found that Fe nitrides are unique, durable catalysts for the FTS that produce large yields of alcohols. Anderson developed equations that predict the isomer and carbon-number distributions of FTS products.	[32]
1957	G. Natta and co-workers	Studied the methanol and higher alcohol syntheses.	[33,34]
1959	Pichler	Resumed work on FTS on Ru which led to the polymethylene synthesis.	

1961	H. H. Storch	He died: he was the architect of the useful scientific and engineering research programs on coal-to-oil processes at the U.S. Bureau of Mines in Pittsburgh and Bruceton, Pennsylvania	[32,35].
1967	U.S. Bureau of Mines workers	Developed methods for flame spraying catalysts onto metals for the platelet assemblies of hot-gas-recycle reactors. These techniques led to the development of a new FTS unit, the tube-wall reactor.	[36]
1975	SASOL II SASOL III	In South Africa, the decision was made to build SASOL II, scheduled for operation in 1980, and in 1979, plans were made for SASOL III, to begin operation in 1982. The new plants are similar to the initial plant, except that fixed-bed FTS reactors were not included in the new installations.	[31]
1976	Mobil	Announced a process for converting methanol to an aromatic gasoline and C to C_4 olefins on the shape-selective catalyst ZSM5. This process may be a serious competitor for FTS.	
1981	New Zealand	A methanol plant operating on natural gas plus the Mobil process was planned, scheduled for competition in 1985.	
1982	The worldwide recession	Sharply decreased demand for petroleum. OPEC was unable to control the production and price of oil among its members. The relatively low cost and abundance of petroleum has discouraged new coal-to-oil ventures.	
1993	Shell in Bintulu, Malaysia	Completed construction and began operating their "Shell Middle Distillate Process". The Bintulu Plant produces 12,500 BPD and in 2000 increase that capacity to 15,000 BPD. This F-T plant has effectively captured the world specialty wax market.	
2000		While Saudi Arabia produced about 8 million barrels of oil per day in 2000, the world flared (burned) or re-injected associated gas equivalent to 7.2 million barrels per day of clean synthetic fuels. Worldwide environmental legislation requiring ultra-low sulphur and aromatic levels in fuel will cost billions in oil refinery upgrading.	
2002		Nearly every major oil company is either developing their own F-T technology, forming joint ventures, or scrambling to do so. Exxon/Mobil has spent over $500 MM, Chevron formed a joint venture with Sasol, Statoil has formed a joint venture with Mossgas, Conoco built a $400MM test plant in Oklahoma, BP completed its pilot/test plant in Alaska, Shell has announced 7 new projects.	
2004		50 new Fischer-Tropsch projects have been announced. These projects total over 900,000 BPD capacity. Some of these projects are pilot plants, some are feasibility studies for clients, and some have started construction.	
2005		In South Africa, Mossel Bay GTL Expansion, operated by PetroSA with a capacity of 15.000bpd	
2006		In Qatar, ORYX GTL Phase 1, operated by Sasol/Qatar Petrol with a capacity of 32.400 bpd	
2011		In Qatar, Pearl GTL Phase 1, operated by Shell with a capacity of 70.000 bpd	
2011		In Qatar, Pearl GTL Phase 2, operated by Shell with a capacity of 70.000 bpd	
2013*		In Nigeria, Escravos, operated by Chevron/NNPC, with a capacity of 34.000bpd	
2017*		In Uzbekistan, Oltin Yo'l GTL, operated by Sasol/UNG/Petron, with a capacity of 38.000bpd	
2018-19*		In USA, Sasol Lousiana, operated by Sasol, with a capacity of 96.000bpd	

*Firm proposed large-scale GTL capacity outlook

Fig. 1.5. The Sasol Synfuels plant at Secunda, South Africa

Fig. 1.6. “Shell Middle Distillate Process” in Bintulu, Malaysia.

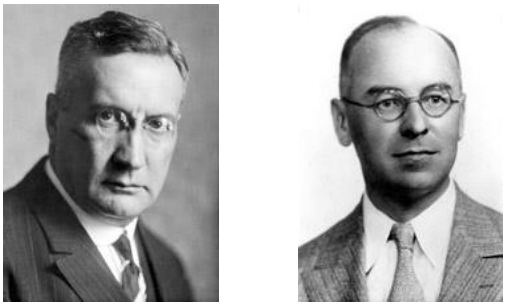

Fig. 1.7. Franz Fischer and Hans Tropsch

1.2 Present Situation of Fischer-Tropsch Technology

High energy prices and concerns about the environmental consequences of greenhouse gases (GHG) emissions lead a number of national governments to provide incentives in support of the development of alternative energy

sources, making renewables the world's fastest-growing source of energy in the outlook.

According to the Annual Energy Outlook 2013 [37], the aggregate fossil fuel share of total energy use falls from 82 percent in 2011 to 78 percent in 2040 in the Reference case, while renewable use grows rapidly (Fig. 1.7). The renewable share of total energy use grows from 9 percent in 2011 to 13 percent in 2040 in response to the federal renewable fuels standard; availability of federal tax credits for renewable electricity generation and capacity during the early years of the projection; and state renewable portfolio standard (RPS) programs.

Increased vehicle fuel economy offsets growth in transportation activity, resulting in a decline in the petroleum and other liquids share of fuel use even as consumption of liquid biofuels increases. Biofuels, including biodiesel blended into diesel, E85, and ethanol blended into motor gasoline (up to 15 percent), account for 6 percent of all petroleum and other liquids consumption by energy content in 2040.

Consumption of petroleum and other liquids peaks at 19.8 million barrels per day in 2019 in the *AEO2013 r*eference case and then falls to 18.9 million barrels per day in 2040 (Figure 1.8).

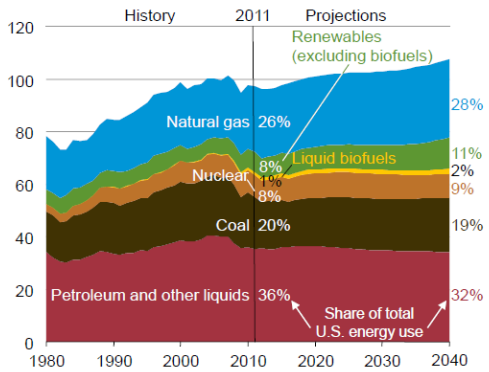

Fig 1.8. Primary energy use by fuel, 1980-2040 (quadrillion BTU).

The transportation sector accounts for the largest share of total consumption throughout the projection, although its share falls to 68 percent in 2040 from 72 percent in 2012 as a result of improvements in vehicle efficiency following the incorporation of CAFE standards for both LDVs and HDVs.

An increase in consumption of biodiesel and next-generation biofuels (*include pyrolysis oils, biomass derived, Fisher-Tropsch liquids, and renewable feedstocks used for on-site production of diesel and gasoline)*, totaling about 0.4 million barrels per day from 2011 to 2040, is attributable to the EISA2007 RFS mandates. The relative competitiveness of CTL and GTL fuels improves over the projection period as petroleum prices rise. In 2040, CTL and GTL together supply 0.3 million barrels per day of nonpetroleum liquids.

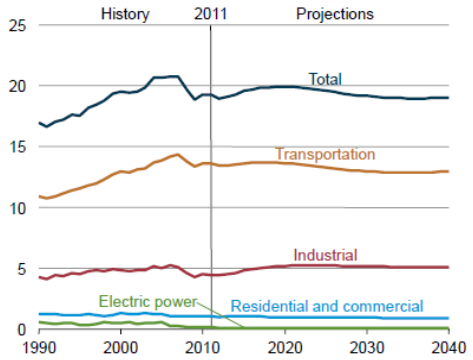

Fig. 1.9 Consumption of petroleum and other liquids by sector, 1990-2040 (million barrels per day)

2. Oil prices and total energy consumption

The importance of the research in FTS is directly dependent of the oil prices and the total energy consumption. So, it is so important to meet the projections of these variables before to make every kind of investments on this area. In *AEO2013*, oil prices are represented by spot prices for Brent crude. Prices rise in the Reference case from $111 per barrel in 2011 to about $117

per barrel in 2025 and $163 per barrel in 2040 (Table 1). The price rise starts slowly, then accelerates toward the end of the projection period.

Market volatility and different assumptions about the future of the world economy are reflected in the range of oil price projections for both the near and long term; however, most projections show oil prices rising over the entire projection period.

Table 1. Comparisons of oil price projections, 2025, 2035, and 2040 (2011 dollars per barrel)

			Projections					
	2011		2025		2035		2040	
	WTI	Brent	WTI	Brent	WTI	Brent	WTI	Brent
AEO2013 (Reference case)	94.86	111.26	115.36	117.36	143.41	145.41	160.68	162.68
AEO2012 (Reference case)	94.82	--	135.35	--	148.03	--	--	--
Energy Ventures Analysis, Inc. (EVA)	--	--	78.18	--	82.16	--	87.43	--
IEA (Current Policies Scenario)	--	107.60	--	135.70	--	145.00	--	--
INFORUM	--	111.26	--	136.77	--	149.55	--	--
IHSGI	94.88	--	93.05	--	86.25	--	81.20	--

As regard the total energy consumption, the in table 2 there are four different projections made by other organizations (INFORUM, IHSGI, ExxonMobil and IEA) [37].

Table 2. Comparisons of energy consumption by sector projections, 2025, 2035 and 2040 (quadrillion BTU)

Sector	*AEO2013* Reference	INFORUM	IHSGI	ExxonMobil	IEA
			2035		
Residential	11.4	11.9	12.5	--	--
Residential excluding electricity	5.7	6.1	5.7	5.0	--
Commercial	9.9	10.3	10.8	--	--
Commercial excluding electricity	4.4	4.5	4.1	3.0	--
Buildings sector	21.2	22.2	23.3	--	23.0
Industrial	27.8	26.8	--	--	24.2
Industrial excluding electricity	23.9	23.4	--	19.0	--
Losses[b]	1.4	--	--	--	--
Natural gas feedstocks	0.5	--	--	--	--
Industrial removing losses and feedstocks	25.9	--	23.4	--	--
Transportation	26.4	28.8	22.9	25.0	22.7
Electric power	44.1	44.1	53.6	39.0	42.7
Less: electricity demand[c]	15.1	15.1	18.1	--	18.6
Electric power losses	29.0	--	--	--	--
Total primary energy	**104.4**	**106.8**	--	**91.0**	**93.6**
Excluding losses[b] and feedstocks	**102.6**	--	**105.1**	--	--
			2040		
Residential	11.6	--	12.9	--	--
Residential excluding electricity	5.5	--	5.7	5.0	--
Commercial	10.2	--	11.1	--	--
Commercial excluding electricity	4.5	--	4.1	3.0	--
Buildings sector	21.8	--	24.0	--	--
Industrial	28.7	--	--	--	--
Industrial excluding electricity	24.8	--	--	18.0	--
Losses[b]	1.9	--	--	--	--
Natural gas feedstocks	0.4	--	--	--	--
Industrial removing losses and feedstocks	26.4	--	23.5	--	--
Transportation	27.1	--	22.0	25.0	--
Electric power	45.7	--	55.9	39.0	--
Less: electricity demand[c]	15.7	--	19.1	--	--
Electric power losses	30.0	--	--	--	--
Total primary energy	**107.6**	--	--	**89.0**	--
Excluding losses[b] and feedstocks	**105.3**	--	**106.3**	--	--

-- = not reported.
*IEA data are for 2010.
[b]Losses in CTL and biofuel production.
[c]Energy consumption in the sectors includes electricity demand purchases from the electric power sector, which are subtracted to avoid double counting in deriving total primary energy consumption.

ExxonMobil includes a cost for carbon dioxide (CO_2) emissions in their projection, which helps to explain the lower level of consumption in their outlook. Although the IEA's central case also includes a cost for CO_2 emissions, its Current Policies Scenario (which assumes that no new policies are added to those in place in mid-2012) is used for comparison in this analysis, because it corresponds better with the assumptions in the AEO2013 Reference case. ExxonMobil and IEA show lower total energy consumption across all years in comparison with the AEO2013 Reference case. Total energy consumption is

higher in all years of the IHSGI projection than in the AEO2013 Reference case but starts from a lower level in 2011.

For the transportation sector, the difference could be related to vehicle efficiency, as the INFORUM projection for motor gasoline consumption (2 quadrillion Btu lower than AEO2013) is comparable with the EIA projection in AEO2012, which did not include the efficiency standard for vehicle model years 2017 through 2025.

IHSGI projects significantly higher electricity consumption for all sectors than in the AEO2013 Reference case, which helps to explain much of the difference in total energy consumption between the two projections.

Then, the projections make possible the investment on research in Fischer – Tropsch synthesis.

The process, known as Gas to Liquid (GTL), was based on two steps:

- Steam reforming of natural gas into syngas
- Fischer Tropsch synthesis from syngas into synthetic liquid fuels.

Recently (2004-2006), the massive growth of GPN (Gross National Product) in China and India has caused crude oil process to rise continuously, and FTS (including both coal and biomass as feedstock, BTL) has become once more an appealing technology. Recent interest in FT technology especially in Europe and South America is driven by a focus on the gasification of biomass into fuel [38] (BTL).

Biomass to Liquid via Fischer–Tropsch (BTL-FT) synthesis is gaining increasing interests from academia and industry because of its ability to produce carbon neutral and environmentally friendly clean fuels.

In the BTL-FT process, biomass, such as woodchips and straw stalk, is firstly converted into biomass-derived syngas (bio-syngas) by gasification.

Bio-syngas resulting from biomass gasification contains CO, H_2, CO_2, CH_4, and N_2 in various proportions [39, 40]. Then, a cleaning process is applied to remove impurities from the bio-syngas to produce clean bio-syngas which meets the Fischer–Tropsch synthesis requirements. Cleaned bio-syngas is then conducted into a Fischer–Tropsch catalytic reactor to produce green gasoline, diesel and other clean biofuels.

Generally, there are three main steps in the Biomass to Liquid via Fischer–Tropsch (BTL-FT) synthesis [41-43]. Biomass is firstly converted into biomass-derived syngas (bio-syngas) by gasification. In a second step, a cleaning process is applied to the bio-syngas in order to remove impurities, resulting in clean bio-syngas which meets the Fischer–Tropsch synthesis requirements. Finally, the cleaned bio-syngas is then conducted into Fischer–Tropsch catalytic reactor to produce green gasoline, diesel and other clean biofuels. The flow sheet of the BTL-FT process is depicted in Figure 1.10.

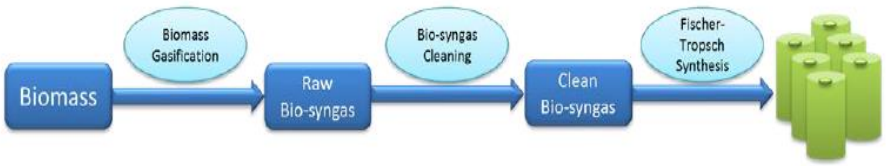

Fig.1.10. Flow sheet of the Biomass to Liquid via Fischer–Tropsch Synthesis (BTL-FT) process. [44]

It is difficult to predict the composition of the gas product from a gasifier due to the complex reactions occurred during the gasification. Table 1.3 shows the typical composition of gas produced from gasification of wood and charcoal with low to medium moisture content with ambient air as the gasifying agent in a downdraft gasifier [45] and composition of bio-syngas from biomass gasification [46–48].

At present, the main commercial interest in FTS is the production of high quality sulphur-free synthetic diesel fuels from natural gas, currently being flared at crude oil production wells [49-52]. This renewed interest in FTS has not just only come about as a result of abundant supply of natural gas, but also because of the global development of fuel supplies and environmental regulations to improve air quality in cities around the world.

All these facts have recently aroused renewed interest in the Fischer–Tropsch Synthesis. Synthetic diesel is being promoted by the fuel industry because it can produce super clean diesel oil fraction with high cetane number (typically above 70) without any sulfur and aromatic compounds, with low particulate formation and low NO_x and CO emission [3-4, 53] as the most viable next step towards the creation of a sustainable transport industry.

Table 1.3. Composition of gas produced from gasification of wood and charcoal in ambient air [45] and also the composition of typical nitrogen free bio-syngas [46–48].

Component	**Wood gas (air)**	**Charcoal gas (air)**	**Bio-syngas (nitrogen free)**
N_2	50–60	55–65	0
CO	14–25	28–32	28–36
CO_2	9–15	1–3	22–32
H_2	10–20	4–10	21–30
CH_4	2–6	0–2	8–11
C_2H_4	n/a	n/a	2–4
BTX	n/a	n/a	0.84–0.96
C_2H_5	n/a	n/a	0.16–0.22
Tar	n/a	n/a	0.15–0.24
Others	n/a	n/a	<0.021

3. Viability of GTL for the gas market

According to Brown [54], between 1950 and 2010, global volumes of GTL product output capacity had materialized at less than 100.000 b/d -roughly equivalent to the output of just one average- sized east European refinery.

However, the recent confluence of several factors has altered the commercial viability of the GTL industry, suggesting that wide margins and robust revenues can be earned by converting natural gas into clean-burning liquid fuels and other high value oil-linked commodities. Broadly speaking, these factors are:

1) Improvements in the lifespan of the catalysts used to derive hydrocarbon chains from natural gas (methane) and efficiency gains in the Fischer Tropsch processes

2) The detachment of natural gas markets from oil prices and the subsequent wide differential between the two prices, courtesy of the unconventional gas boom

3) Long-term global demand trends favouring low-emissions fuels in the transport sector.

Despite these auspicious circumstances, however, this paper argues that GTL fuels will have only a limited reach into oil product markets and the transport sector going forward. While downward pressure on natural gas prices and increasing demand for clean-burning motor fuels have ushered in "visions of a new future of transport fuels (that) will soon go global" [55], the transient conditions that had supported a favourable outlook for the proliferation of GTL liquid fuels over the period of 2009-12 have, more recently, shown signs of deterioration. Moreover, alternative and less capital-intensive pathways to natural gas monetization are emerging via small-scale "modular" GTL plants, whose development has been encouraged by the rapidly increasing supply of

unconventional and associated gas which has necessitated more practical and localized gas monetization solutions.

Commodity prices for transport fuels such as diesel are closely correlated to crude price movements (see Fig 1.10) and, moreover, trade at a premium to crude benchmarks depending on regional dynamics such as product balances and cyclical demand conditions. GTL products sharing identical physical characteristics with crude-refined diesel have the potential to exploit not only the market price differential between gas feedstock and oil prices, but, in addition, the spread between oil benchmark prices and oil product markets. The confluence of these dynamics leads to significantly wider margin potential than that experienced by crude-refined alternatives in oil product markets, at least in a context defined by high oil and low gas prices. Accordingly, the upside revenue potential of large-capacity GTL builds is dictated by the relatively straightforward principle that the more capacity dedicated to products trading at a premium to crude a plant has the higher the plant's revenues will be.

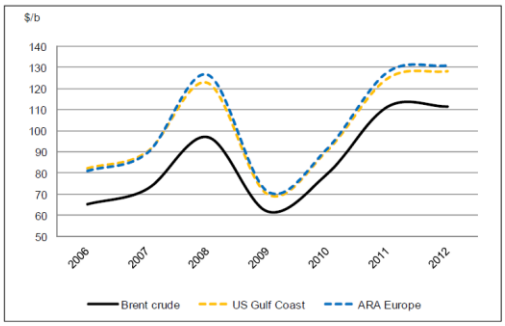

Source: EIA, Bloomberg. f.o.b. spot prices for ARA ULSD and USGC Diesel 2.

Fig. 1.11. Correlation between ultra-low sulphur diesel spot prices and Brent crude

Europe offers an ideal destination for GTL-derived diesel. A combination of stringent fuel quality specifications and declining domestic supply supports a healthy environment for gasoil and diesel imports. Moreover, the oil product market is predominately driven by gasoil/diesel consumption, which accounted

for well over half (56 per cent, see Fig. 1.11) of main product demand in 2012. As such, the current application and commercialization of GTL diesel in Europe reflects the potential of GTL diesel to impact global gasoil markets.

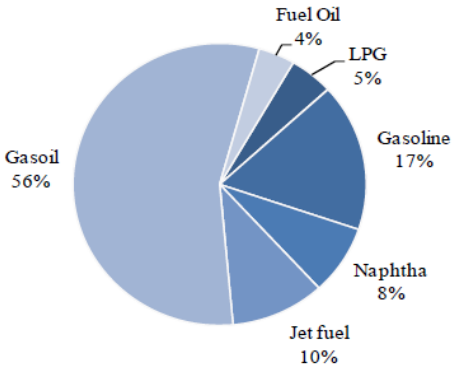

Source: IEA, national sources, and PFC Energy

Fig. 1.12. Europe main oil product demand (2012)

In order to meet supranational carbon emissions targets, progressively tighter EU-wide Fuel Quality Directives have mandated a sharp reduction of sulphur content in gasoil/diesel marketed within the European Union. The specifications for sulphur content in motor fuels (gasoline and diesel) in the road sector were reduced from 350 parts per million (ppm) in 2000 to just 10 ppm in 2009. The legislation was amended in 2011 to encompass gasoil and diesel consumed in off-road sectors such as railways and inland navigation, and, by 2012, 10 ppm gasoil accounted for an estimated 80 per cent of Europe-wide gasoil demand [54]

The gasoil produced by refineries in Europe has varying physical characteristics in terms of sulphur content (affecting particulate emissions), cetane index (influencing ignition quality in combustion engines), and viscosity (affecting energy content and fuel efficiency), each influencing market value.

It has been estimated that FT-GTL should be viable at crude oil prices of about $20 per barrel. The oil price has been well above $70 per barrel (more recently

it has even topped above $100 per barrel), making it a very appealing for countries, that have huge reserves of natural gas, but little local market for it and no major pipeline infrastructure to ship it to larger economies.

In Fig. 1.12 it can be seen a geographical representation of the world proved reserves for 2011.

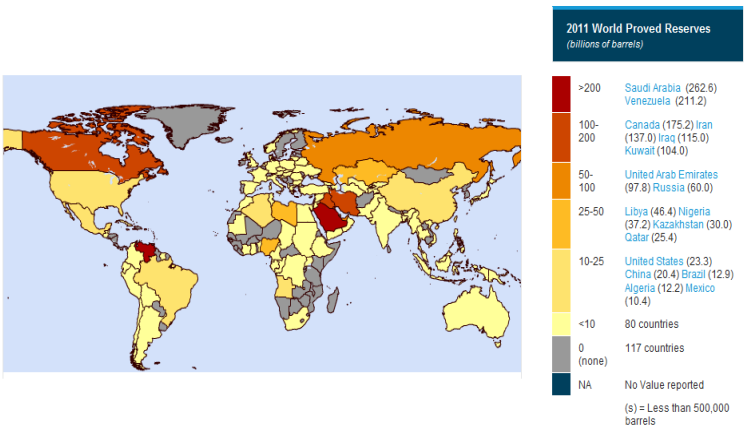

Fig. 1.13 World proved reserves 2011. [37a]

1.2 Fischer Tropsch GTL Process and Chemistry

According to [56] the basic FT-GTL process consists of three fundamental steps, which require significant supporting infrastructure and a secure feed gas supply to function effectively (Fig. 1.13).

1. The production of synthesis gas (syngas). The carbon and hydrogen are initially divided from the methane molecule and reconfigured by steam reforming and/or partial oxidation. The syngas produced, consists primarily of carbon monoxide and hydrogen.
2. Catalytic Fischer Tropsch synthesis. The syngas is processed in Fischer-Tropsch reactors of various designs depending on technology creating a wide range of paraffinic hydrocarbons product (synthetic crude, or

syncrude), particularly those with long chain molecules (e.g. those with as many as 100 carbons in the molecule).

3. Cracking-product workup. The syncrude is refined using conventional refinery cracking processes to produce diesel, naphtha and lube oils for commercial markets [57]. By starting with very long chain molecules the cracking processes can be adjusted to an extent in order to produce more of the products in demand by the market at any given time. In most applications it is the middle distillate diesel fuel and jet fuels that represent the highest-value bulk products with lubricants offering high-margin products for more limited volume markets. In modern plants, FT-GTL unit designs and operations tend to be modulated to achieve desired product distribution and a range of products slates [58]

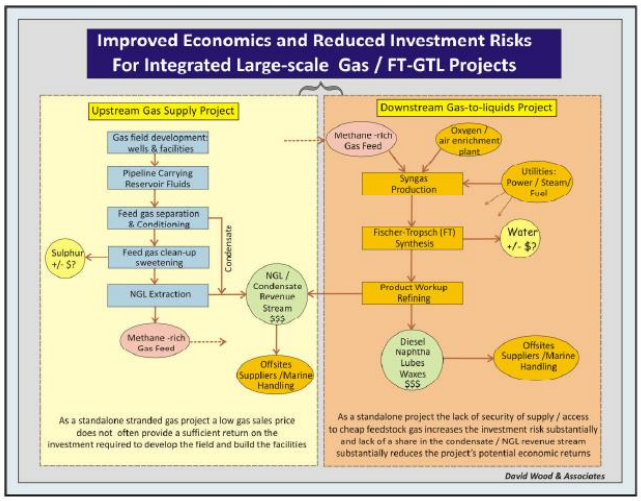

Fig. 1.14 Large scale FT-GTL projects become more economically robust for the developer if they involve integrated upstream and downstream components securing feed gas supplies and additional revenues from NGL and condensate extracted from the feed gas. [56]

The Fischer Tropsch processes are not limited to using gas derived from large conventional, non- associated natural gas as a feedstock; coal seam gas, associated gas, coal or biomass can all be processed using FT technologies by changing the catalysts and work conditions (Pressure and temperature). A secure supply of feed gas, from whatever origin, is important for the commercial viability of large-scale FT-GTL plants. Integrated upstream and downstream projects therefore offer GTL project developers lower-risk returns.

1) The production of synthesis gas (syngas)

Synthesis gas ("syngas") is typically produced using either partial oxidation or steam reforming processes [59]. Syngas is an intermediate gas feed for many different petrochemical processes including a range of GTL alternative technologies:

• Partial Oxidation	$CH_4 + ½O_2 \rightarrow CO + 2H_2$ (exothermic)	The key components required for this approach include: A combustion chamber operated at high temperatures (1200-1500°C) without catalysts. Process designs to impede a competing reaction to syngas formation which involves the decomposition of methane to carbon black (due to high temperature, non-catalytic nature of the chemistry) [59]
• Steam Reforming	$CH_4 + H_2O \rightarrow CO + 3H_2$ (endothermic)	Steam reforming is usually carried out in the presence of catalyst –e.g. nickel dispersed in alumina in operating conditions involving temperatures of 850-940°C and pressure of about 3MPa. The process is typically conducted in tubular, packed reactors with heat recovery from flue gas used to pre-

heat the feed gas or to raise steam in waste heat boilers. Several well-established engineering companies offer their own variants of this process.

- Other possible reactions are:

$$CO + H_2O \leftrightarrow CO_2 + H_2$$
$$CH_4 + CO_2 \leftrightarrow 2CO + 2H_2$$

2) Fischer-Tropsch synthesis

According to [55] Fischer-Tropsch synthesis is one of a several technologies to polymerise the carbon and hydrogen components into long-chain molecules:

$$CO + 2H_2 \rightarrow -CH_2- + H_2O \text{ (very exothermic)}$$

Which in practice operates more typically as:

$$2CO_{(gas)} + H_{2\,(gas)} \rightarrow (-CH_2-)_{n\,(liquid)} + CO_{2\,(gas)} + H_2O$$

The process involves some carbon dioxide emission and water/steam production along with the hydrocarbon liquid production.

The typical FT reactions compete with the methanation (reverse of steam reforming) reaction (and reactions that lead to the production of propane and butane (LPG), which are also highly exothermic:

$$CO + 3H_2 \leftrightarrow CH_4 + H_2O$$

In order to promote FT reaction in preference to methanation (or LPG reactions), the synthesis is run at low temperatures: 220-350°C; pressure: 2-3 MPa with carefully selected catalysts (i.e. commonly cobalt) in reactors that encourage the growth of long-chain hydrocarbon molecules. Several companies hold patents associated with XTL catalysts, process vessels and process sequences (e.g. Conoco Phillips, CompactGTL, ExxonMobil, Rentech, Sasol, Shell, Syntroleum and others), however, it is only Sasol and Shell that have built large-scale commercial plants (i.e.>5000 barrels/day of GTL product)

rather than pilot-scale or demonstration plants. The industry therefore remains in its infancy and the many patents held by relatively few companies act as a costly barrier to entry for resource-rich gas companies and countries wishing to use GTL as an alternative means of monetizing their gas.

There are two major categories of natural gas-based FT process technology: the high-temperature and the low-temperature types.

HTFT (High-Temperature Fischer-Tropsch): In HTFT, because of the process conditions and the catalysts involved, the syncrude produced includes a high percentages of short chain (i.e., <10 carbon atoms) with significant amounts of propane and butane mixed with olefins (e.g. propylene and butylene). These short-chain hydrocarbons gases are typically extracted from the tail gas stream, utilizing cryogenic separation. The resultant lean tail gas is recycled and, mixed with additional lean feed gas for further syngas production [60]. The high-temperature (HT), iron catalysts-based FT GTL process produces fuels such as gasoline and diesel that are closer to those produced from conventional oil refining. The resultant GTL fuels are sulphur-free, but contain some aromatics [61]. Typical process operation conditions for HTFT are temperatures of approximately 320°C and pressures of approximately 2.5MPa. Conversion in HTFT can be>85% efficient [62], but not all the products are readily usable or capable of producing high-quality transport fuels. HTFT processes tend to be conducted in either circulating fluidized bed reactors or fluidized bed reactors [63].

LTFT (Low-Temperature Fischer-Tropsch): LTFT involves the use of low-temperature (LT), cobalt-catalyst-based processes, either in slurry-phase bubble-column reactors (e.g. Sasol) or in multi-tubular fixed bed reactors (e.g. Shell). LTFT produces a synthetic fraction of diesel (GTL diesel) that is virtually free of sulphur and aromatics. Typical process operation conditions for LTFT are

temperatures of approximately 220°C to 240°C and pressures of approximately 2.0 to 2.5 MPa. Conversion in LTFT is typically only about 60% with recycle or the reactors operating in series to limit catalyst deactivation [62].

The primary focus of most large-scale FT technologies in current market conditions is to produce, high-quality low-emissions GTL diesel, jet fuel and naphtha (for petrochemical feedstock or gasoline blending).

3) Cracking – product workup

From [56] FT GTL plants can be configured to produce a wide range of products, from lubricating base oils and waxes through to petrochemical naphtha and specialty chemicals. Most of the already developed and planned plants target the production of diesel fuels (C_{14}-C_{20}) together with some kerosene/jet fuel (C_{10}-C_{13}), naphtha (C_5-$C1_0$), lubricants (>C_{50}) and a little LPG (C_3-C_4)- By adjusting operating conditions in the Fischer Tropsch reactor, the mix of products can be altered. This enables FT GTL products to be produced in quantities that enable them to target the high-value product markets of petroleum products produced by conventional oil refineries.

However, the yield pattern from a typical FT GTL plant is significantly different to that rom a catalytic cracking crude oil refinery (Fig. 1.14). Typically, the diesel yield of FT GTL plant is around 70%, much higher than for crude oil refineries, which is typically some 40% [64].

From Fig. 1.14, the products derived from upgrading syncrude produced by FT-GTL differ significantly from those produced by refining barrel of crude oil. Notably FT GTL produces more high-value, zero-sulphur products, especially middle distillates. On the other hand refining crude oil, particularly heavy oil produces substantial quantities of low-value fuel oil, i.e. more than prevailing markets can consume. Source modified from [65].

Most oil refineries yield some low-value fuel oil, the yield depending on the quality of the fuel processed and the type and capacity of the refinery's fuel-oil conversion units. By contrast, the FT GTL plants are configured to yield only higher-value (relative to crude oil) light and middle distillate products. From a plant with existing technology, the yield of middle distillates (gasoil/diesel and kerosene) is nearly a third more of the total product slate than that from a typical oil refinery [66].

As predicted a decade ago [67] globally, diesel demand is growing rapidly at some 3% a year, more quickly than other refinery products. Against this backdrop, refiners face significant challenges to meet diesel demand and quality in the future as crude oil supply becomes heavier and sourer [68].

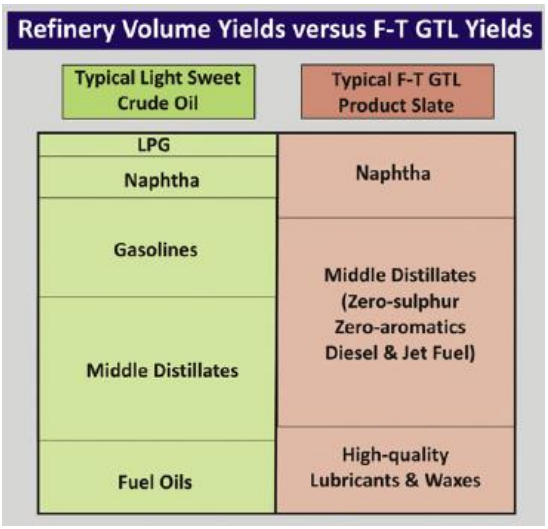

Fig. 1.15. Refinery Volume Yields versus FT GTL Yields.

From [56], for FT-GTL to be commercial at oil prices of less than about 40$/barrel, plant capital costs, operating costs and feed gas costs all have to be substantially lower on a unit basis than large-scale plants built in recent years have been able to deliver. If the unit capital cost of an FT-GTL plant is close to 100.000$/barrel/day, the operating cost of that plant is close to 20$/barrel of

product and the feed gas costs in the vicinity of 5$/MMBtu the liquid products would cost in the vicinity of 100$/barrel and the economics of such as a plant do not look so inviting in 2012 market conditions. The industry has to achieve lower plant and feed gas costs to be economically attractive.

Fischer- Tropsch Synthesis. Opportunities and challenges

GTL technologies offer the potential to reduce global dependency on crude-oil derived transportation fuels. They also offer substantial opportunities for the owners of stranded gas to diversify the markets into which they deliver their gas-derived liquid products, particularly targeting the large and rapidly growing global middle distillate markets (See Fig. 1.16).

However, the technologies are complex, costly and tightly held by a few companies holding patents for the key process steps, which present significant barriers to entry for building large-scale plants. This also renders the building of large-scale plants challenging for the gas resource holders in terms of capital costs, access to technology and long-term transfer of GTL technologies.

At the current time Fischer Tropsch technologies dominate GTL applications for large scale-plants. Technology breakthroughs are required if methane-to-gasoline or methane-to-olefin plants are to displace traditional refinery and petrochemical routes to those products. On the other hand dimethyl-ether (DME) has a growing market in Asia, particularly in China, which is likely to expand if the one-step process, avoiding the production route via methanol, is successfully scaled up as planned, and transportation fuel markets are developed for DME.

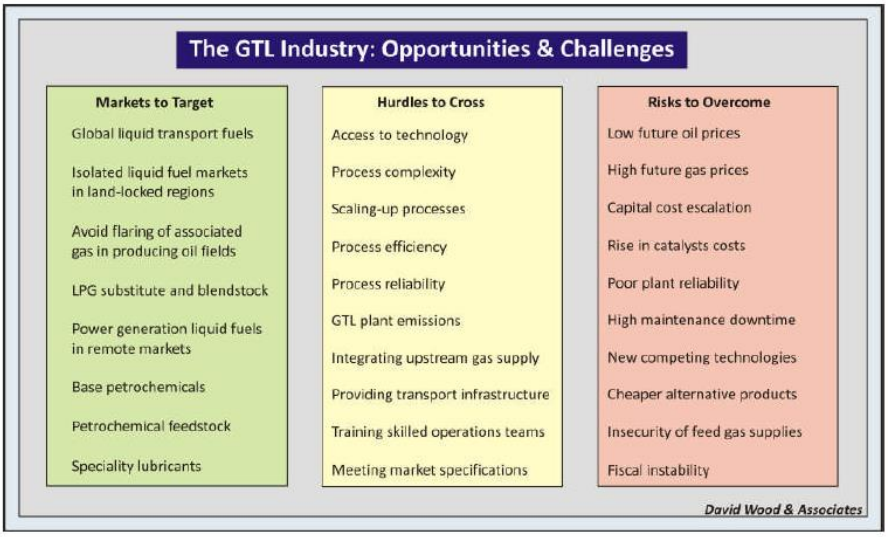

Fig. 1.16. The GTL Industry: Opportunities and Challenges

References

[1] Michael Talmadge, Mary Biddy, and Abhijit Dutta; Syngas Upgrading to Hydrocarbon Fuels Technology Pathway; *National Renewable Energy Laboratory;* Technical Report; NREL/TP-5100-58052, PNNL-22323 March 2013; http://www.osti.gov/bridge

[2] C. Pirola, C. Bianchi, A. Di Michele, P. Diodati, S. Vitali, V. Ragaini, Catal Lett 131. 294-304 (2009)

[3] M. S. Hadnadev-Kostic, J. Tatjana, T. Vulic, R. Marinkovic-Neducin, A. D. Nikolic, B. Jovic, Journal of Serbian Chemical Society. 76 (12) (2011) 1661–1671;

[4]E. Lira, C. López, F. Oropeza, M. Bartolini, J. Alvarez, M. Goldwasser, F. López, J. Lamonier, J. Pérez, Journal of Molecular Catalysis A: Chemical 281 (2008) 146–153;

[5] Qinghong Zhang, Jincan Kang, and Ye Wang, ChemCatChem 2 (2010), 1030 – 1058

[6] C. Perego, M. Ricci, Catalysis Science & Technology, (2012), 2, 1776–1786

[7] G.W.Huber, S.Iborra, A.Corma, Chemical Reviews 106 (2006) 4044

[8] P.L. Spath and D.C. Dayton, Preliminary Screening - Technical and Economic Assessment of Synthesis Gas to Fuels and Chemicals with Emphasis on the Potential for Biomass-Derived Syngas; NREL/TP-510-34929; December 2003
[9] F. Fischer and H.Tropsch, Brennst.Chem. 4 (1923) 276
[10] A. Martinez, C. Lopez, F. Marquez, I.J. Diaz, Catalysis 220 (2003) 486
[11] John L. Casci, C. Martin Lok, Mervyn D. Shannon, Catalysis Today 145 (2009) 38–44
[12] M.E.Dry in Enciclopedia of Catalysis. I.T.Horvarth Ed. J.Wiley&Sons, New York (2003) 247
[13] Fischer-Tropsch Technology in: Studies in Surface Science and Catalysis, Elsevier, New York, (2004)
[14] G.P.Vaan Deer Laan, A.A.C.M.Beenackers, Catalysis Reviews-Sci.Eng. 41(3&4) (1999) 255
[15] H.Schulz, Applied Catal. A 186 (1999) 3
[16] G.P. van der Laan, A.A.C.M.Beenackers, Applied Catal. A 193 (2000) 39
[17] R.J.O'Brien, L.Xu, S.Bao, A.Raje, B.H.Davis Applied Catalysis A: general 196 (2000) 173
[18] V. Roberto Calderone, N. Raveendran Shiju, Daniel Curulla Ferré and Gadi Rothenberg, Green Chemistry, 2011, 13, 1950–1959
[19] E. D. Smit and B. M.Weckhuysen, *Chem. Soc. Rev.*, 2008, 37, 2758– 2781.
[20] Qinghong Z, Weiping D, Ye W. Review. Recent advances in understanding the key catalyst factors for Fischer-Tropsch synthesis. J Ener Chem 2013; 22:27–38
[21] A.Y. Khodakov, W.Chu, P. Fongarland Chem. Rev. 107 (2007), 1692
[22] B.H.Davis, Catal. Today 84 (2003) 83.
[23] G.W.Huber, S.Iborra, A.Corma, Chem.Rev. 106 (2006) 4044
[24] J. Xu, C.H.Bartholomew, J. Phys. Chem. B 109 (2005) 2392.
[25] H.B. Zhang, G.L. Schrader, J.Catal. 95 (1985) 325
[26] E.S. Lox, G.B. Marin, E. de Graeve, P. Bussiere, Appl. Catal A 40 (1988) 197
[27] P.Sabatier and J.D.Senderens, C.R.Hebd.Seance, Acad.Sci. 134, 514, 680 (1902)
[28] A.Mittash, Adv.Catal. 2, (1950) 81
[29] E.Houdry, W.F.Burt, A.E.Pew, W.A.Peters, Pet. Refiner 17 (1938) 574
[30] H. Pichler, Adv.Catal. 4 (1952) 271
[31] M.E.Dry, Chemtech 12 (1982) 744
[32] R.B.Anderson, ACS Symp.Ser. 222 (1983) 389
[33] G.Natta, in "Catalysis" (P.H. Emmett, ed.), Vol.3, p.349. Van Nostrand-Reinhold, Priceton, New Jersey, 1955
[34] G.Natta, U.Colombo, I.Pasquon, in "Catalysis" (P.H. Emmet, Ed.), Vol.5, p.131. Van Nostrand-Reinhold, Princeton, New Jersey, 1957

[35] R.B.Anderson, Fuel 41 (1962) 295
[36] M.J. Baird, R.R.Schehl, W.P.Haynes and J.T.Cobb, Ind. Eng. Chem. Prod. Res. Dev. 19 (1980) 175.
[37] EIA, Annual energy outlook 2013. Available at: http://www.eia.gov/forecasts/aeo/pdf/0383(2013).pdf , accessed on 16 august 2013
[37a] U.S. Energy. Information Administration. Available at: http://www.eia.gov/countries/index.cfm?view=reserves, accesed on 16 august 2013.
[38] M.J. Prins, K.J. Ptasinski, F.J.J.G. Janssen, Fuel Process. Technol., 86 (2005) 375
[39] Klass, DL Biomass for Renewable Energy, Fuels and Chemicals; Academic Press: San Diego, CA, USA, 1998.
[40]Beenackers, A.A.C.M.; Swaaij, W.P.M. Thermochemical Processing of Biomass; Butterworth: London, UK, 1984.
[41] Demirbas, A. *Energy Educ. Sci. Technol.*, *17*, (2006) 27–63.
[42] Tijmensen, M.J.A.; Faaij, A.P.C.; Hamelinck, C.N.; van Hardeveld, M.R.M, Biomass Bioenergy, *23*, (2002) 129–152.
[43]Hamelinck, C.N.; Faaij, A.P.C.; den Uil, H.; Boerrigter, H. *Energy*, *29*, (2004) 1743–1771.
[44] J. Hu, F. Yu, Y. Lu, Catalysts, 2, (2012) 303-326
[45]. Stassen, H.E.M.; Knoef, H.A.M. Biomass Technology Group, University of Twente: Enschede, The Netherlands, 1993.
[46] Demirbas, A. Prog. Energy Combust. Sci., 33, (2007)1–18.
[47] Demirbas, A. Energy Sources A, 29, (2007) 1507–1512.
[48] Demirbas, A. Energy Sources A, 30, (2008) 924–931.
[49] M.J.Prins, K.J.Ptasinski, F.J.J.G.Janssen, Fuel Process Technol. 86 (2005) 375
[50] C.L.Iandoli, S.Kjelstrup, Energy&Fuels 21 (2007) 2317
[51] J.Jacometti, A.Ekvall, Shell in the Middle East 17 (2002) 1
[52] G.Coupe, Step on the gas, in The Engineer, 6 (2004)
[53] T. Fu, Y. Jiang, J. Lv, Z. Li, Fuel Process Technol. 110 (2013) 141–149
[54] C. Brown, The Oxford Institute for Energy Studies, May 2013, ISBN 978-1-907555-74-9. Available on: http://www.oxfordenergy.org/wpcms/wp-content/uploads/2013/05/WPM-50.pdf
[55]K. MacKenzie, Financial Times, 30 April 2013. http://ftalphaville.ft.com/2013/04/30/1473572/where-are-all-those-natural-gas-fleet-conversions/
[56] D. Wood, C. Nwaoha, B. Towler, Journal of natural gas science and engineering, 9 (2012) 196-208

[57] Agee, K, Fundamentals of gas to liquids. 2nd ed. London: Petroleum economist. 2.9 (2005) 30-31
[58] Rahmin, II, Oil and gas Journal (2005)
[59]Rahmin, II, Gas-to-liquid technologies: Recent advances, Economics, Prospects. 26th IAEE Annual International Conference, June 2003, Prague. Pp. 1-36
[60] Minnie, R, et a, 2005. Where it all began. In: Fundamentals of Gas to Liquids, second ed. Petroleum Economist, London, pp. 27e29 (Chapter 2.8).
[61] Waddacor, M., 2005. Converting gas into ultra-clean diesel in three steps. In: Fundamentals of Gas to Liquids, second ed. Petroleum Economist, London, pp. 46-49 (Chapter 4.1).
[62] De Klerk, A, 2012. Gas-to-liquids conversion. In: Natural Gas Conversion Technologies Workshop of ARPA-E. US Department of Energy, Houston, TX. 13 January 2012.
[63] Velasco, JA, Lopez, L, Velasquez, M, Boutonnet, M, Cabrera, S, Jaras, S, 2010. Gas to liquids: a technology for natural gas industrialization in Bolivia. Journal of Natural Gas Science and Engineering 2 (5), 222e228.
[64] Pytte, T, 2005. GTL diesel: the way forward. In: Fundamentals of Gas to Liquids, second ed. Petroleum Economist, London, pp. 32e35 (Chapter 3.1).
[65] Fleisch, TH, Sills, R, Briscoe, M, Freide, JF, 2003. GTL-FT in the Emerging Gas Economy. Fundamentals of Gas to Liquids, Petroleum Economist, p. 39e41.
[66] Corke, M, 2005. Securing a market. In: Fundamentals of Gas to Liquids, second ed. Petroleum Economist, London, pp. 36e38 (Chapter 3.2).
[67] Cherrillo, RA, Clark, RH, Virrels, IG, 2003. Shell Gas to Liquids in the Context of a Future Fuel Strategy e Technical Marketing Aspects. 9th Diesel Engine Emissions Reduction Workshop. Newport RI, 24e28 Aug 2003.
[68] Wood, DA, 2007. Consequences of a heavier and sourer barrel. Petroleum Review, April ed., 30e32.

Chapter 2 Chemistry of Fischer-Tropsch Synthesis

The Fischer–Tropsch (FT) reaction is a heterogeneous catalytic reaction that converts synthesis gas, that is, a mixture of carbon monoxide (CO) and hydrogen (H_2), into mainly linear hydrocarbons in the range C_1 to C_{100}. It is a surface polymerization reaction that uses monomers formed by hydrogenation of adsorbed CO in order to produce hydrocarbons and oxygenated products with a broad range of chain length and functionality.

The chemistry of the process can be described by the set of irreversible and equilibrium reactions.

According to Glasser et al [1] the Fischer–Tropsch (FT) reaction mechanism is still an issue of contention [2, 3]. Many apparently different mechanisms have been proposed, but common to them all is the concept that a stepwise chain growth process is involved. This is supported by the fact that the carbon number product distributions calculated on probabilities of chain growth match the experimentally observed results obtained in different reactor types and sizes over widely varying process conditions with different catalysts [1].

There are some important aspects related to the FTS that will be discuss in this chapter to better understand the chemistry of this process:

1) FT thermodynamics
2) FT reaction mechanism
3) FT products selectivity
4) FT kinetics
5) Influence of FT process conditions

2.1 FT Thermodynamics

The Fischer-Tropsch Synthesis is a highly exothermic reaction [4]:

$$n\,CO + (2n+1)\,H_2 \rightarrow C_nH_{2n+2} + n\,H_2O \qquad \Delta H° \cong -40\ kcal/mol \qquad (1)$$

$$n\,CO + 2n\,H_2 \rightarrow C_nH_{2n} + n\,H_2O \qquad \Delta H° \cong -35\ kcal/mol \qquad (2)$$

$$n\,CO + 2n\,H_2 \rightarrow C_nH_{2n+1}OH + (n-1)\,H_2O \qquad \Delta H° \cong -35\ kcal/mol \qquad (3)$$

Thermodynamically, the formation of methane and other hydrocarbons is energetically favourable, that means negative Gibbs energy values for reaction (1)-(3).

In figure 2.1 standard Gibbs energy variation for the production of hydrocarbons and alcohols is reported as a function of temperature.

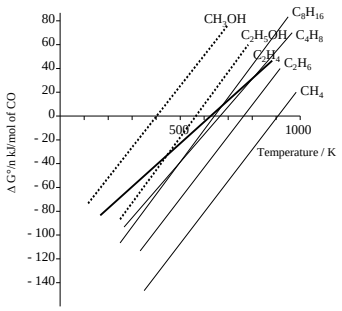

Figure 2.1. Standard Gibbs energy of some FTS products [5]

From the diagram reported in figure 2.1 it can be deduced that methane formation is highly favoured over that of the alcohols, olefins and hydrocarbons of heavier molecular weight. In Fig. 2.1 to keep all of the curves on the same scale, the enthalpy and free energy changes are divided by the number of carbons atoms in the product. Thus, the equilibrium constant for the reaction is given by $K = \exp\left[-n\left(\Delta G^0 / n\right)\right] / RT$.

On the basis of thermodynamics, a vast variety of molecules can be produced in synthesis reaction up to 400°C and for some up to 500°C, particularly at elevated pressures, including acetaldehyde and higher aldehydes, ketones, esters. Usually a broad spectrum of types of molecules, carbon numbers, and carbon-chains structures is produced, and the distribution of molecules depends on the selectivity of the catalyst employed. Generally the reaction products are not in thermodynamic equilibrium with other product molecules or reactants.

Summarizing, it is important to highlight some important aspects of the FT thermodynamics:

It is energetically possible to produce a vast array of hydrocarbons and organic molecules by the hydrogenation of CO and related process such as the $H_2 + CO_2$ and the $H_2O + 3$ CO reactions. Most of these reactions are highly exothermic;

A variety of reactions of synthesis products are thermodynamically possible, such as dehydration of alcohols, hydrogenation of olefins, hydrogenolysis of paraffins, and a number of isomerization reactions;

On an energetic basis, olefins and alcohols can be “incorporated” into synthesis reactions to produce higher molecular weight hydrocarbons in any amount. Paraffins, element carbon, or carbidic carbon can be “incorporated” into synthesis reactions to only a limited extent, that is, part of the carbon of the hydrocarbon must come from $H_2 + CO$.

2.2 FT Reaction Mechanism

According to [6] FT synthesis follows the polymerization mechanism. It is generally accepted that CO undergoes dissociative or hydrogen-assisted dissociative chemisorption on the surface of Ru, Co or Fe metal or metal

carbide nanoparticles, forming CH_x (x = 0–3) intermediates as the monomers for polymerization. The coupling between CH_x monomers leads to chain growth, providing C_nH_m intermediates. C_nH_m intermediates with different carbon numbers can then undergo hydrogenation or dehydrogenation to afford paraffins or olefins as the final products. An early work pointed out that the coupling between methylene (CH_2) groups mainly accounted for the chain growth, but recent theoretical studies suggested that the situation was more complicated [7-12]. Depending on the identity and the structure of the surface concerned, the monomeric CH_x species for polymerization may be different.

The calculation of energy barriers suggests that the couplings of (CH+CH), (C+CH), (C+CH_2) or (CH_x+HCO) may all be possible [7-12].

Since its discovery, many efforts have been made to identify the surface species that lead to chain initiation and chain growth. The FT reaction mechanism is still an issue of contention.

There are some mechanisms, like the mechanism proposed by Fischer in 1926 (‘carbide’ theory), but it has a problem, he did not explain the production of relatively large amounts of oxygenated products, i.e. alcohols.

According to [13] elementary steps of FTS can be grouped into few basic sets, including:

(1) reactant (CO and H_2) adsorption;

(2) CO activation (or chain initiation);

(3) chain propagation; and

(4) chain termination (product formation).

Fig. 2.2 shows possible CO activation steps in the carbide (also referred to as the alkyl or methylene) and the CO-insertion mechanisms. For the classical carbide mechanism, the CO activation step consists of a direct CO dissociation (i.e. the C O bond is severed before C is hydrogenated), whereas in the CO-

insertion pathway CO is first hydrogenated and only then is the C O bond broken to give the chain starter (CH_3S). Newer modification of the carbide mechanism assumes that hydrogen assists in the C O bond scission. The primary difference between the two mechanisms is the type of species being inserted into the growing chain: CH_x for the carbide (most often CH_2) and adsorbed CO for the CO-insertion mechanism. Storsæter et al. [14] compared versions of the two mechanisms– carbide (including direct and H-assisted CO dissociation) and CO-insertion – using the UBI-QEP (unity bond index – quadratic exponential potential) method [15] and micro-kinetic modeling ofC_1 and C_2 species formation. Their results showed that the chosen CO-insertion pathway had a lower activation barrier compared to both direct and H-assisted CO dissociation mechanisms that were utilized. Based on these findings, they suggested that the CO-insertion mechanism is likely the main mechanism of FTS.

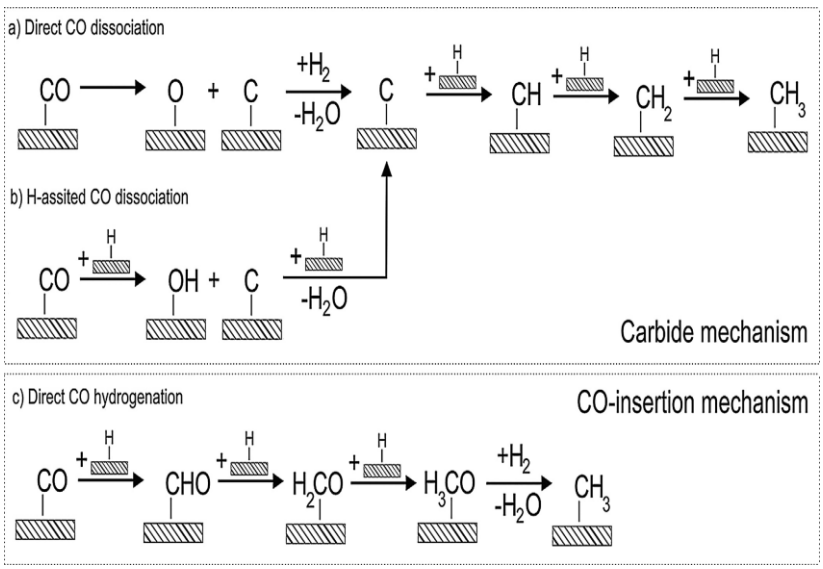

Fig. 2.2 Examples of CO activation pathways: (a) direct CO dissociation (carbide mechanism); and (b) H-assisted CO dissociation (carbide mechanism); (c) CO hydrogenation (CO-insertion mechanism) [13].

The following Figure (2.3) [16] shows another representation of the chain initiation, growth and termination deeply find in literature.

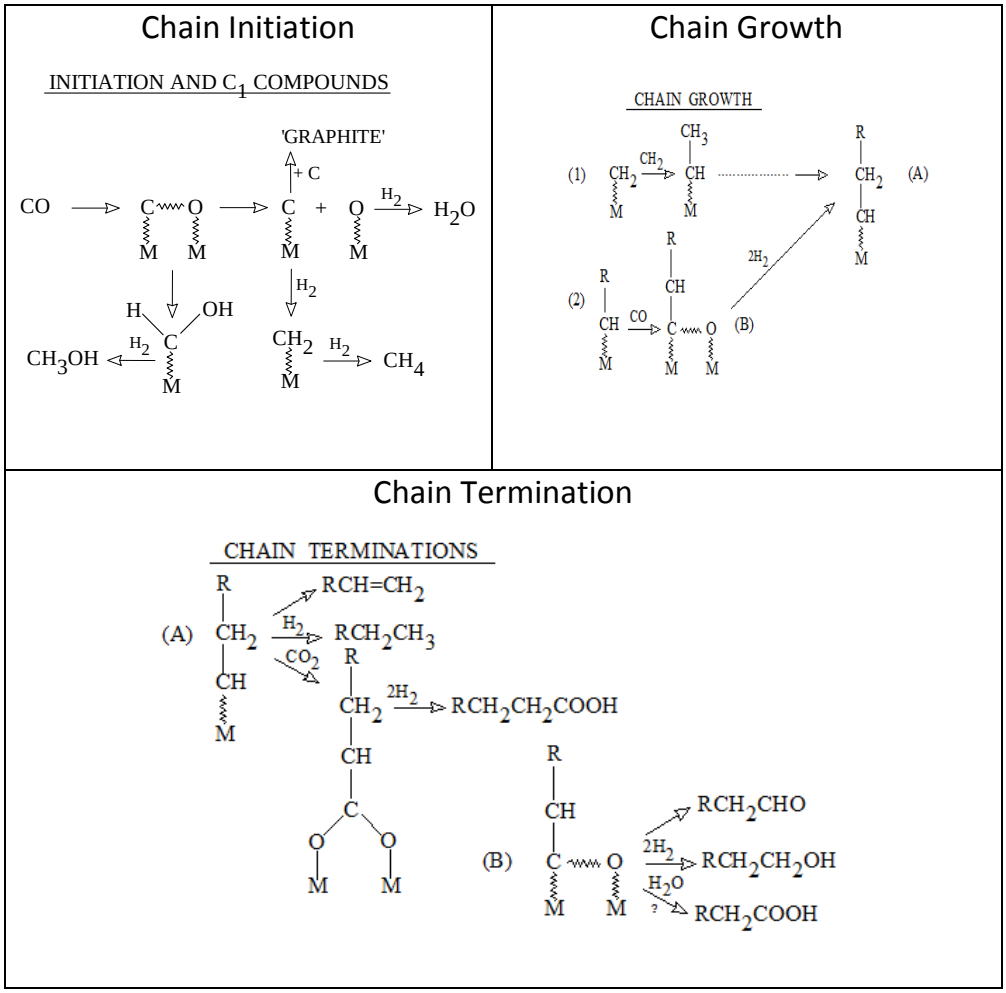

Fig. 2.3 Different steps of the reaction mechanism in FTS

Fig. 2.4 shows a simplified scheme for the formation of chain starters and incorporation into growing chains. The CH_3 groups formed as a precursor to methane are assumed to act as chain growth centres. Addition of a hydrogen atom produces methane while insertion of a CH_2 group into the metal-carbon

bond of a CH_3 group produces an ethyl group, and continuation of this type of reaction gives rise to a spectrum of adsorbed alkyl groups.

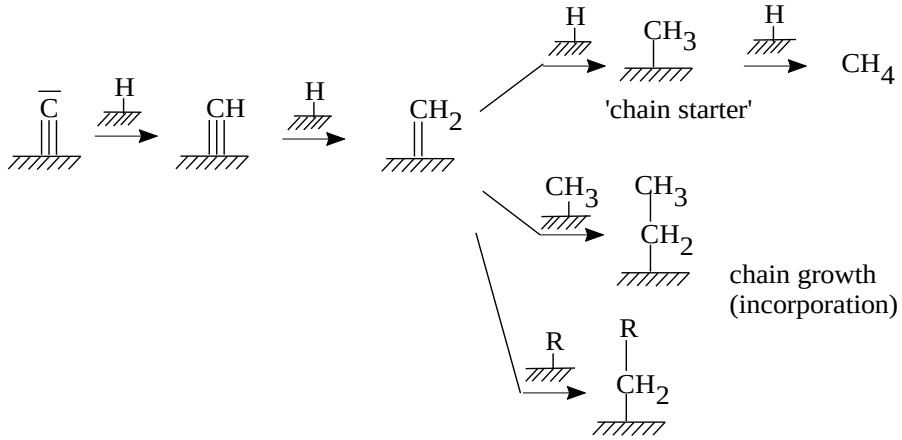

Fig 2.4. Simplified kinetic scheme of the successive hydrogenation of surface carbon yielding chain starters and incorporation into growing chains

The oxygen released by CO dissociation is removed from the catalyst as either H_2O or CO_2.

As far as hydrogenation process is concerned, there is still controversy on the reaction mechanism: first of all, it is uncertain if the monomer formation proceeds via hydrogenation of dissociated or undissociated CO. Moreover, methyne, methylene, and methyl groups are assumed to be in equilibrium by some authors, on the basis of studies with metal clusters containing these as ligands, while others postulate that the hydrogenation of surface carbon and of CH_x species is an irreversible reaction.

The nature of primary FT products reflects the nature of the surface bonded intermediates from which they originate. Primary hydrocarbon FT products are preferentially straight chain terminal olefins and straight chain paraffins. The formation of primary paraffin molecule is represented as:

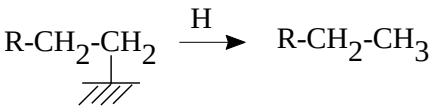

Terminally bonded (alpha) alkyl species on the catalyst surface can be considered the most common intermediates.

Olefin formation is represented as dissociative desorption from the alkyl species (β-elimination):

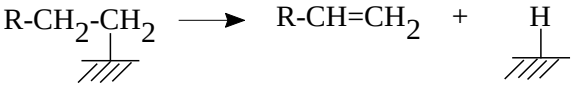

The ratio probabilities of primary desorption as a paraffin or as an olefin is commonly 0.25. That means that the reaction of desorption as a paraffin is much less probable than the reaction of desorption as an olefin. It is suggested that the chain propagation is favoured against chain termination because of the principle of 'selective inhibition', i.e. termination reaction are more inhibited than propagation reaction by steric hindrance. This effect is more pronounced with paraffin than with olefin formation. In fact, while paraffin desorption, requiring the reaction between alkyl and H, involves two metal sites, olefin desorption need an intermediate, i.e. a transition state with π and σ bonding at the same metal site.

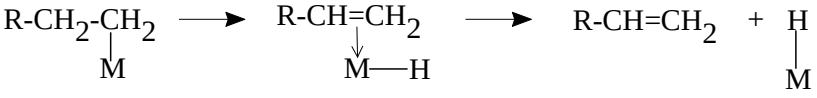

In both cases however, this might not be easily accessible under the condition of strong competitive chemisorption and strong spatial constraints.
Chain termination can also occur by CO insertion into surface alkyls, a step that leads to the formation of predominantly primary alcohols. [16]

2.3 FT Products Selectivity

The products from the FT on Co, Fe and Ru show the following characteristics [17]:

1) the carbon-number distributions for hydrocarbons gives the highest concentration for C_1 and decrease monotonically for higher carbons number, although around C_3-C_4 often a local maximum is observed
2) Monomethyl-substituted hydrocarbons are present in moderate amounts, whereas dimethyl products are present in significantly smaller amounts than monomethyl. None of these branched products contain quaternary carbons atom on Co, Fe, and Ru.
3) Olefins from iron catalysts exceed 50% of the hydrocarbon products at low carbon numbers, and more than 60% of these α-olefins. The ethane selectivity is low in comparison to propene. The olefin content decrease asymptotically to zero with increasing carbon number on Co, Ru and Fe catalysts.
4) A change in chain growth parameter in the distribution is only observed for linear paraffins and not for olefins
5) Yields of alcohols are maximal at C_2 and decrease with carbon number. Low yields of methanol are probably the result of thermodynamic limitations.

Investigations of the carbon number spectrum based on the assumption of a stepwise chain mechanism were carried out in considerable detail by several authors.

Herrington [18] described the distribution of paraffins wax using individual chain termination probabilities for each chain size and he found that the probability of chain growth in FT synthesis over a cobalt catalyst did not change much with the chain length of the hydrocarbon.

Anderson investigated the spectrum of a number of different catalysts. The plot of log W_n/n against carbon number gave straight line over a fairly large carbon number range (W_n is the mass fraction and n the carbon number). This indicated again that the probability of chain growth was fairly constant [18].

Schulz modified and applied to the FT product spectrum the Flory equation dealing with the product distribution in a polymerization process. As pointed out by Anderson, the Schulz-Flory treatment was no different from the earlier treatment, and led to the equation, henceforth referred as the Anderson-Schulz-Flory (ASF) model:

$$W_n/n = (1- \alpha)^2 \alpha^{n-1} \qquad (1)$$

where n is the number of carbon atoms in the product, W_n is the weight fraction of product containing n carbon atoms, α is the chain growth propagation probability expressed by the equation:

$$\alpha = r_p/ (r_p + r_t) \qquad (2)$$

where r_p is the propagation rate constant and r_t is the termination rate constant.

The α value is independent of carbon number; it is estimated by a least-squares linear regression of the logarithmic form of equation (3), the slope and intercept both yielding α:

$$\ln (W_n/n) = \ln (1-\alpha)^2 + (n-1) \ln \alpha \qquad (3)$$

Different factors have an influence on the alpha parameter such as process conditions, type of catalyst, and chemical promoters [19, 20] The ASF product distribution as a function of α is depicted in Figure 2.5.

The ASF equation did not distinguish between different product types. In practice, a multicomponent product mixture is formed. According to the ASF model, the maximum selectivity toward C_2–C_4 olefins is achieved with an alpha value between 0.4 and 0.5. One of the most efficient ways of shifting product selectivity to low alpha values is by increasing reaction temperature. However, a decrease on the chain growth probability results in an increase of methane selectivity as indicated by the ASF product distribution. This effect was long considered a major restriction for the industrial application of the direct conversion of syngas into lower olefins via the Fischer−Tropsch synthesis [21, 22] Negative deviations of the ASF model for methane selectivity have been observed for iron-based catalysts [23, 24]. Schwab et al. [23] proposed that Fe catalysts possess different catalytic sites, some in charge of C−C coupling for the growth of the carbon chain and others responsible for methane formation.

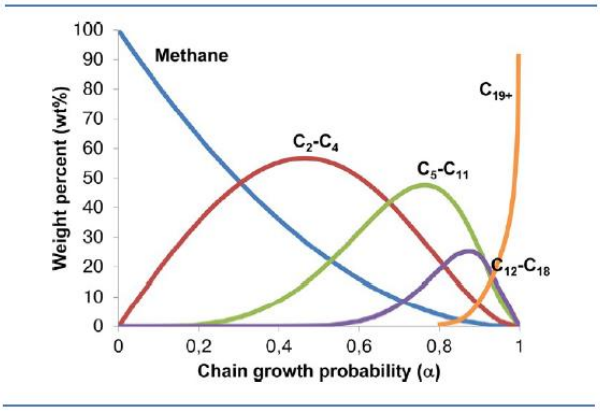

Fig. 2.5 Anderson−Schulz−Flory (ASF) model for the prediction of product distribution.

Deviations from ASF Distribution Anderson-Schulz-Flory Distribution is a well-accepted model for describing product selectivity in FT synthesis, especially for

its simplicity, nevertheless significant deviations have been noticed and reported in literature.

1) Methane selectivity is in general higher than predicted theoretically by ASF kinetics. Several mechanisms have been postulated to explain these experimental data [25-26]

2) Anomalies of Ethane and Ethene: The maximum C_2 selectivity is expected to be about 30 wt.% while in practice the maximum found is only about 18 %wt. It is commonly observed for iron as well as for cobalt and ruthenium catalysts that the C_2 selectivity is lower than the C_1 and C_3 selectivity [17].

3) Change in Chain Growth Parameter α: α is defined by ASF model as a parameter independent of the product carbon number n; nevertheless, it has been observed that at a carbon number of about 10, the slope of the semilogarithmic mole fractions of hydrocarbons against carbon number increases. This phenomenon has been described on iron, cobalt and ruthenium catalysts [27]. Suggestions for the increased chain growth parameter or two probabilities of chain growth are the occurrence of different catalytic sites [28] or the existence of different chain termination reactions [25]. Several attempts to model hydrocarbon distribution with two different values of α have been reported. However, the assumption of multiple catalytic sites cannot explain the decrease of the olefin-to-paraffin ratio with increasing chain length, decreasing space velocity, and increasing H_2/CO ratios in the reactor. Kuipers et al. [29] stated that the occurrence of secondary reactions gives the most reasonable explanation for the deviations from the ASF distribution.

2.4 FT kinetics

According to Glasser et al [1] kinetic models of FTS on cobalt, iron and ruthenium catalysts have received considerable attention [30-35] from

researchers in the past but not recently. The major problem in describing the FT reaction kinetics is the apparent complexity of the reaction mechanism and the large number of species involved. When one looks at the kinetic studies in the literature, one finds that there are a variety of rate expressions as well as a wide range of activation energies for both Co and Fe catalysts. This raises questions about which of these data, kinetic parameters and rate expressions can be relied on for estimating reaction rates and/or conducting preliminary reactor design [36.]. This strongly suggests that the complex FT reaction behavior may not be described efficiently by kinetics alone. This point is addressed at a later stage.

However, the proposed mechanism used a variety of surface species and different elementary reaction steps, resulting in empirical power-law expressions for the kinetics. However, also Langmuir-Hinshelwood-Hougen-Watson (LHHW) and Eley-Rideal type of rate equations have been applied, based on a reaction mechanism for the hydrocarbon-forming reactions. In most cases, the rate-determining step was assumed to be the formation of the monomer. These rate expressions for the consumption of synthesis gas mainly differ in the monomer's nature and in the adsorption of CO, H_2, and products (H_2O and CO_2) on the catalyst surface. Ideally, the development of kinetic rate expressions should be based on each possible rate determining process in a well-defined mechanistic scheme in the hydrocarbon forming reactions. Kinetic studies of the consumption of synthesis gas on cobalt and, in particular way, iron catalysts will be discussed in detail in this chapter. Kinetic models which describe the rate of formation of products and the water gas shift reaction will not be discussed here, their studies are reported in [17, 37].

1) Overall conversion of synthesis gas

The kinetic rate equations presented for the synthesis-gas consumption do not present a uniform picture. In general, the FT synthesis is simplified as a combination of the FT reaction and the water-gas-shift reaction:

$$CO + (1 + m/2n)\, H_2 \rightarrow 1/n\, C_nH_m + H_2O \quad (R_{FT}) \qquad (4)$$

$$CO + H_2O \leftrightarrow CO_2 + H_2 \quad (R_{WGS}) \qquad (5)$$

where n is the average carbon number and m is the average number of hydrogen atoms of the hydrocarbon products. Water is a primary product of the FT reaction, and CO_2 can be produced by the water-gas-shift reaction (WGS). Iron based catalysts show a high WGS activity unlike Co and Ru based catalysts. That is reflected by the different kinetic expressions.

Kinetic equation can be based on the overall synthesis gas consumption ($-R_{H2+CO} = -R_{CO} - R_{H2}$), which is independent of the WGS equilibrium, or based on CO consumption to hydrocarbon product ($R_{FT} = -R_{CO} - R_{WGS}$). The rate of synthesis gas consumption only differs from the FT reaction rate by reaction stoichiometry, $-R_{H2+CO} = (2 + m/2n)\, R_{FT}$. The kinetic rate equations presented for the synthesis gas consumption do not present a uniform picture. Table 2.1 [17] gives an overview. In general, catalyst composition as well as reaction conditions determine the numerical values of the intrinsic rate parameter. Moreover, the rate equations are not identical; thus, k can be decomposed of different combinations of kinetic and adsorption constant. There is experimental evidence that the FT activity of Fe and Co depends on the preparation method, metal loading of the catalyst, and catalyst support.

Table 2.1. Reaction rate equation for overall synthesis gas consumption rate, proposed in Ref. [17]

Kinetic expression type	**Kinetic expression**
(a)	kP_{H_2}
(b)	$kP_{H_2}^{a}P_{CO}^{b}$
(c)	$\frac{kP_{H_2}P_{CO}}{P_{CO}+aP_{H_2O}}$
(d)	$\frac{kP_{H_2}^{2}P_{CO}}{P_{CO}P_{H_2}+aP_{H_2O}}$
(e)	$\frac{kP_{H_2}^{2}P_{CO}}{1+aP_{CO}P_{H_2}^{2}}$
(f)	$\frac{kP_{H_2}P_{CO}}{P_{CO}+aP_{CO_2}}$
(g)	$\frac{kP_{H_2}P_{CO}}{P_{CO}+aP_{H_2O}+bP_{CO_2}}$
(h)	$\frac{kP_{CO}^{1/2}P_{H_2}^{1/2}}{\left(1+aP_{CO}^{1/2}+bP_{H_2}^{1/2}\right)^{2}}$
(i)	$\frac{kP_{CO}P_{H_2}^{1/2}}{\left(1+aP_{CO}+bP_{H_2}^{1/2}\right)^{2}}$
(h)	$\frac{kP_{CO}P_{H_2}}{\left(1+bP_{CO}\right)^{2}}$

2.5 Influence of FT process conditions

A. Temperature

The influence of temperature on the selectivity is considerable for all FT catalysts. As the operating temperature is increased, the product selectivity shifts to products with a lower carbon number on iron, ruthenium and cobalt catalysts. Increasing the temperature the CO conversion increases, but the WGS reaction increases too, mainly with iron based catalysts.

B. Partial pressure of H_2 and CO

Most studies show that the product selectivity shifts to heavier products and to more oxygenates while increasing total pressure. Increasing H_2/CO ratios in the reactor results in lighter hydrocarbons and lower olefin content. Donnelly and Satterfield [38] observed a decreased of the olefin to paraffin ratio from 6 to 1 by increasing the H_2/CO ratio from 0.3 to 4. Sufficiently high CO pressures inhibit secondary reactions i.e. olefin isomerization, hydroformilation, hydrogenation, and oligomerization.

C. Space Velocity

The influence of space velocity of the synthesis gas (residence time) on the selectivity has been investigated. The increase of the olefin to paraffin ratio with increasing space velocity (thus a decrease of the conversion) was observed. The selectivity to methane and olefins decreases with a decrease of the space velocity, whereas the selectivity toward paraffins remains unchanged. These findings can be ascribed by an enhancement of secondary reactions as the residence time and the concentration of reactive α-olefins increase within bed interstices and catalyst pellets [17].

D. Time-on-stream

It is known that catalyst deactivation may occur at reaction conditions and that may affect the activity and selectivity of a catalytic system. An increase of the

methane selectivity and low molecular weight products is observed on iron catalyst [17]. These selectivity changes can be ascribed to carbonaceous deposits formed on sites with potassium promoters. Moreover, sintering leads to a reduction of the surface area, hence lowering the catalyst activity. High water pressures enhance agglomeration of initially small crystallites.

E. Conversion

The influence of CO conversion on the reaction selectivity must be related to the decrease of CO partial pressure and the increase of water partial pressure with high levels of conversion. Low CO partial pressures (i.e. high CO conversion) imply that secondary hydrogenation reaction are less inhibited, hence olefins are hydrogenated to inactive paraffins so that olefin selectivity decreases. Moreover, secondary-cracking reactions may occur especially if high temperature is adopted to increase conversion, hence methane selectivity increases.

A schematic view of the general influence of different parameters on the selectivity is given in Table 2.2.

Table 2.2. Selectivity control in F-T synthesis by process conditions (↑ = increase with increasing parameter; ↓ = decrease with increasing parameter; * = complex relation). From [17]

Parameter	Chain Lenght	Chain branching	Olefin Selectivity	Alcohol Selectivity	Carbon deposition	Methane Selectivity
Temperature	↓	↑	*	↓	↑	↑
Pressure	↑	↓	*	↑	*	↓
H_2/CO	↓	↑	↓	↓	↓	↑
Conversion	*	*	↓	↑	*	↑
Space Velocity	↑	↓	↑	↑	↑	↑

References

[1] David Glasser, Diane Hildebrandt, Xinying Liu, Xiaojun Lu and ornelius M Masuku; Current Opinion in Chemical Engineering 2012, 1:296–302
[2] Gaube J, Klein H-F. J Mol Catal A Chem 2008, 283:60-68.
[3] Davis BH. Catal Today 2009, 141:25-33.
[4] R.B.Anderson, Academic Press (Harcourt Brace Jovanovich, Publishers (1984), Chapter 2
[5] R.B.Anderson, C.B.Lee, J.C.Machiels, Can.J.Chem.Eng 54 (1976) 590
[6] Qinghong Z, Weiping D, Ye W. J Ener Chem 2013; 22:27–38
[7] Ciobıca I M, Kramer G J, Ge O, Neurock M, van Santen R A. *J Catal*, 2002, 212(2): 136
[8] Cheng J, Gong X Q, Hu P, Lok C M, Ellis P, French S. *J Catal*, 2008, 254(2): 285
[9] Lo J M H, Ziegler T. *J Phys Chem C*, 2007, 111(35): 13149
[10] Cheng J, Hu P, Ellis P, French S, Kelly G, Lok C M. *J Phys Chem C*, 2008, 112(15): 6082
[11] Cao D B, Li Y W, Wang J G, Jiao H J. *J Mol Catal A*, 2011, 346(1-2): 55
[12] Zhao Y H, Sun K J, Ma X F, Liu J X, Sun D P, SuH Y, Li WX. *Angew Chem Int Ed*, 2011, 50(23): 5335
[13] B. Todic, Wenping M, G. Jacob, B.H. Davis, Dragomir B. Bukur, Catal. Today (2013), http://dx.doi.org/10.1016/j.cattod.2013.08.008
[14] S. Storsæter, D. Chen, A. Holmen, Surf. Sci. 600 (2006) 2051–2063.
[15] E. Shustorovich, H. Sellers, Surf. Sci. Rep. 31 (1998) 1–119.
[16] C. Pirola, PhD 2007-2008, Novel supported iron based Fischer-Tropsch catalysts: Preparation, characterization and applications.
[17] G.P.Van Der Laan, A.A.C.M. Beenackers, Catal.Rev.-Sci.Eng., 41 (3&4), (1999) 255
[18] A.P.Steynberg, M.E.Dry (Editors) Fischer Tropsch Technology, Studies in surface science and catalysis 152 (2004) p.623
[19] Hirsa M. Torres Galvis and Krijn P. de Jong. ACS Catal. 2013, 3, 2130−2149
[20] Abello, S.; Montane, D. ChemSusChem 2011, 4, 1538−1556.
[21] Wang, C.; Xu, L.; Wang, Q. J. Nat. Gas Chem. 2003, 12, 10−16.
[22] Janardanarao, M. Ind. Eng. Chem. Res. 1990, 29, 1735−1753.
[23] Schwab, E.; Weck, A.; Steiner, J.; Bay, K. Oil Gas Eur. Mag. 2010, 1, 44−47.
[24] Torres Galvis, HM; Bitter, JH; Khare, CB; Ruitenbeek, M; Dugulan, AI; De Jong, KP Science 2012, 335, 835−838.
[25] Sarup and B. W. Wojciechowski, Can. J. Chem. Eng., 66, (1988) 831.
[26] C. H. Bartholomew, W. Lee, Stud. Surf. Sci. Catal., 130 (2000) 1151.
[27] R.B.Anderson, The Fischer Tropsch Synthesis, Academic Press, inc (1984)

[28] G. A. Huff, Jr and C. N. Satterfield, Ind. Eng. Chem. Process Des. Dev., 24 (1985) 407.
[29] E. W. Kuipers, I. H. Vinkenburg, and H. Oesterbeek, J. Catal., 152 (1995) 137
[30] Dry ME: Conversion of Syngas to Fuels and Chemicals. Int Conf on Catal & Catal Proc; Cape Town, South Africa: 1993:57-66.
[31] Dry ME, Appl Catal A 1996, 138:319-344.
[32] Maitilis PM, Quyoum R, Long HC, Turner ML, Appl Catal A 1999, 186:363-374.
[33] Ribeiro FH, von Wittenau AES, Bartholemew CH, Somorjai GA. Catal Rev Sci Eng 1997, 39:49-76.
[34] Huff GA Jr, Satterfield CN. Ind Eng Chem Process Des Dev 1984, 23:696-705.
[35] Zimmerman WH, Bukur DB. Can J Chem Eng 1990, 68:292-301.
[36] Bartholomew CH, Farrauto RJ. New Jersey: Wiley; 2006.
[37] D.Pinna, E.Tronconi, L.Lietti, R.Zennaro, P.Forzatti, La Rivista dei Combustibili 56 fasc.2 (2002), 69
[38] T.J.Donnelly and C.N.Satterfield, Appl.Catal.A 52 (1989) 93

Chapter 3. Catalysts for Fischer Tropsch Synthesis

The core of any FT process is its catalyst. Only a few metals show catalytic activity in the FT synthesis [1]. As explained before, the reaction is generally assumed to start with the adsorption of CO on the catalyst surface where it reacts with adsorbed hydrogen to afford a methylene group which, in its turn, is responsible for the C–C chain growth. Probably, at least two reaction paths co-exist for the initial steps of the FT reaction: one in which carbon monoxide is adsorbed in a dissociative way (i.e., its C–O bond is cleaved before any possible reaction with hydrogen), and another in which some hydrogenation by adsorbed hydrogen atoms precedes the C–O cleavage [2]

So, a good catalyst should adsorb both CO, possibly in a dissociative way, and H_2. Furthermore, since metal oxide formation is always possible under FT conditions either by dissociative CO absorption or by metal reaction with co-produced water, the metal oxide should be easily reduced under the reaction conditions. With this respect, most early transition metals are not good FT catalysts because, despite their favorable CO adsorption, they form very stable oxides that are not reduced under FT conditions. Iridium, platinum and palladium adsorb CO in a non-dissociative manner, while metals of groups 11 and 12 hardly adsorb it: none of them is an effective FT catalyst. The specific activities (i.e., the reaction rates per unit surface area of metal) of most of the metals of the former Group VIII (all but osmium) were assessed under comparable conditions, and ruthenium proved to be the most active catalyst. As expected on the basis of the classical work by Sabatier (1902), nickel (and, even to a larger extent, palladium) showed very high selectivity towards

methane formation, obviously a feature not appreciated in a FT catalyst [2]. Osmium was successively evaluated, but turned out to be ca. 100 times less active than ruthenium. So, the best FT catalysts are based on iron, cobalt and ruthenium, with nickel, rhodium, and osmium (and, possibly, rhenium) being moderately active (Fig. 3.1) [3].

3	4	5	6	7	8	9	10	11	12
IIIb	IVb	Vb	VIb	VIIb	VIIIb			Ib	IIb
Sc	Ti	Vb	Cr	Mn	Fe	Co	Ni	Cu	Zn
Y	Zr	Nb	Mo	Tc	Ru	Rh	Pd	Ag	Cd
La	Hf	Ta	W	Re	Os	Ir	Pt	Au	Hg

Fig. 3.1 Catalytic activity of transition metals in the FT reaction. Blue denotes early transition metals able to adsorb CO in a dissociative way; they, however, show poor or no capability to adsorb H2 and their oxides are not reduced under usual FT conditions: accordingly, these metals are not active FT catalysts. Orange denotes late transition metals and a few main group elements which show poor or no CO adsorption and no FT activity. Yellow shaded elements have good H2 adsorption capability and reducible oxides; they, however, adsorb CO in a non-dissociative way and, as a matter of fact, are poor FT catalysts. Brilliant green denotes the best FT catalysts. Nickel, rhodium, osmium and possibly rhenium (pale green) are moderately active. [3]

However, FT industrial plants require huge amounts of catalyst and ruthenium is too rare and expensive to be used on this scale. As a matter of fact, cobalt and iron are the only metals of choice for industrial applications. Iron is obviously cheaper than cobalt but, to select between them, a key issue is the carbon feedstock. Iron is a good water gas shift catalyst and, for this reason, is particularly suitable for hydrogen-poor syngas, such as those obtained from coal or biomasses. Cobalt performs better with an almost stoichiometric ratio between hydrogen and carbon monoxide, so it is preferred when the carbon feedstock is natural gas. Alternatively, cobalt can also be used with hydrogen-poor syngas, provided that the H_2/CO molar is adjusted by a WGS unit between the gasification and the FT reactors [1].

Apart from methane (which usually forms in amounts higher than expected), the FT products distribution follows the Anderson–Schulz–Flory model [2]. So, the FT output is always a complex mixture of products ranging from methane to waxes formed by high molecular weight linear paraffins, as explained before. A proper choice of catalyst and reaction conditions allows tuning, to some extent, the composition of the final mixture, but it is impossible to force the process to produce selectively a well-defined range of products, i.e. middle distillates. So, the best strategy to maximize diesel production is to select conditions which allow obtaining the maximum amount of long chain linear paraffins that can be then fed to a hydrocracking stage, transforming them into a most valuable fuel.

Cobalt and iron are the metals which were proposed by Fischer and Tropsch as the first catalysts for syngas conversion. Both cobalt and iron catalysts have been used in the industry for hydrocarbon synthesis. A brief comparison of cobalt and iron catalysts [4] is reported in Table 3.1. Cobalt catalysts are more expensive, but they are more resistant to deactivation. Although the activity at low conversion of two metals is comparable, the productivity at higher conversion is more significant with cobalt catalysts. Water generated by FT synthesis slows the reaction rate on iron to a greater extent than on cobalt catalysts. At relatively low temperatures (200 - 250°C), chain growth probabilities of about 0.94 have been reported [5] for cobalt-based catalysts and about 0.95 for iron catalysts. The water-gas shift reaction is more significant on iron than on cobalt catalysts [4].

Iron catalysts usually produce more olefins. Both iron and cobalt catalysts are very sensitive to sulphur, which could readily contaminate them. For iron-based catalysts, the syngas should not contain more than 0.2 ppm of sulphur. For Co catalysts, the amount of sulphur in the feed should be much less than

0.1 ppm. Cobalt catalysts supported on oxide supports are generally more resistant to attrition than iron co precipitated counterparts; they are more suitable for use in slurry-type reactors. Iron catalysts produce hydrocarbons and oxygenated compounds under different pressures, H_2/CO ratios, and temperatures (up to 340°C). Cobalt catalysts operate at a very narrow range of temperatures and pressures; an increase in temperature leads to a spectacular increase in methane selectivity. Iron catalysts seem to be more appropriate for conversion of biomass-derived syngas to hydrocarbons than cobalt systems because they can operate at lower H_2/CO ratios [4].

Table 3.1. Comparison of Cobalt and Iron FT catalysts [4]

Parameter	Cobalt catalyst	Iron Catalyst
Cost	More expensive	Less expensive
Lifetime	Resistant to deactivation	Less resistant to deactivation (coking, carbon deposit, iron carbide)
Activity at low conversion	comparable	
Productivity at high conversion	Higher; less significant effect of water on the rate of CO conversion	Lower; strong negative effect of water on the rate of CO conversion
Maximal chain growth probability	0.94	0.95
Water gas shift reaction	Not very significant; more noticeable at high conversion	Significant
Maximal sulphur content	< 0.1 ppm	< 0.2 ppm
Flexibility (temperature and pressure)	Less flexible; significant influence of temperature and pressure on hydrocarbon selectivity	Flexible; CH_4 selectivity is relatively low even at 340°C
H_2/CO ratio	2	0.5-2.5
Attrition resistance	Good (always supported)	Not very resistant if not supported

A large number of studies have pointed out that various factors can influence the catalytic behaviors of a FT catalyst. As summarized in Table 3.2, besides the engineering factors such as reactor design and operation conditions [6-10], there exist many catalyst factors, which can exert significant influences on the activity and product selectivity.

Table 3.2. Typical key factors influencing the activity and product selectivity of a FT catalyst [11]

Engineering factors	Catalyst factors
(i) Reactor design (ii) Operation conditions	(i) identity of active metal (Ru, Co or Fe) (ii) chemical state of active phase (metal, oxide or carbide) (iii) support (identity, pore structure, physicochemical properties) (iv) promoter (typically including noble metals, oxides of Mn, Zr or rare earth metals, alkali metal ions) (v) size of active phase (vi) microenvironment of active phase

3.1 Iron and Cobalt industrial FT catalysts

i) Iron catalysts: With iron catalysts two directions of selectivity have been pursued. One direction has aimed at a low molecular weight olefinic hydrocarbon mixture to be produced in an entrained phase or fluid bed process (Sasol Synthol process). Due to the relatively high reaction temperature (340°C), the average molecular weight of the product is so low that no liquid product phase occurs under reaction conditions. The catalyst particles moving around in the reactor are small (d_p =100 mm) [12] and carbon deposition on the catalyst does not disturb reactor operation. Thus low catalyst porosity with

small pore diameters as obtained from fused magnetite (plus promoters) after reduction with hydrogen is appropriate. For maximising the overall gasoline yield the olefins C_3, C_4 have been oligomerised at Sasol. However, recovering the olefins for use as chemicals in e.g. polymerisation processes is advantageous today [13].

The second direction of iron catalyst development has aimed at highest catalyst activity to be used at low reaction temperature where most of the hydrocarbon product is in the liquid phase under reaction conditions. Typically, such catalysts are obtained through precipitation from nitrate solutions. A high content of a carrier provides mechanical strength and wide pores for easy mass transfer of the reactants in the liquid product filling the pores. The main product fraction then is a paraffin wax, which is refined to marketable wax materials at Sasol, however, also can be very selectively hydrocracked to a high quality Diesel fuel. Thus iron catalysts are very flexible. Selective FT synthesis of linear terminal olefins seems only possible with iron catalysts. Alkalised iron FT catalysts exhibit water gas shift activity (in contrast to cobalt catalysts). This is a favourable feature for FT synthesis with CO-rich syngas as obtained from high temperature coal- or heavy-oil-gasification through partial oxidation (H_2/CO molar ratio =1.0), however, it is undesirable for FT synthesis with hydrogen-rich syngas as produced from natural gas. The activity of iron catalysts decreases through product inhibition by water [14]. This feature restricts the attainable degree of conversion and leads to gas recycle operation after water removal together with the organic condensate.

ii) Cobalt catalysts: Cobalt catalysts have been applied in the first FT plant of Ruhrchemie in 1935. Present catalyst design makes use of several preparation techniques, however the intention to produce a well-dispersed cobalt phase in a wide pore support remains the same. Today cobalt catalysts for FT Diesel

production from natural gas are designed for a maximum wax selectivity, the waxy product then being the feed for hydrocracking. Hydrocracking of FT paraffins follows the kinetic regime of 'ideal hydrocracking' as observed by Schulz and Weitkamp [15]: always the largest molecules are cracked selectively and no secondary cracking occurs. With cobalt catalysts olefin readsorption on FT sites takes place and this contributes significantly to the desired high wax selectivity. This implies that olefin secondary hydrogenation and double bond shift should be kept low. Diesel fuel selectivity approaching 80% can be obtained by the process combination FT synthesis/hydrocracking [15].

3.2 Chemical State of active phase

As explained before, the typical active metals used for FT synthesis are Fe, Co and Ru. According to [11] the current consensus is that metallic Co and Ru, i.e., Co^0 and Ru^0 nanoparticles, function as the active phases for CO hydrogenation to heavier hydrocarbons, whereas iron carbides are responsible for CO hydrogenation [16]. However, deeper knowledge about the effects of different chemical states of these active phases on catalytic performances is still needed for the rational design of an efficient FT catalyst.

2.1. Co-based catalysts

Metallic Co may exist in two different crystalline forms, .i.e., fcc and hcp phases. For bulk Co, the hcp phase is more stable at lower temperatures, but the fcc phase becomes more stable when the size of Co particles becomes less than 20 nm [17]. However, the actual crystalline structure of Co catalyst under working conditions is not well known. The formation of Co_2C may cause the catalyst deactivation. Another recent work also demonstrated that the deactivation of Co-based catalyst was due to the carbide formation and carbon deposition [18]. The prolonging of the time on stream caused the partial

decomposition of the bulk Co_2C to Co0 and increased the conversion of CO and the selectivity to heavier hydrocarbons.

2.2. Fe-based catalysts

Iron carbides are easily formed under FT reaction conditions because of the lower or similar activation energy for iron carbide formation as compared with that of CO hydrogenation. Many types of iron carbides such as ε-Fe_2C, ε_ -$Fe_{2.2}C$, Fe_7C_3, χ-Fe5C2 and θ-Fe_3C all have been observed in FT synthesis [19-20]. However, the true active species under working conditions remains still unsettled. Many studies have been devoted to characterizing the active iron carbide phase. Because the carburized iron catalysts are very sensitive to air exposures even under controlled passivation [21], the in situ or operando characterizations under working conditions are quite important.

3.3 Size of active phase

According to [11], the size of the active phase is one of the most important factors determining the catalytic behaviors of a heterogeneous catalyst [23]. For Co-based catalysts, Iglesia once analyzed data obtained over different metal oxide-supported Co catalysts, and the results suggested that the turnover frequency (TOF) for CO conversion, i.e., the amount of CO converted per surface Co per time, was independent of the size of Co particles loaded on different metal oxides in a Co-size range of 9−200 nm [24]. The selectivity to CH4 was higher over the catalysts with smaller Co particles, and decreased with increasing Co size particularly in the range of 2.6−8 nm. C5+ selectivity increased with the mean size of Co nanoparticles monotonically, and the increase became insignificant when Co size exceeded 6−8 nm. Thus, Co-catalyzed FT synthesis is a structure sensitive reaction in the Co-size range of <10 nm. Size effect studies for Ru- and Fe-based catalysts are not numerous. A

few early studies pointed out the increase in TOF for CO hydrogenation with increasing the size of Ru or Fe particles (or decreasing the metal dispersion) [25-27].

In general, the results obtained for many Co- and Ru-based catalysts all indicate that the TOF for CO conversion increases with the size of metal nanoparticles up to a critical point (6−10 nm) and then changes slightly. For Fe-based catalysts, the results are still inconsistent.

References

[1] C. Perego, M.Ricci. Catalysis Science & Technology, 2012, 2, 1776–1786
[2] P. M. Maitlis, V. Zanotti, Chem. Commun., 2009, 1619–1634.
[3] C. Perego, R. Bortolo and R. Zennaro, Catal. Today, 2009, 142, 9–16.
[4] A.Y. Khodakov, W. Chu, P. Fongarland, Chem.Rev. 107 (2007) 1692
[5] B. Jager, Stud. Surf. Sci. Catal. 119 (1998) 25
[6] Luque R, de la Osa A R, Campelo J M, Romero A A, Valverde J L, Sanchez P. *Energy Environ Sci*, 2012, 5(1): 5186
[7] Hao X, Dong G Q, Yang Y, Xu Y Y, Li YW. *Chem Eng Technol*, 2007, 30(9): 1157
[8] van Steen E, Claeys M. *Chem Eng Technol*, 2008, 31(5): 655
[9] Davis B H. *Ind Eng Chem Res*, 2007, 46(26): 8938
[10] Gao J H, Wu B S, Zhou L P, Yang Y, Hao X, Xu Y Y, Li Y W. *Chin J Catal (Cuihua Xuebao)*, 2011, 32(12): 1790
[11] Qinghong Z, Weiping D, Ye W. Review. J Ener Chem 2013; 22:27–38
[12] O.G.Malan, J.D.Louw, L.C.Ferreira, Brennstoff-Chem. 42 (1961) 209
[13] A.P. Steynberg, R.L. Espinoza, B. Jager, A.C. Vosloo, Appl.Catal.A 186 (1999) 41
[14] M.E. Dry, J.R. Anderson, M. Boudart (Eds.), Catalysis Science and Technology M., Springer, Berlin (1981) 159.
[15] H.Schulz, Appl. Catal. A 186 (1999) 3
[16] Zhang Q H, Kang J C, Wang Y. *ChemCatChem*, 2010, 2(9):1030
[17] Kitakami O, Sato H, Shimada Y, Sato F, Tanaka M. *Phys Rev B*, 1997, 56(21): 13849
[18] Tan K F, Xu J, Chang J, Borgna A, Saeys M. *J Catal*, 2010, 274(2): 121
[19] De Smit E, Weckhuysen B M. *Chem Soc Rev*, 2008, 37(12): 2758

[20] Zhang Q H, Kang J C, Wang Y. *ChemCatChem*, 2010, 2(9): 1030
[21] Janbroers S, Louwen J N, Zandbergen H W, Kooyman P J. *J Catal*, 2009, 268(2): 235
[22] P.J. Van Berge, J. Van de Loosdrecht, J.Caricato, E.A. Barradas, Patent WO 99/42214
[23] Zhang Q H, Deng W P, Wang Y. *Chem Commun*, 2011, 47(33): 9275
[24] Iglesia E. *Appl Catal A*, 1997, 161(1-2): 59
[25] Kellner C S, Bell A T. *J Catal*, 1982, 75(2): 251
[26] Jones V K, Neubauer L R, Bartholomew C H. *J Phys Chem*, 1986, 90(20): 4832
[27] Boudart M, McDonald M A. *J Phys Chem*, 1984, 88(11): 2185

Chapter 4. Experimental: FT plant and analytical methods

Two different FTS units, were used in this PhD's research work in order to homologate some results. The first one, is located at the *Università degli Studi di Milano* in Italy, while the second one, is located at the *Universidad Central de Venezuela* in Venezuela. Following there is the description of both FTS unit.

First FTS Unit (Unit 1). *Università degli Studi di Milano* in Italy:

FT reaction tests were performed into a fixed bed reactor (d_i =0.6 cm, l = 56 cm), using 1 g of fresh catalyst mixed with 1 g of diluting material (α-Al_2O_3, Fluka). This diluting material must be inert for FT and a good thermal conductor to control the process temperature [1]. The catalysts were tested, after their activation, in a 46.8 NmL min^{-1} flow of syngas with H_2/CO ratios of 2/1 (total flow = 46.8 Nml min^{-1}) and nitrogen as internal analytical standard (flow = 5.0 NmL min^{-1}) at P = 20 bar and temperature range between 220-260°C, for a duration between 20 and 90 h in continuous. Analyses of the gas-phase products (C_1-C_7) were performed with an on-line micro-gaschromatograph (Agilent); measurements were carried out every 60 min, during the reaction. Liquid products were collected in a trap (V=400mL), operating at 5°C and at the same pressure of the reactor (20 bar), and analyzed by a gas chromatograph (Agilent) equipped with a Porapack-Q columns (able to separate C_7-C_{30} hydrocarbon fraction) after the reaction duration. The aqueous phases collected in the cold trap were analyzed by a TOC (Schimadzu) for the quantification of carbonaceous species dissolved in water. Using all the data

collected, for each run a mass molar balance has been verified, with a maximum error of ± 5%$_{moles}$.

Second FTS Unit (Unit 2). *Universidad Central de Venezuela* in Caracas-Venezuela):

FTS was performed in a continuous flow system with a fixed bed stainless-steel reactor (d_i =0.95 cm, l = 30 cm). The reactor was loaded with 0.3 g of fresh catalyst mixed with 0.3 g of see sand as a diluting material [2]. The calcined catalysts were initially reduced in situ by flowing hydrogen for 4 hours at 90.0 $Nml \cdot min^{-1}$, 350°C and 0.8 MPa. After the reduction step, the temperature was lowered to 220°C under H_2. They were then tested in the standard conditions by flowing syngas (H_2: CO: N2, 63:32:5, v/v, N_2 as internal standard) at 15.6 $Nml \cdot min^{-1}$, increasing the system pressure slowly up to 2.0 MPa and 220-260°C. Once the reaction temperature was achieved, the reaction was led to proceed during a period of 280 h.

During reaction, the reactor effluent passed through a hot trap kept at 150°C and 0.2 MPa to collect waxes, and the products leaving this trap were passed through a second trap kept at 0°C and 0.2MPa to collect the lighter products (water, alcohols and hydrocarbons). The analyses were performed in various chromatographs according to the nature of the sample to be analyzed. Permanent gases and light hydrocarbons were analyzed on-line in a PerkinElmer 3000GC Autosystem fitted with TCD detectors using a Carbosieve SII Supelco column .The liquid products (collected at 150ºC and 0ºC) were weighted and analyzed in a PerkinElmer chromatograph fitted with a 50m long Alumina RT capillary column connected to a FID.

A mass molar balance was performed for each FT run, resulting in a maximum error of ± 5%$_{moles}$

4.1 FT Laboratory plant

a) First FTS unit (Unit 1):

As explained by Pirola [3-5] the experimental tests were performed in a laboratory plant with a tubular reactor (made by "Renato Brignole" Company) with a fixed bed of catalyst vertically placed. The feed (CO, H_2 and N_2 as internal standard) is prepared in situ mixing three different flow of pure CO, pure H_2 and pure N_2 using three different flow meters. Then the feed goes into the catalytic reactor from the top part, reacts with the catalyst and then the reacted flow comes out from the lower part. The plant pipes are heated till the cold trap to avoid the heavy products condensation. In this cold trap, cooled at 5°C, the heavy products and the water condense. The not reacted gas and the light hydrocarbons go in a flow meter for their quantification and finally in an analytical zone where they are analyzed by a micro gaschromatograph. In the condensed liquid in the cold trap there are two phases: the first one is an aqueous phase (in which water and small quantities of light hydrocarbons and oxygenated compounds are present) and the second one is an organic phase (in which hydrocarbons in the range C_7-C_{30} are present).

In Fig. 4.1 the detailed flow-sheet of FT plant has been reported.

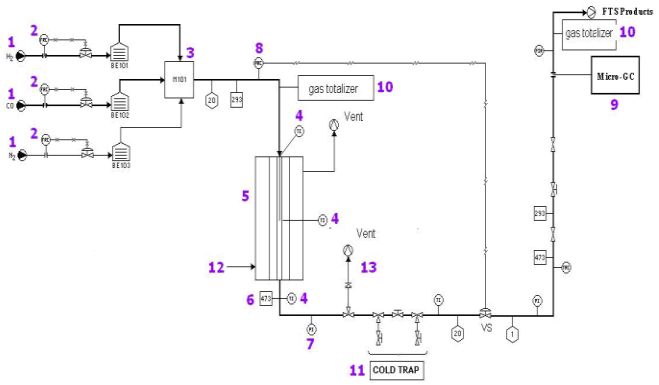

Fig. 4.1. Laboratory plant flow-sheet

The key for the Fig.4.1 is the following:

1: valve

2: flow meter (Brooks ® mod. 5850TR); for H_2 and CO operating in the range 0-100 Nml min^{-1}, for N_2 operating in the range 0-20 Nml min^{-1}

3: gas mixer

4: thermocouples for the control of temperature in the catalytic bed, in the reactor and in the heated pipe

5: Tubular reactor

6: Security valve

7: Pressure indicator

8: Pressure control and regulation tool

9: micro GC "Agilent ® 3000 series"

10: gas totalizer for the control of the total flow of gas

11: Cold trap operating at 5°C and 20 bar

12: Cooling air for the temperature control of the reactor

13: vent (usually closed)

In figure 4.2 a photo of the plant is reported.

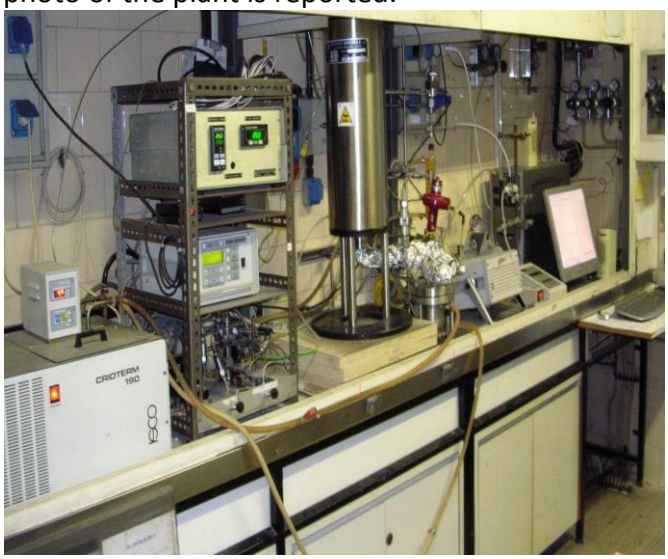

Fig. 4.2. FT laboratory plant

In the following paragraphs the main parts of this plant will be described.

4.1a Main parts of the plant

4.1a.1 Apparatus for the regulation and control of temperature, pressure and flow of reagents

In the plant the pressure is controlled and regulated by an electronic controller (Brooks®) that interacts with a pressure valve able to work till 25 bars (Fig 4.3), located after the reactor and the cold trap.

Fig. 4.3. Pressure valve

This system can control the plant pressure with a care of 0.1 bar respect the set up.

The reactor temperature is regulated by a heating oven (Renato Brignole) and the pipe lines after the reactor are heated at 220°C to prevent the heavy products condensation by two electrical cables (both with a resistance of 7 Ω/m) controlled by a Ascon ® apparatus. The CO, H_2 and N_2 flows are regulated by Brooks® 5850TR series flow meters (Fig. 4.4).

4.4. Flowmeters for CO, H_2, N_2

In table 4.1 the main characteristics of these flow meters are reported

Table 4.1. Flowmeters characteristics

	Range (Nml/min)	I/O signal (vdc)	Max Pressure (Bar)
H_2	0-50	0-5	100
CO	0-50	0-5	100
N_2	0-20	0-5	100

4.1a.2: FT reactor

The FT plant reactor (Fig. 4.5) has been made by Renato Brignole ® Company (Legnano, Italy). It is a fixed bed tubular reactor with the catalyst vertically located. It is made of AISI 316 stainless steel and in the internal surface of reactor there is a coaxial copper tube (thickness = 1 mm) to prevent some catalytic activities of steel and to uniform the heating of reactor. The technical characteristics of reactor are summarized in Table 4.2.

Table 4.2. Reactor Characteristics

Volume (cm^3)	Max operating pressure (Bar)	Max. operating temperature (°C)	Internal diameter (mm)	Height (mm)
15.8	100	400	6	560

In this reactor it is possible to charge till 3 g of the mixture catalyst-diluting material. The feed goes into the reactor at the top and goes out from the lower part. The operation of opening and closing of reactor is made using the disks illustrated in Fig. 4.6 and this is an operation that needs a particular attention, to avoid gases losses or mechanical damage.

Fig. 4.5. FT tubular reactor

Fig. 4.6. Reactor opening disks

The temperature inside the reactor is monitored by two thermocouples: the first one is vertical and it is inside the catalyst, the second one is horizontal and it is inside the reactor. The values of temperatures recorded are quite the same (max. difference = 2°C).

4.1a.3 Cold Trap

The condensation of heavy FT products (mainly hydrocarbons higher than C_7 and water) is made using a cold trap in stainless steel able to work at 20 bar and a T=5°C (Fig. 4.7). The low temperature is maintained by an external circulation of water coming from a "Crioterm ® 190 isco" thermocriostat. The

volume, height and width of the cold trap are, respectively, 125 ml, 100 mm and 40 mm.

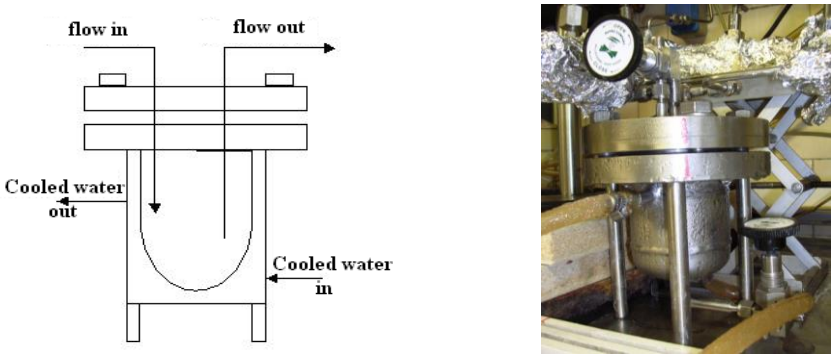

Fig. 4.7. Cold trap

The cold trap, at the end of each kinetic run, is opened and the liquid condensed inside is quantified and analyzed. There are two phases: the first one is an organic phase made by hydrocarbons in the range C_7-C_{30} and it is analyzed by a GC, the second one is an aqueous phases with some organic, mainly oxygenated, compounds and the quantification of all the present carbon is made by a TOC analysis. The results obtained in this way give an average value of all the time of kinetics. It is not possible to open the cold trap during the experiment. In fact, opening the cold trap the pressure and flow equilibrium of the plant is broken.

4.1a.4 Flow totalizers

The calculation of CO conversion and products selectivity of the plant needs to know exactly the quantity of gas incoming and out coming. Moreover, adding those data to the quantity of liquid condensed in the cold trap and to analytical data it is possible to verify the mass balance on the plant. The calculation of the mass balance is very important to verify the goodness of the experimental data collected.

In FT plant it is possible to quantify all flow passed in a fixed time. The incoming flow of H_2, N_2 and CO is totalized by the same flow meters that regulate the flow (Brooks ® Instruments) and the out coming flow (mixture of not reacted CO and H_2, N_2 and non-condensed FT products) is totalized by a Ritter ® mod. TG01-5 (Fig. 4.8) instrument.

Fig. 4.8. Ritter ® totalizer

4.2a Analytical instruments

FT plant needs three different analysis for the quantification of the composition of:

i) out coming gas (mixture of not reacted CO and H_2, N_2 and non-condensed FT products) by a micro-GC Agilent ® mod. 3000A,
ii) organic phase of condensed liquid in cold trap (hydrocarbons in the range C_7-C_{30}) by a GC "Fison Carlo Erba ® Mod. 8000 series" and
iii) liquid phase of condensed liquid in the cold trap (water with hydrocarbon, mainly oxygenated, dissolved inside) by a Total Organic Carbon "Shimadzu ® mod. 5000A".

4.2a.1 micro Gas Chromatograph "Agilent ® mod. 3000A"

In the micro GC Agilent ® there are two different columns: the first one is a molsieves module, by which it is possible to separate, in order of retention time, He, H_2, Ne, Ar, O_2, N_2, CH_4 and CO; the second one is a OV-1 module (filled with polydymethylsiloxilane) by which it is possible to separate CO_2 and

all the hydrocarbons in the range C_2-C_7. In this instrument the gas sample is splitted in the two modules and then analyzed in the same time. For each sample then we obtain two different analyses. In our application, using the first module the CO, N_2 and CH_4 were quantified with a column temperature of 45°C, using the second module CO_2 and hydrocarbons were quantified with a column temperature of 100°C. Each module is equipped with a TCD detector. The sensibility limit of the analyses is about 50 ppm for each compound and the carrier gas is helium. The instrument scheme is reported in Fig. 5.9 and the instrument is represented in Fig. 4.10. An example of analyses is reported in Fig. 4.11.

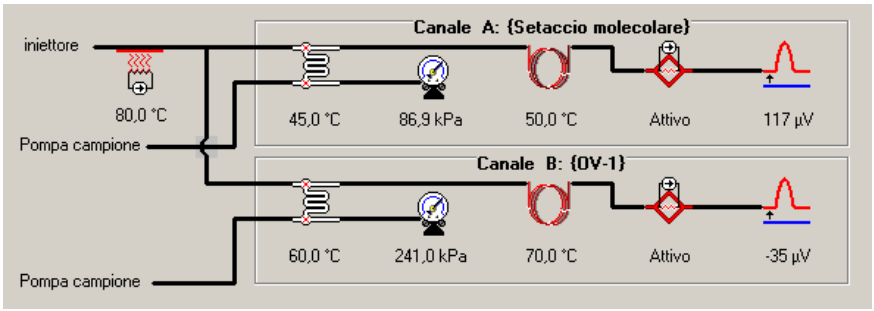

Fig. 4.9. Agilent Micro GC scheme

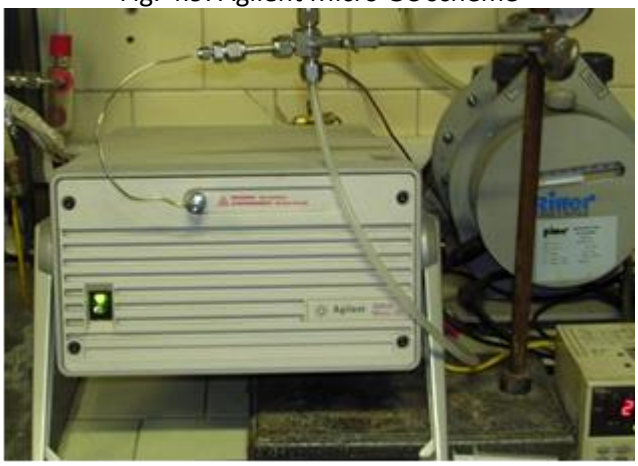

Fig. 4.10. Micro GC Agilent

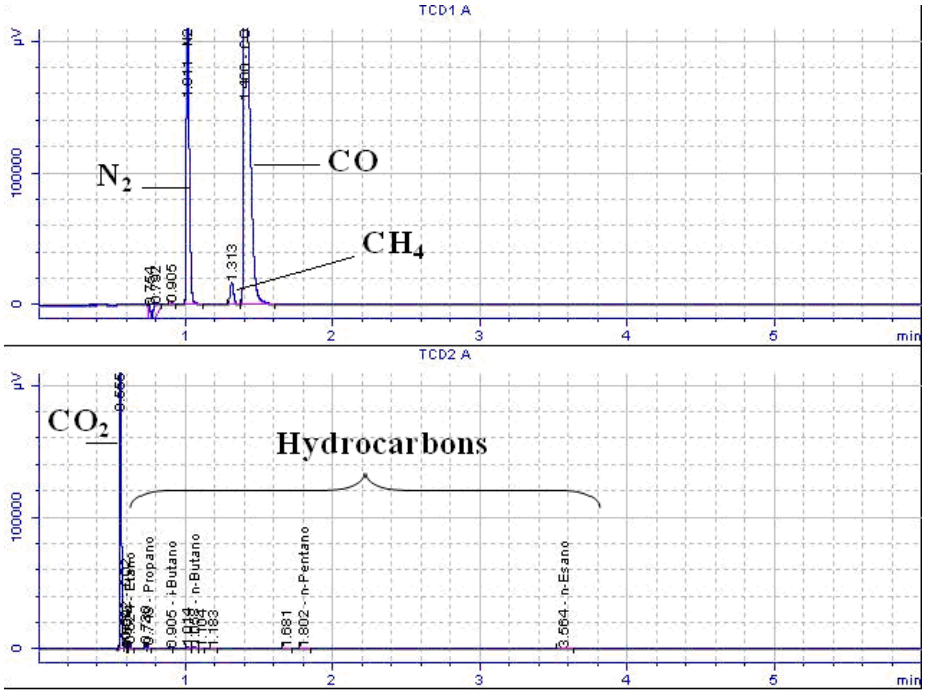

Fig. 4.11. Example of Agilent micro GC analyses on FT out coming gas

4.2a.2 Gas Chromatograph "Fision Carlo Erba ® Mod. 8000 series"

In this traditional Gas Chromatograph (GC), equipped with a wide bore Varian (model VF-1ms) (dymethylpolyxolane) column (length = 25 m, diameter = 0.25 mm) it is possible to separate and quantify the hydrocarbons in the range C_7-C_{30}. The GC detector is a FID, with a sensibility limit of about 100 ppm for each compound, and the carrier is helium. The column temperature is maintained at 60°C for 3 minutes, then heated till 260°C at 7°C/min for 15 minutes, after that heated at 280°C for 40 minutes at 5°C/min and then heated till 310°C for 5 minutes. In Fig. 4.12 and 4.13 the gas chromatograph in its column.

Fig. 4.12. Example of GC analysis for the quantification of heavy FT products

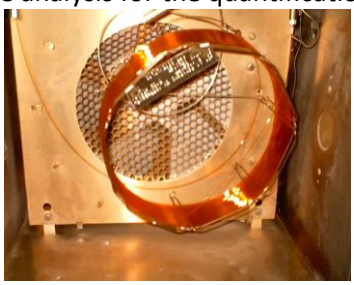

Fig 4.13: Wide bore Varian VF-1ms column

4.2a.3 Total Organic Carbon "Shimadzu ® mod. 5000A"

Using this instrument it is possible to quantify the organic carbon dissolved in water. The sample passes through an oxidation catalyst (Pt) at high temperature (700°C) and then all the organic carbon is converted to CO_2. This CO_2 is then exactly quantified by an IR detector. In Fig. 4.14 it can be seen the instrument

Fig. 4.14. SHIMADZU TOC-5000A

4.3a Analytical instruments calibration

4.3a.1. Flow meters calibration

All flow meters have been calibrated comparing the flow measured by these instruments and that measured using a "soap-bubble" flow meter at the end of the plant. This calibration has been made using the FT plant both in FT work condition (T=250°C, P=20 bar) and at room condition (T=20°C, P=1 bar). For each flow meter some tests at different flow have been made, always in the range between 0 and 40 Nml/min. For each flow meter a diagram has been made where the real flow (y) is reported in function of the set-up flow (x). The result for all the instruments is a straight line (y = ax + b). In Tab. 4.3 the results for all the instruments have been reported in term of "a" and "b" coefficient and "R^2" value.

Tab. 4.3. Flow meters calibrations

Flow meter	Calibration conditions	a	b	R^2
1: CO	T = 20°C; P = 1 bar	1.1364	1.2727	0.9996
2: H_2	T = 20°C; P = 1 bar	1.008	-1.749	0.999
3: N_2	T = 20°C; P = 1 bar	1.2744	6.7994	0.9935
4: Mix CO: H_2: N_2	T = 20°C; P = 1 bar	0.968	1.816	0.9998

The conclusion is that the instruments give a very good calibration and their indications of the flow are quite perfect.

4.3a.2. micro GC calibration

This calibration has been made in Cernusco sul Naviglio (MI) in the laboratory of "SRA Instruments Italia" Company. This company is an Agilent Technologies Premier Solution Partner, directly present in Italy and France, and it is constantly engaged in research and development of solutions based on portable and ultra-fast Micro Gas chromatograph (www.srainstruments.com).

The calibration has been made analyzing two mixture of certified gas and is reported by [5]

The calibration of CO_2 and light hydrocarbon is a direct calibration. As the volume of gas injected in column is always the same, it is possible to calibrate directly (without an internal standard) the peaks area with the concentration of different compounds, i.e. the concentration is directly proportional to chromatographic area. In "SRA Instruments Italia" all calibration factors fc_i (chromatographic area / compound concentration) and all retention times have been found, and they are reported in table 4.4

Table 4.4. Calibration results for CO_2 and light hydrocarbons

Module	Compound	Retention time (min)	Calibration factor
Molsieves	N_2	1.007	35119
	CH_4	1.203	27027
	CO	1.402	45799*
OV-1	CO_2	0.592	16722
	Ethane	0.624	19230
	Propane	0.745	25706
	I-butane	0.918	28248
	N-butane	1.061	27027
	I-pentane	1.556	32051
	N-pentane	1.808	32326
	N-hexane	3.578	33670

*CO quantification has been performed using another calibration

Using these data it is possible to calculate the concentration of each compound using the formula:

$$\%_v compound_i = area_i \cdot fc_i \quad (1)$$

Nevertheless, it is important to remember that in FT plant there is N_2 as internal standard for CO quantification, and then the equation (1) must be corrected, because the N_2 flow is not to be considered as FT gas:

$$\%_v compound_i = area_i \cdot fc_i \cdot \frac{flow_{total}}{flow_{FT}} \quad (2)$$

Where

$$flow_{FT} = flow_{total} - flow_{N_2} \quad (3)$$

To better understand this calculation, an example is here reported:

If we assume to have a real FT flow of 20 Nml/min with a CO_2 %v = 2%, it means to have 0.4 Nml/min CO_2.

If we have 10 Nml min/min of N_2 as standard and 30 Nml/min of FT flow and we calculate the CO_2 percentage using the total flow we obtain

$\frac{0.4}{30} \cdot 100 = 1.33\% vCO_2$, making a mistake. If we use the correction in the equation (2), we obtain $\left(\frac{0.4}{30} \cdot 100 \right) \cdot \frac{30}{20} = 2.0\% vCO_2$, the true value.

The CO calibration concerns only the CO and N_2 flow. The CO is the compound to be quantified and the N_2 is the standard gas, in fact N_2 is not involved in FT reactions and it pass through the FT plant without any modification, then the incoming and out coming N_2 is the same. The necessity with CO to have a calibration with a standard is explained considering that the CO quantification gives the CO conversion of FT process, then a more accurate measure is convenient. Moreover it is not possible to use N_2 as internal standard also for CO_2 and light hydrocarbons because they are not analyzed in the same module (OV-1) of N_2 (molsieves). Another important consideration is that in literature the CO conversion for FT reactor is always calculated using this method.

In this calibration method the ratio (flow CO / flow N_2) is directly proportional to ratio (area CO / area N_2). Using FT plant in reaction conditions (T=250°C, P=20 bar, CO = 15.6 Nml/min, H_2 = 31.2 Nml/min, N_2 = 10.0 Nml/min) obviously

without catalyst inside, we have calculated these ratios and the co-relation between them. The results are reported in Table 4.5.

Table 4.5 CO-N_2 calibration results

Flow N_2 (Nml/min)	Flow CO (Nml/min)	Flow H_2 (Nml/min)	Area N_2	Area CO	R flow CO/N_2	R area CO/N_2	Rarea / Rflow
10,0	15,6	31,2	411142	782455	1,56	1,9031	1,2199
10,0	15,6	31,2	390220	793329	1,56	2,0330	1,3032
10,0	15,6	31,2	388002	794913	1,56	2,0487	1,3133
10,0	15,6	31,2	384672	795362	1,56	2,0676	1,3254

The mean value of ratio between area and flow ratios is 1.2905 and this is the calibration factor (fc) for the system, as reported in the equation (4):

$$\frac{COarea}{N_2 area} = f_c \cdot \frac{COflow}{N_2\, flow} \tag{4}$$

then, the CO flow out coming from the FT plant is:

$$CO_{out}\, flow = \frac{COarea}{N_2 area} \cdot \frac{N_2\, flow}{1.2905} \tag{5}$$

finally, the CO conversion is:

$$COconversion = \frac{CO_{in} flow - CO_{out}\, flow}{CO_{in} flow} x100 \tag{6}$$

<u>The H_2 calibration</u>

To optimize the kinetic model of the FT synthesis was necessary to develop a measurement method to quantify the hydrogen leaving the plant. For this, it was performed a calibration of the micro-gas chromatograph using N_2 as standard in different streams of H_2.

To identify and quantify the hydrogen, it is necessary to change the carrier in the micro-gas chromatograph (from He to Ar).

Using Argon as a carrier the response of the micro-GC is about ten times smaller than the response compared with He. For this reason it has been

necessary to modify the injection time for the analysis and set to 40ms instead of the usual 30ms.

In Table 4.6 and Fig. 4.15 are shown the results relating to the calibration of the system H_2-N_2:

Table 4.6. H_2-N_2 calibration results

Flow N_2 (Nml/min)	Flow H_2 (Nml/min)	F H_2 / F N_2	Area N_2	Area H_2	A H_2 /A N_2
20	3	0.15	31511	33480	1.062
20	3.5	0.175	29525	36348	1.231
20	4.1	0.205	28420	40995	1.442
20	4.9	0.245	26747	45908	1.716
20	5.6	0.28	20897	41151	1.969
20	6.1	0.305	20748	44040	2.123

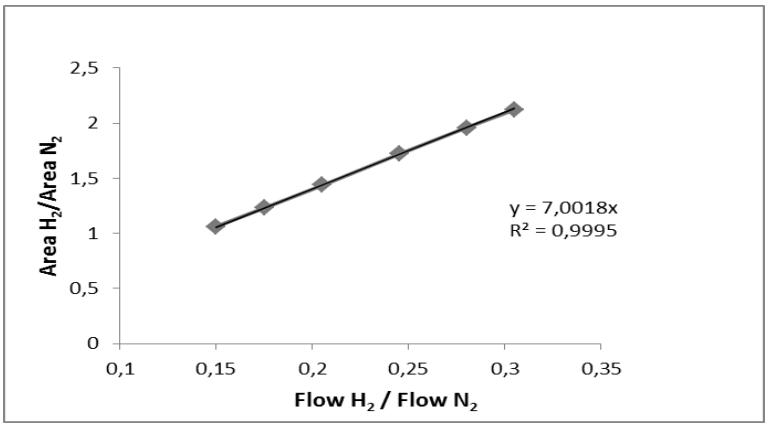

Fig. 4.15 Calibration results for the micro-GC for the system H_2 –N_2

From the equation of the straight line is obtained a correction factor equal to 7.0018.

By this correction factor (Fc) is possible to deduce the flow of the H_2 outflowing from the reactor and its conversion during the reaction using the following equation:

$$conversion \quad H_2 = \frac{FlowH_{2_{in}} - FlowH_{2_{out}}}{FlowH_{2_{in}}} \cdot 100$$

The calculation set to detect the flow of H_2 in output is based on the fact that the ratio between the areas H_2/N_2 is equal to the ratio between the respective flows multiplied by Fc (correction factor), according to the following equation:

$$\frac{AreaH_2}{AreaN_2} = Fc \cdot \frac{FlowH_2}{FlowN_2}$$

So from this equation it is possible to determine the flow of H_2 at the out of the reactor:

$$Flow \quad H_{2OUT} = \frac{AreaH_2}{AreaN_2} \cdot \frac{FlowN_2}{7.0018}$$

In Fig. 4.16 is shown an example of a gas chromatographic analysis of hydrogen

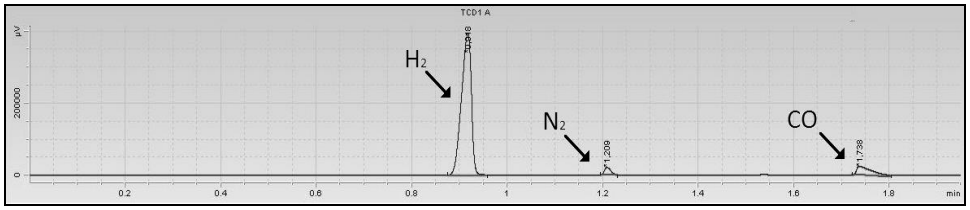

Fig. 4.16. Gas chromatographic analysis of a system H2-N2

4.3a.3 GC calibration

In this instrument, as before discussed, it is possible to analyze the heavy hydrocarbons condensed in the cold trap. Obviously, for their quantification we need a calibration with some standard compounds because the detector quantification is not the same for all the species. For this reason the equation

$$\frac{area_i}{\%mol_i} = \frac{area_j}{\%mol_j} \qquad (7)$$

it is not correct and we must use

$$\frac{area_i}{\%mol_i} \cdot F_i = \frac{area_j}{\%mol_j} \cdot F_j \quad (8)$$

where F_i and F_j are the calibration factor for the compound i and j respectively.

The calibration method used is the "internal standard method", in which one of the compounds to be analyzed is chosen as internal standard and his calibration factor (F) is established equal to 1. N-heptane has been chosen as internal standard because it is normally present in FT products. Analyzing a calibration hydrocarbon mixture it is possible to calculate the calibration factor of all the hydrocarbon present inside this mixture, using the following equation:

$$F_i = F_j \cdot \frac{area_j}{\%mol_j} \cdot \frac{\%mol_i}{area_i} \quad (9)$$

The composition of the calibration mixture is reported in table 4.7 and the calibration results in table 4.8.

In FT runs all hydrocarbons in the range C_1-C_{19} were obtained. To find the calibration factor and the retention times of hydrocarbons not present in the calibration mixture, an interpolation calculation was made. In the following figure are reported the diagram of the calibrations factors (Fig. 4.17) and of the retention times (Fig. 4.18) in function of carbon number. Starting from these experimental results an interpolation curve were calculated and then the calibrations factors and retention times for each carbon number was calculated too. The results are reported in Table 4.9. It is important to outline that for each single carbon number there is only one calibration factor for all the isomers, as they are not well separated by the GC column and the detector answer for the isomers is the same.

Table 4.7. Composition of GC calibration mixture

Hydrocarbon	PM (g/mol)	Quantity (g)	% Mol
n-Heptane (C7)	100,2	0,229	0,2295
Nonane (C9)	128,26	0,2389	0,1871
Decane (C10)	142,28	0,1284	0,0906
Undecane (C11)	156,31	0,1197	0,0769
Dodecane (C12)	170,33	0,1139	0,0672
Tridecane (C13)	184,36	0,1202	0,0655
Tetradecane (C14)	198,4	0,1577	0,0798
Pentadecane (C15)	212,41	0,1123	0,0531
Hexadecane(C16)	226,44	0,1817	0,0806
Octadecane (C18)	254,5	0,0919	0,0363
Nonadecane (C19)	268,52	0,0895	0,0335

Table 4.8. GC calibration results

Mix	%Mol	Chromatographic areas					Fc mean
		Analysis 1	Analysis 2	Analysis 3	Analysis 4	Analysis 5	
C7	0,229522	7,763	9,384	8,81	9,036	8,981	1,00
C9	0,18706	16,343	16,475	15,226	13,896	15,051	0,47
C10	0,090631	8,463	8,8707	7,902	7,588	7,856	0,43
C11	0,076907	8,716	7,627	8,235	7,916	8,239	0,36
C12	0,067157	8,485	7,313	8,137	7,709	8,168	0,32
C13	0,065478	8,47	7,654	8,253	7,859	8,271	0,31
C14	0,079826	11,095	9,689	10,988	9,685	11,042	0,29
C15	0,053096	8,309	8,19	8,876	8,844	8,535	0,24
C16	0,080586	12,395	11,571	12,863	12,834	13,014	0,25
C18	0,036265	6,059	6,061	6,679	6,817	6,59	0,22
C19	0,033474	6,134	5,958	6,527	6,663	6,549	0,20

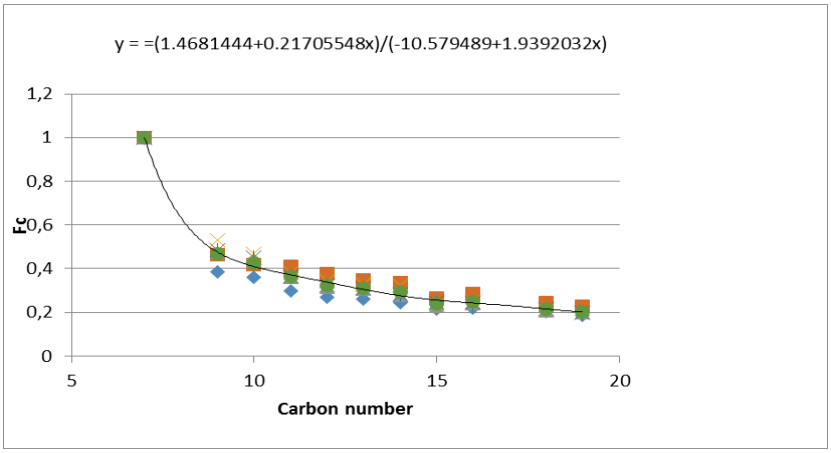

Fig 4.17. GC calibration factor vs. carbon number

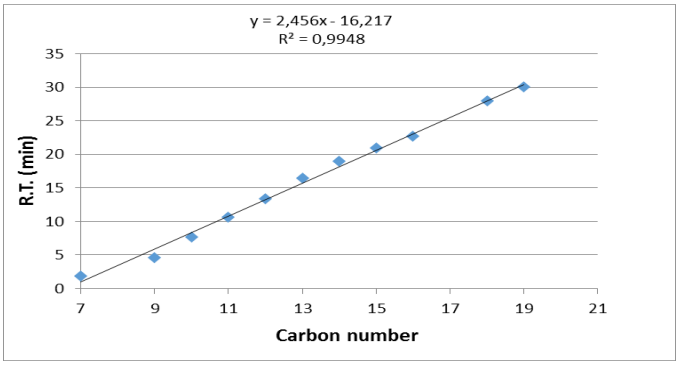

Fig. 4.18. GC retention time vs. carbon number

Table 4.9. GC Calibration factor and retention times for all the hydrocarbons $C_7 – C_{30}$

Carbon number	Fi	Retention time (min)
7	0,997	0,975
8	0,649	3,431
9	0,497	5,887
10	0,412	8,343
11	0,358	10,799
12	0,320	13,255
13	0,293	15,711
14	0,272	18,167
15	0,255	20,623
16	0,241	23,079
17	0,230	25,535
18	0,220	27,991
19	0,212	30,447
20	0,205	32,903
21	0,199	35,359
22	0,194	37,815
23	0,189	40,271
24	0,185	42,727
25	0,181	45,183
26	0,178	47,639
27	0,175	50,095
28	0,172	52,551
29	0,170	55,007
30	0,167	57,463

4.3a.4 TOC calibration

The detector of the instrument (type NDIR) is able to analyze and quantify by means of infrared spectroscopic technique, the CO_2 produced by the sample. For this calibration is not necessary to use a standard equal to the analyte (in the case of the synthesis of FT the carbonaceous species dissolved in water), but it is necessary to use a stable standard such as potassium hydrogen phthalate, because due to its physical nature (solid) is therefore inherently more reliable than a liquid and allows the exact correlation between the ppm of carbon present in solutions of standards and the areas provided by the instrument after analysis.

There were prepared different solutions at known concentrations (200 and 100 ppm) from a stock solution of 300 ppm obtained by dissolving 0.31895 g in 100ml of distilled water.

Standard solutions were corrected by a correction factor "f" according to the following equation:

$$f = \frac{real \quad sample \quad mass}{theoretical \quad sample \quad mass} \qquad (10)$$

The calculated value of "f" is equal to 1.000627 and the table 4.10 and the Fig. 4.19 show the correct ppm standard and the areas supplied by the instrument.

Table 4.10: calibrationTOC

Corrected ppm	Area
300.2	28679
200.1	17261
100.1	6568

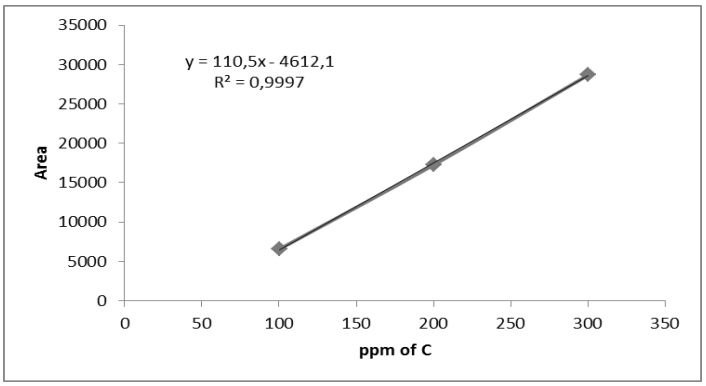

Fig. 4.19. Interpolation of areas obtained in function of the concentration (ppm) of the standard

4.4a Experimental procedure

All the kinetic FT runs were made on the plant following the same experimental procedure:

1) Catalyst preparation
2) Catalyst loading on the plant in the FT reactor
3) Catalyst activation
4) FT run
5) When FT finish, opening of cold trap and separation of organic from aqueous phases
6) Catalyst removal from reactor
7) Reactor cleaning and micro-GC column regeneration

4.4a.1 Catalyst preparation

Before the catalyst was loaded in the reactor, a standard procedure was followed on the same catalyst:

- Catalyst mesh operation between 106 and 150 micron
- Heating in oven at 120°C for a night
- Mixture catalyst - αAl_2O_3 (inert material – diluent) 1:1

In table 4.11 the main characteristics of α-Al_2O_3 are reported. The role of this material is to help the heating removal from the catalyst (FT reaction is highly exothermic).

Table 4.11. Main characteristics of α-Al_2O_3

Superficial area (m^2/g)	Bulk density (g/cm^3)	Composition %	Humidity %
0,7-1,3	1,72	99,6 Al_2O_3 <0,05 SiO_2 0,1 FeO <0,01 TiO_2	26

4.4a.2 Catalyst loading

The catalyst loading is obviously an essential operation. The catalyst must be charged in the middle of reactor because this is the isothermal zone, as it is possible to observe in Figure 4.20.

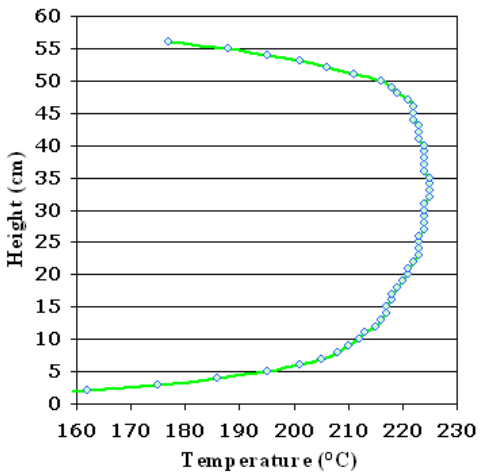

Fig. 4.20. Thermic profile of FT reactor

As the height of the mixture catalyst + α-Al_2O_3 is about 7 cm (using a pipe with an internal diameter of 6 mm), if this material is charged in the middle of the reactor, this work surely at the same temperature in each point. The final arrangement of the reactor is reported in Fig. 4.21.

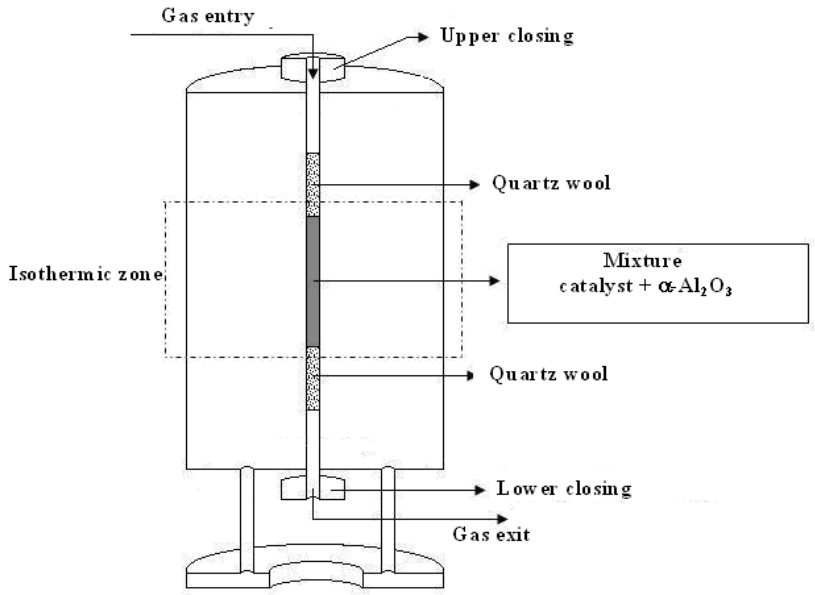

Fig. 4.21. FT reactor internal loading arrangement

Finally, after the closing, the pressure inside the reactor is raised till 4 bar, with the activation gases. The gas flow is stopped and then the held of reactor is checked to control possible gas losses. If the reactor pressure is stable, the activation catalyst step will be performed. The same procedure for the check of possible gas loss will be performed when the pressure of the reactor will be raised till 20 bar for FTS.

4.4a.3 Catalyst activation

The catalyst activation is the process in which the catalyst is reduced from the oxidised state in the reduced or metallic state. In the FT reaction the active form for the Cobalt based catalysts is the Cobalt metallic and for the iron based catalysts are the carbide iron forms. All the catalysts were charged into the reactor in the oxidised form because the last operation in the catalysts preparation is the calcination (T=500°C) in air. The catalyst activation-reduction is performed, in this PhD's research work, at 350°C and using H_2 for Co based

catalysts and CO+H_2 for iron based catalysts always for 4 h at 3 bar of pressure. At the end of this step the FT process start.

4.4a.4 Fischer Tropsch runs

After the catalyst activation the plant is raised at standard reactions conditions:

- Temperature = 220-260°C (depending of the test);
- Pressure = 20 bar;
- Feed ratio H_2/CO = 2/1; 1/1; 1.75/1; 1.5/1 (depending on the test were varied the feed ratio too);
- H_2 flow = 31.2 Nml/min;
- CO flow = 15.6 Nml/min;
- N_2 flow = 5.0 Nml/min;

These are the "standard" reaction conditions, but for some specific studies they have been changed. When the plant reaches the set-up values, this is the "zero-time" of the FT runs. The first operation is to annul the totalizers, both in the entrance and in the exit of the plant. Then every one hour the micro-GC make one analysis on the out coming flow (also during the night) and the operator takes the flow out coming from the plant. Each data is reported and elaborate using an excel database. The FT run has duration between 48 and 90 hours. At the end of run the cold trap is opened (Fig. 4.22) and both the organic phase (GC) and the aqueous phase (TOC) are separated and then weighed and analyzed. Also these data is collected in the excel database, and now it is possible to calculate the CO conversion, the products selectivity, the alpha parameter and to verify the final mass balance.

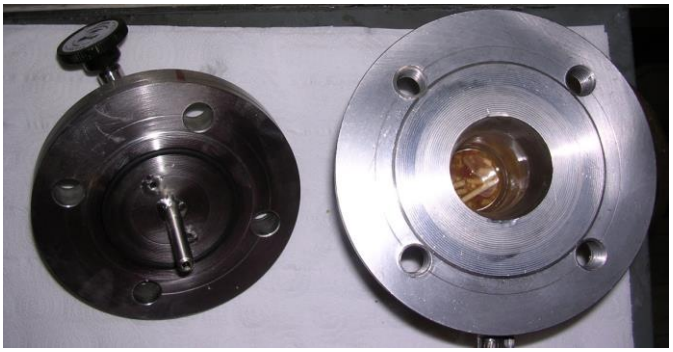

Fig. 4.22. Opening cold trap operation

After the reactor cooling, the catalyst is unloaded and recovered for possible characterization after its use. The reactor and the cold trap are obviously cleaned carefully. The last operation is the micro-GC column regeneration, using the condition reported in Table 4.12

Table 4.12. Micro-GC column regeneration conditions

Parameter	Module 1 (molsieves)	Module 2 (OV-1)
Sample Injector temperature (°C)	80	80
Column Injector temperature (°C)	45	60
Column temperature (°C)	160	160
Sampling time (s)	--	--
Injection time (ms)	--	--
Analysis time (s)	--	--
Post-analysis time (s)	--	--
Column pressure (kPa)	120	241
Detector sensibility	Detector off	Detector off

b) Second FTS unit (Unit 2):

At the end of the second and the beginning of the third year of the PhD, there were performed a serious of catalytic tests in a FT unit at the *Universidad Central de Venezuela* in Caracas-Venezuela in order to homologate the results obtained in the first FTS unit as regard the cobalt based catalysts, specifically the hydrotalcites. The experimental tests were performed in a laboratory plant with a tubular reactor with a fixed bed of catalyst vertically placed. They were then tested in the standard conditions by flowing syngas (H_2: CO: N2, 63:32:5, v/v, N_2 as internal standard) at 15.6 $Nml \cdot min^{-1}$ using a flow meter. Then the feed goes into the catalytic reactor from the top part, reacts with the catalyst and then the reacted flow comes out from the lower part. The plant pipes are heated at 220°C. During reaction, the reactor effluent passed through a hot trap kept at 150ºC and 20 bar to collect waxes, and the products leaving this trap were passed through a second trap kept at 0ºC and 20 bar to collect the lighter products (water, alcohols and hydrocarbons). The analyses were performed in various chromatographs according to the nature of the sample to be analyzed. Permanent gases and light hydrocarbons were analyzed on-line in a PerkinElmer 3000GC Autosystem fitted with TCD detectors using a Carbosieve SII Supelco column. The liquid products (collected at 150ºC and 0ºC) were weighted and analyzed in a PerkinElmer chromatograph fitted with a 50m long Alumina RT capillary column connected to a FID.

In Fig. 4.23 the detailed flow-sheet of FT plant has been reported.

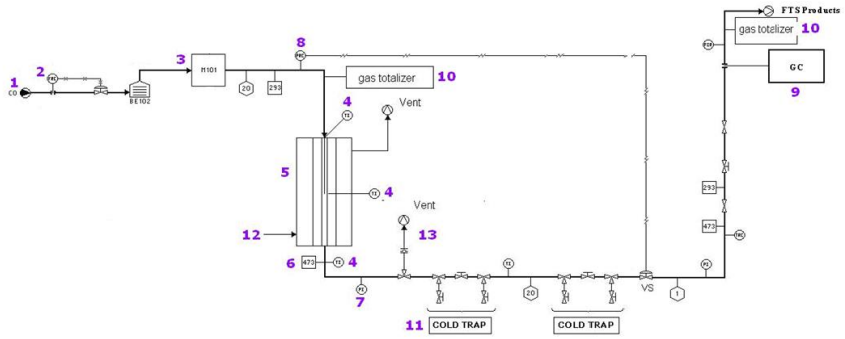

Fig. 4.23. Laboratory plant flow-sheet

The key for the Fig.4.23 is the following:

1: Valve

2: Flow meter for H_2 and syngas operating in the range 0-100 Nml min^{-1}

3: Gas mixer

4: Thermocouples for the control of temperature in the catalytic bed, in the reactor and in the heated pipe

5: Tubular reactor

6: Security valve

7: Pressure indicator

8: Pressure control and regulation tool

9: GC “Perkin Elmer”

10: Gas totalizer for the control of the total flow of gas

11: Cold trap operating at 150°C and 20 bar to collect waxes

11.1 Second cold trap kept at 0ºC and 20 bar to collect the lighter products (water, alcohols and hydrocarbons)

12: Cooling air for the temperature control of the reactor

13: vent (usually closed)

In figure 4.24 a photo of the plant is reported.

Fig. 4.24. FT laboratory plant

In the following paragraphs the main parts of this plant will be described.

4.1b Main parts of the plant

4.1b.1 Apparatus for the regulation and control of temperature, pressure and flow of reagents:

In the plant the pressure is controlled by a pneumatic valve that interacts with a pressure valve able to work till 1000 psi (Fig 4.25), located after the reactor and the cold trap.

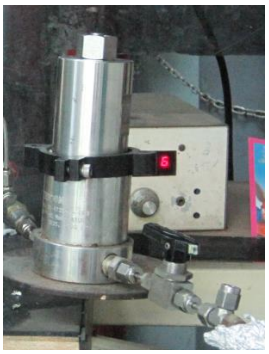

Fig. 4.25. Pressure valve

This system can control the plant pressure with a care of 10 psi respect the set up.

The reactor temperature is regulated by a heating jacket and the pipe lines after the reactor are heated at 220°C to prevent the heavy products condensation by a heater. The CO, H_2 and N_2 flows are regulated by Brooks Instrument Control and Read out Equipment for Thermal Mass Flow meters Model 5878 series flow meters (Fig. 4.26).

4.26. Flow meters for H_2, and syngas

4.1b.2 FT reactor

The FT plant reactor is a fixed bed tubular reactor vertically placed. It is made of AISI 316 stainless steel. The technical characteristics of reactor are summarized in Table 4.13.

Table 4.13. Reactor Characteristics

Volume (cm^3)	Max. operating pressure (Bar)	Max. operating temperature (°C)	Internal diameter (mm)	Height (mm)
85,0	69	400	9,5	300

In this reactor it is possible to charge a quantity of catalysts equivalent to occupy 1 cm of length of the reactor. The feed goes into the reactor at the top and goes out from the lower part.

Fig. 4.27. FT tubular reactor

The temperature inside the reactor is monitored by one thermocouple inside the catalyst.

4.1b.3 Cold Trap

The reactor effluent passed through a hot trap kept at 150°C and 0.2 MPa to collect waxes, and the products leaving this trap were passed through a second trap kept at 0°C and 0.2MPa to collect the lighter products (water, alcohols and hydrocarbons). See Fig. 4.28.

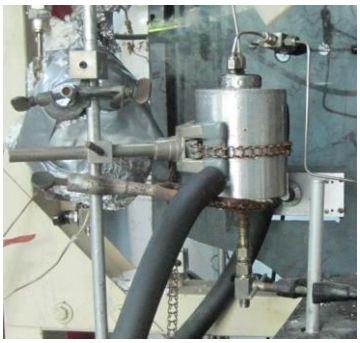

Fig. 4.28. Cold trap

The two cold traps, can be opened at any time of the reaction and the liquid condensed inside can be quantified and analyzed.

The analyses were performed in various chromatographs according to the nature of the sample to be analyzed. Permanent gases and light hydrocarbons were analyzed on-line in a PerkinElmer 3000GC Autosystem fitted with TCD detectors using a Carbosieve SII Supelco column .The liquid products (collected at 150°C and 0°C) were weighted and analyzed in a PerkinElmer chromatograph fitted with a 50m long Alumina RT capillary column connected to a FID.

4.2b Analytical instruments

Two different analysis were made for the quantification of the composition of:

i) Out coming gas (mixture of not reacted CO and H_2, N_2 and non-condensed FT products) by an on-line in a PerkinElmer 3000GC Autosystem fitted with TCD detectors using a Carbosieve SII Supelco column.

ii) Organic phase of condensed liquid products (collected in a cold trap at 150ºC and 0ºC), hydrocarbons in the range C_7-C_{30}, were weighted and analyzed in a PerkinElmer chromatograph fitted with a 50m long and 0.53 mm diameter of Alumina RT capillary column connected to a FID.

An example of analyses of the permanent gases is reported in Fig. 4.29, and an example of analysis of heavy FT hydrocarbons is reported in Fig. 4.30 and Fig. 4.31.

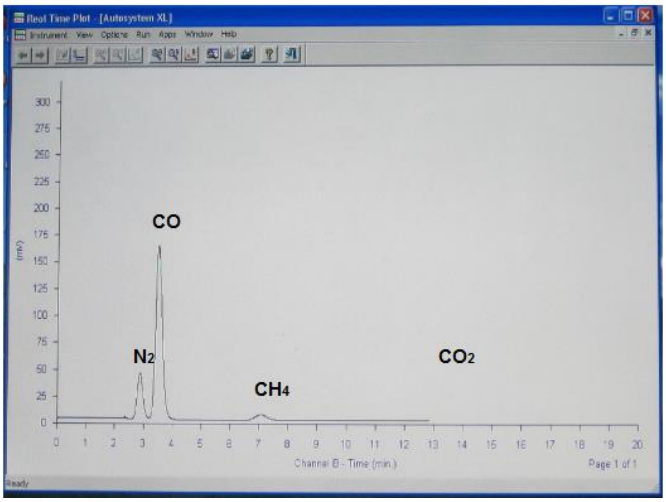

Fig. 4.29. Example of analyses of the permanent gases in the TCD

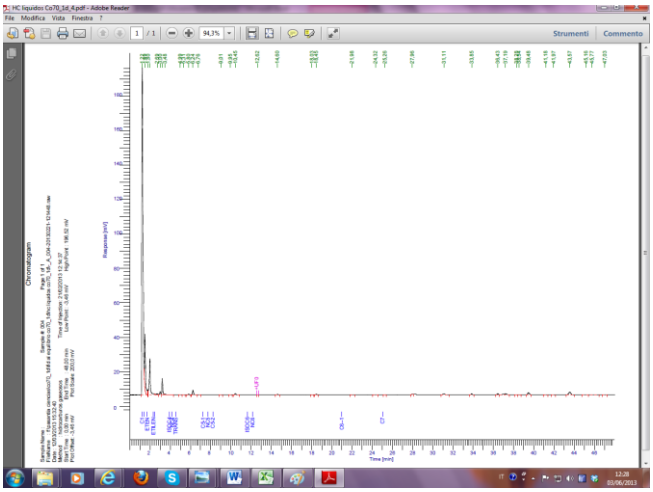

Fig. 4.30. Example of not-condensed products GC analyses on FT out coming gas

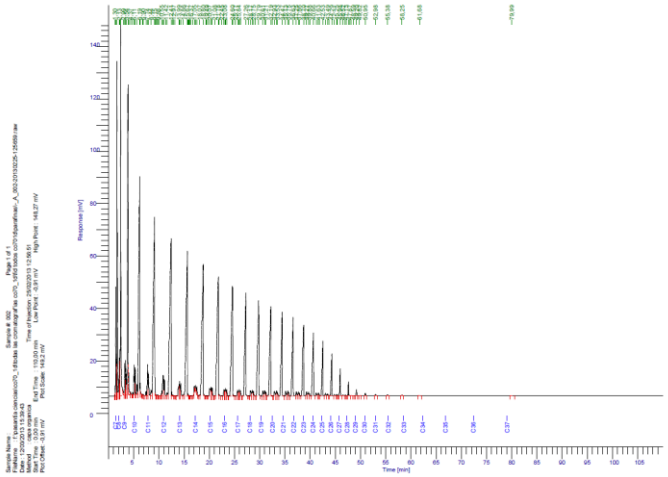

Fig. 4.31. Example of GC analysis for the quantification of heavy FT products

4.3b Experimental procedure

All the kinetic FT runs were made on the plant following the same experimental procedure:

1) Catalyst preparation
2) Catalyst loading on the plant in the FT reactor
3) Leak test
4) Catalyst activation
5) FT run
6) Opening of cold trap and separation of organic from aqueous phases
7) Catalyst removal from reactor
8) Reactor cleaning

4.3b.1 Catalyst preparation

Before the catalyst was loaded in the reactor, a standard procedure was followed on the same catalyst:

- Catalyst mesh operation between 106 and 150 micron
- Heating in oven at 120°C for a night

- Mixture catalyst – sea sand (inert material – diluent) 1:1

In table 4.14 the main characteristics of sea sand are reported. The role of this material is to help the heating removal from the catalyst (FT reaction is highly exothermic). [**5]**

Table 4.14. Main characteristics of sea sand

Particle Size (µm)	Specific Surface Area (m^2/g)	Bulk density (Kg/m^3)	Pore Volume (mL)	Interstitial Velocity (m/d)	Porosity (-)	Composition %
100-300	0,74	200-1430	11,7	2,6	0,44	SiO_2

4.3b.2 Catalyst loading

As the height of the mixture catalyst + sea sand is about 1 cm (using a pipe with an internal diameter of 9.5 mm), if this material is charged in the middle of the reactor, this work surely at the same temperature in each point. The final arrangement of the reactor is reported in Fig. 4.32.

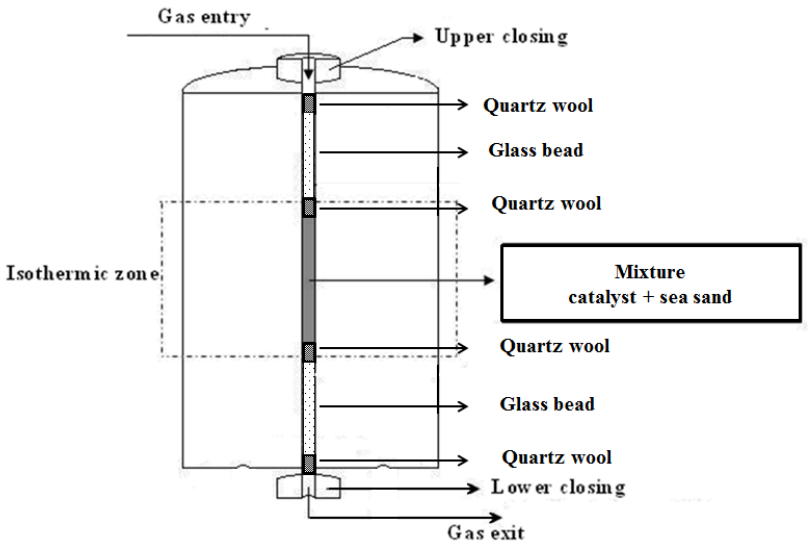

Fig. 4.32. FT reactor internal loading arrangement

Finally, after the closing, the pressure inside the reactor is raised till 3 bar, with the activation gases. The gas flow is stopped for one night and then the reactor is checked to control possible gas losses. If the reactor pressure is stable, the activation catalyst step will be performed. The same procedure for the check of possible gas loss will be performed when the pressure of the reactor will be raised till 20 bar for FTS.

4.3b.3 Catalyst activation

The catalyst activation is the process in which the catalyst is reduced from the oxidised state in the reduced or metallic state. The samples tested in this reactor, were the Co based hydrotalcites. In the FT reaction the active form for the cobalt based catalysts is the cobalt metallic. All the catalysts were charged into the reactor in the oxidised form because the last operation in the catalysts preparation is the calcination (T=500°C) in air. The catalyst activation-reduction is performed in this part of the PhD's research work at 350°C, using H_2, always for 4 h at 3 bar of pressure. At the end of this step the FT process start.

4.3b.4 Fischer Tropsch runs

After the catalyst activation the plant is raised at standard reactions conditions:

- Temperature = 220-260°C;
- Pressure = 20 bar;
- Feed ratio H_2/CO = 2/1;
- Syngas (H_2 + CO + N_2) flow = 15.6 Nml/min (in order to work with the same space velocity used for the same samples tested in the Unit 1 in Italy);

These are the "standard" reaction conditions. When the plant reaches the set-up values, this is the "zero-time" of the FT runs. Every one hour the GC make

one analysis of the permanent gases (CO, CO_2, CH_4, N_2) on the out coming flow (also during the night). Each data is reported and elaborate using an excel database. The FT run has a duration between 200-280 hours. During the reaction and before the changes of temperatures the valves of the two cold trap are opened and both the organic phase (GC) and the aqueous phase are separated and then weighed and analyzed. Also these data is collected in the excel database, and now it is possible to calculate the CO conversion, the products selectivity, the alpha parameter and it is possible to verify the final mass balance.

After the reactor cooling, the catalyst is unloaded. The reactor is cleaned carefully.

4.2 Experimental data elaboration

The experimental data collected in the laboratory are the gas-chromatographic area (with micro and traditional GC), the gas flows, the temperatures, the pressure, the weight of condensed products and the TOC value of organic compounds in aqueous phase. For each run, all these data were put in the excel file where in an automatic way the CO conversion, the products selectivity, the molar balance, the α parameter were calculated.

There were used two different file excel for the two different FTS unit.

a) First FTS unit (Unit 1)

The file excel is split in nine pages: data, results, heavy hydrocarbons analysis, molar balance (CO, hydrogen and oxygen), hydrogen analysis, oxygen analysis and alpha calculation. As example the pages of one FT run (made with a Co base catalyst Co35_2d) are reported in Fig. 4.33a-f.

Data page (Fig. 4.33a)

This worksheet contains the mathematical elaboration of the experimental data obtained from the various analyzes and is composed of different parts

- Conditions: It is referred to the number of tests carried out by the micro-gas chromatograph, the time at which the analysis were made and the outside temperature at the time of sampling;
- Flow in: It is referred to the flow in (Nml/min) of the reactants (H_2 and CO) and the internal standard (N_2) that remain constant during the entire kinetic energy;
- Volumes totalizers: It is referred to the values of the three volumes of gas consumed while the kinetic is in progress (this values are read from the totalizer just before performing the analysis) and the total volume of gas output in ml and Nml. Furthermore it also evaluates an error in percentage between the volume of gas out and the gas in;
- Flow out is measured by a flow meter bubbles and a counter "Ritter"; the flow rates are calculated with the output flow measured from the bubble flow meter and the Ritter counter and then compared:

$$\text{Flow from bubble flow meter } \left(ml/\text{min}\right) = \frac{V}{t} \cdot 60 \qquad (11)$$

V[ml]: Volume path from the bubble

t[min]: Time it takes the bubble to traverse this volume

$$\text{Flow from Ritter counter } \left(ml/\text{min}\right) = \frac{(V_{OUT} - V_{IN})}{t} \cdot 100 \qquad (12)$$

- V_{IN} [ml] and V_{OUT} [ml]are the volume of gas in and out.

- Both values of flow are converted in Nml/min by the next equation:

$$\frac{\frac{ml}{\text{min}} \cdot 273}{273 + T} \text{ ; T[°C]} \qquad (13)$$

- CO Conversion: It is referred to the quantity of gas reacted or converted referred to the gas entering inn the plant. From the micro-gc analysis are taken the chromatographic areas of CO and N_2 and used to calculate the flow out-coming of CO from the equation:

$$flow \quad CO_{OUT} = \frac{Area \quad CO}{Area \quad N_2} \cdot \frac{flow \quad N_{2_{OUT}}}{1{,}2912} \qquad (14)$$

Where 1.2912 is the calibration factor. As the flow in and the flow out of N_2 is the same:

$$flow \quad CO_{OUT} = \frac{Area \quad CO}{Area \quad N_2} \cdot \frac{5{,}02}{1{,}2912} \qquad (15)$$

5.02 is the flow of the internal standard N_2.

Now it is possible to calculate the CO conversion using the next formula:

$$CO \quad Conversion = \frac{flow \quad CO_{IN} - flow \quad CO_{OUT}}{flow \quad CO_{IN}} \qquad (16)$$

- Selectivity: Concerning the gas flow out-coming from the FT plant, made of not reacted CO, CO_2, CH_4 and light hydrocarbons

% CO in reaction mixture: $$\% \quad CO = \frac{flow \quad CO_{OUT}}{flow_{TOT} - flow_{N_2}} \cdot 100 \qquad (17)$$

% product i in reaction mixture:

$$\% \quad product_i = \frac{\frac{area_i}{F.c._i} \cdot flow_{OUT}}{flow_{TOT} - flow_{N_2}} \cdot 100 \qquad (18)$$

where

$flow_{TOT}$ is the total flow out-coming from the FT plant and $concentration_i$ is the amount ($\%_m$) of product *i* found using the micro-GC.

$F.c._i$ is the calibration factor for each compound.

- Carbon molar flow for the i compound:

$$\frac{moles_{C_i}}{\min} = \frac{\frac{flow_{tot} \cdot 0.001}{100}}{22.4 \cdot \%_i} \cdot number_{C_i} \quad (19)$$

where $number_{C_i}$ is the number of carbon atom of compound i.

0,001 transform Nml to Nl and 22,4 let to transform Nl to moles.

- Molar balance.
- CO moles entering in the plant:

$$\frac{moles \quad C_{CO_{in}}}{\min} = \frac{flow_{CO_{in}}}{22.4x1000} \quad (20)$$

- CO moles out coming:

$$\frac{moles \quad C_{CO_{OUT}}}{\min} = \frac{flow_{CO_{out}}}{22.4x1000} + \sum_{i=1}^{6} \frac{molesC_i}{\min} \quad (21)$$

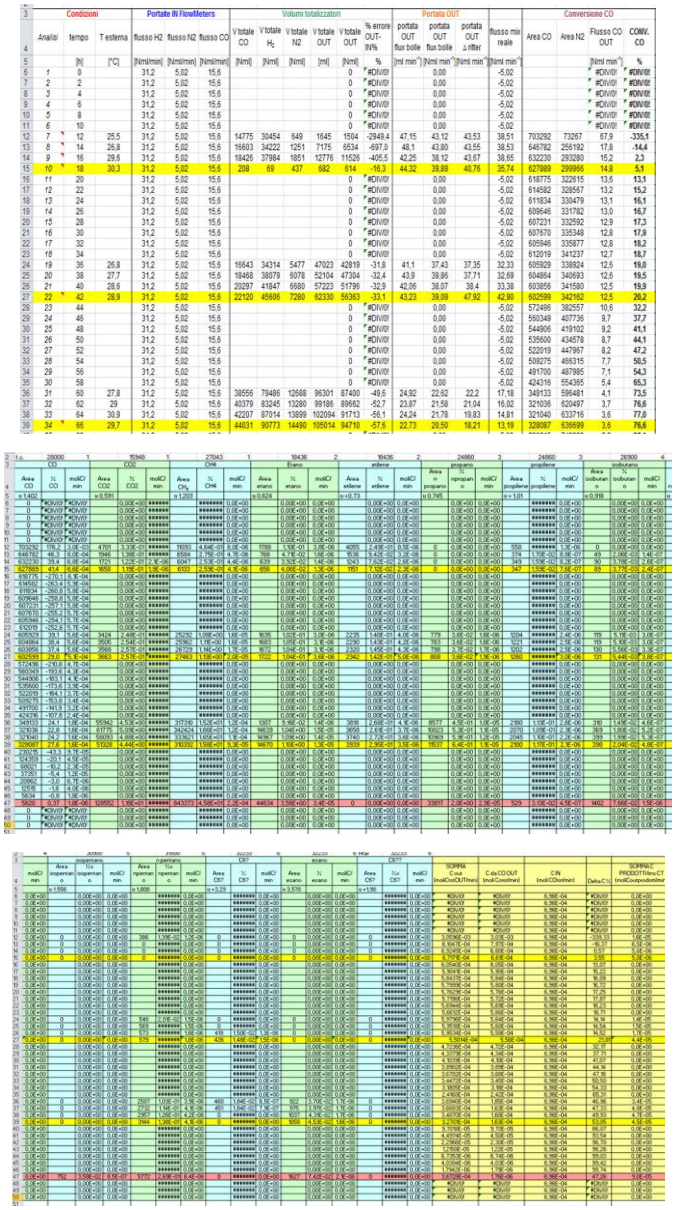

Fig. 4.33a Example of “data page” in FT data elaboration excel file

Results page (Fig. 4.33b)

Concerning the products selectivity:

- Light products ($<C_7$) j selectivity:

$$S_j = \frac{\frac{moles_{C_j}}{\min}}{\frac{molesCO_{in}}{\min} - \frac{molesCO_{out}}{\min}} \cdot 100 \quad (22)$$

where $moles_{C_j}$ means the moles of carbon atom in the j products.

- Heavy products (≥C_7) i selectivity:

$$S_i = \frac{\frac{moles_{C_i}}{\min}}{\frac{molesCO_{in}}{\min} - \frac{molesCO_{out}}{\min}} \cdot 100 \quad (23)$$

where $moles_{C_i}$ means the moles of carbon atom in the i products.

- Total light products selectivity: $S_{light} = \sum S_j$ (24)

- Total heavy products selectivity: $S_{heavy} = \sum S_i$ (25)

.

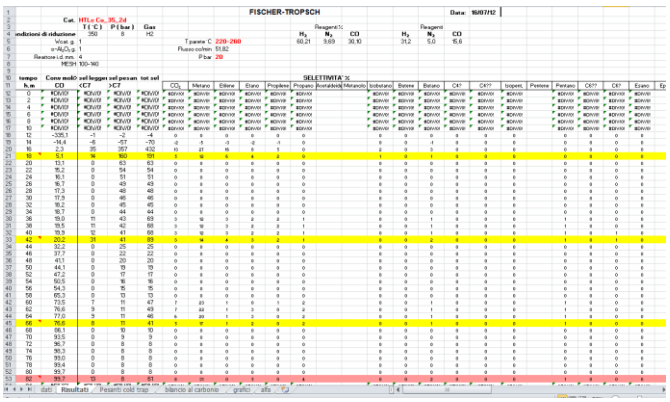

Fig. 4.33b. Example of "results page" in FT data elaboration excel file

Concerning the **heavy product (organic phase condensed in the cold trap)** elaboration: (Fig. 4.33c)

- %moles of i compound: $\%moles_i = \frac{CA_i \cdot fc_i}{\sum CA} \cdot 100$ (26)

where CA is the chromatographic area and fc is the calibration factor

- Total moles of "-CH_2-" unit in organic phase: $$moles_{CH_2} = \frac{weight_{OP}}{14} \quad (27)$$

- Where $weight_{OP}$ means the weight of the organic phase in gram and 14 is the molecular weight of the unit "-CH_2-"

Carbon moles of compound *i*: $$moles_{C_i} = \frac{moles_{CH_2}}{\%moles_i} \cdot 100 \quad (28)$$

- Moles of carbon per minute of each component

$$\frac{moles \quad C_i}{\min} = \frac{moles \quad C_i}{reaction \quad time \cdot 60} \quad (29)$$

	A	B	C	D	E	F	G	H	I	J
1										
2	t ritenz	n Carboni	Aree	Fattori correzione	Aree corrette	%mol miscela	moli C	moliC/min		
3		5	0	1,00	0	0,0	0,0000	0		
4		6	0	1,00	0	0,0	0,0000	0		
5	1,67	7	191127	0,9975	190654,7	34,3	0,1540	3,13039E-05		
6	2,52	8	191674	0,6495	124487,1	22,4	0,1006	2,04398E-05		
7	4,18	9	118295	0,4978	58888,89	10,6	0,0476	9,66907E-06		
8	6,39	10	90190	0,4129	37239,45	6,7	0,0301	6,11441E-06		
9	8,26	11	91790	0,3586	32917,42	5,9	0,0266	5,40477E-06		
10	11,14	12	78970	0,3209	25343,24	4,6	0,0205	4,16115E-06		
11	14,02	13	65091	0,2932	19086,04	3,4	0,0154	3,13377E-06		
12	18,13	14	54358	0,2720	14785,56	2,7	0,0119	2,42767E-06		
13	20,52	15	44906	0,2552	11461,45	2,1	0,0093	1,88188E-06		
14	22,85	16	37345	0,2416	9024,109	1,6	0,0073	1,48168E-06		
15	25,09	17	30120	0,2304	6939,824	1,2	0,0056	1,13946E-06		
16	27,24	18	25641	0,2210	5665,67	1,0	0,0046	9,30257E-07		
17	29,38	19	18595	0,2129	3959,089	0,7	0,0032	6,5005E-07		
18	31,29	20	17084	0,2060	3518,766	0,6	0,0028	5,77753E-07		
19	33,13	21	13728	0,1999	2744,486	0,5	0,0022	4,50622E-07		
20	34,89	22	14029	0,1946	2730,051	0,5	0,0022	4,48252E-07		
21	36,55	23	9435	0,1899	1791,598	0,3	0,0014	2,94166E-07		
22	38,21	24	7866	0,1857	1460,595	0,3	0,0012	2,39818E-07		
23	39,76	25	6252	0,1819	1137,307	0,2	0,0009	1,86737E-07		
24	41,25	26	4025	0,1785	718,4811	0,1	0,0006	1,17969E-07		
25	42,66	27	4504	0,1754	790,067	0,1	0,0006	1,29723E-07		
26	44,12	28	2152	0,1726	371,4321	0,1	0,0003	6,09861E-08		
27	45,80	29	1575	0,1700	267,7843	0,0	0,0002	4,3968E-08		
28	47,88	30	1261	0,1677	211,4129	0,0	0,0002	3,47123E-08		
29										
30		totale			556194,5	100	0,449307	Peso fase organica	6,2903	g
31								moli CH2	0,449307	moli
32								tempo cinetica	82	ore
33										
34								somma >C13	1,42E-05	

Fig. 4.33c. Example of "heavy hydrocarbons analysis page" in FT data elaboration excel file

Molar balance page (Fig. 4.33d)

The molar balance is verified using the following equation:

$$moles_{CO_{in}} = moles_{CO_{out}} - moles_{Clight_{out}} - moles_{Cheavy_{out}} - moles_{Cwater_{out}} \quad (30)$$

Where:

$moles_{CO_{in}}$ and $moles_{CO_{out}}$ are respectively the moles of CO in entrance and escape of the FT plant in all the run's time; $moles_{Clight_{out}}$ are the carbon atom moles of light FT products came out from the FT plant in all the run's time; $moles_{Cheavy_{out}}$ are the carbon atom moles of the heavy hydrocarbons in the organic phase condensed in the cold trap and $moles_{Cwater_{out}}$ are the carbon atom moles inside the water phase condensed in the cold trap. In particular:

- $$moles_{Clight_{out}} = \sum \frac{\left(flow_{tot_{out}} - flow_{N_2}\right) \cdot n°C_i \cdot \%_i \cdot 0.01}{22.4} \quad (31)$$
- $$moles_{Cheavy_{out}} = \frac{weight_{OP}}{PM_{CH_2}} \quad (32)$$
- $$moles_{Cwater_{out}} = \frac{ppm_{TOC} \cdot weight_{OP} \cdot fd}{10^6 \cdot 12} \quad (33)$$

where ppm_{TOC} are the ppm of Total Organic Carbon measured by TOC instrument and fd is a diluting factor (normally 1:500), as the aqueous phase must be diluted before the TOC analysis.

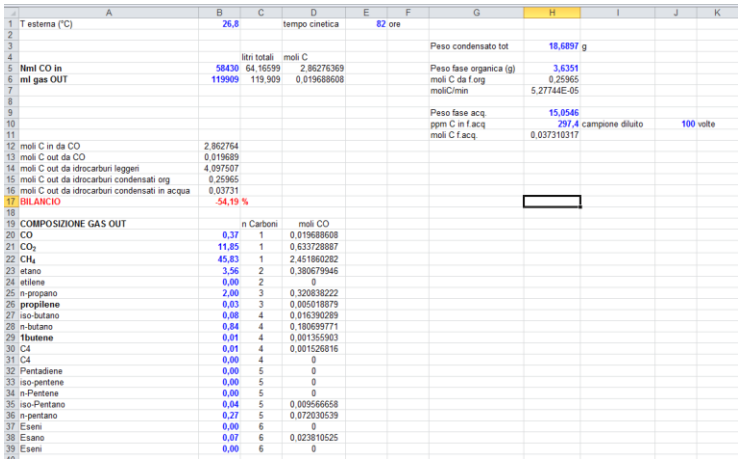

	A	B	C	D	E	F	G	H	I	J	K
1	T esterna (°C)	26,8		tempo cinetica	82	ore					
2											
3							Peso condensato tot	18,6897	g		
4			litri totali	moli C							
5	**Nml CO in**	58430	64,16599	2,86276369			Peso fase organica (g)	3,6351			
6	**ml gas OUT**	119909	119,909	0,019688608			moli C da f.org	0,25965			
7							moliC/min	5,27744E-05			
8											
9							Peso fase acq	15,0546			
10							ppm C in f.acq	297,4	campione diluito	100	volte
11							moli C f.acq	0,037310317			
12	moli C in da CO	2,862764									
13	moli C out da CO	0,019689									
14	moli C out da idrocarburi leggeri	4,097507									
15	moli C out da idrocarburi condensati org	0,25965									
16	moli C out da idrocarburi condensati in acqua	0,03731									
17	BILANCIO	-54,19 %									
18											
19	**COMPOSIZIONE GAS OUT**		n Carboni	moli CO							
20	**CO**	0,37	1	0,019688608							
21	**CO_2**	11,85	1	0,633728887							
22	**CH_4**	45,83	1	2,451860282							
23	etano	3,56	2	0,380679946							
24	etilene	0,00	2	0							
25	n-propano	2,00	3	0,320838222							
26	**propilene**	0,03	3	0,005018879							
27	iso-butano	0,08	4	0,016390289							
28	n-butano	0,84	4	0,180699771							
29	**1butene**	0,01	4	0,001356903							
30	C4	0,01	4	0,001526816							
31	C4	0,00	4	0							
32	Pentadiene	0,00	5	0							
33	iso-pentene	0,00	5	0							
34	n-Pentene	0,00	5	0							
35	iso-Pentano	0,04	5	0,009566658							
36	n-pentano	0,27	5	0,072030539							
37	Eseni	0,00	6	0							
38	Esano	0,07	6	0,023810525							
39	Eseni	0,00	6	0							

Fig. 4.33d. Example of "molar balance page" in FT data elaboration excel file

alpha parameter (Fig. 4.33e):

This parameter represents a prediction of the distribution related to the number of carbon atoms according to the Anderson-Schulz-Flory distribution.

In the excel file of data elaboration it is possible to calculate the alpha parameter in different range of hydrocarbons: C_1-C_6, C_3-C_{12}, C_{13}-C_{30}, C_3-C_{30}. The hydrocarbon range is chosen depending of the FT results: if, as example, the heavy product selectivity is very low, it is not convenient to consider these products in the α calculation. The equation for the α calculation is

- $$\log\left(\frac{W_n}{n}\right) = n\log\alpha + \log\left(\frac{(1-\alpha)^2}{\alpha}\right) \qquad (34)$$

where W_n is the weight fraction of product with n carbon atom number. In the excel file the equation used are:

- $$moles_{C_i} = \frac{moles_{C_i}}{\min} \cdot 60 \cdot t_{tot} \qquad (35)$$

where t_{tot} is the total time of FT run in hours

- $$g_i = moles_{C_i} \cdot PM_i \qquad (36)$$

- $$W_n = \frac{g_i}{\sum_{i=1}^{n} g_i} \qquad (37)$$

The calculation of α is then performed making a diagram in which the $\log\left(\frac{W_n}{n}\right)$ is reported vs the carbon atom number.

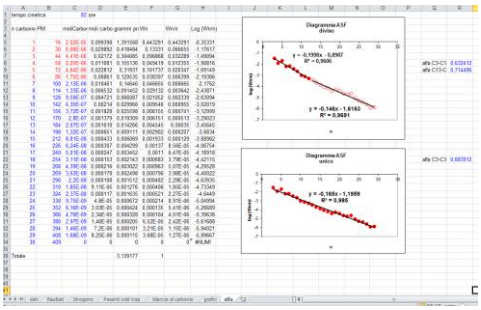

Fig. 4.33e. Example of "α calculation page" in FT data elaboration excel file

"α calculation page"

The product distribution can be predicted using the Anderson−Schulz−Flory (ASF) model that depends on the chain growth probability α. Different factors have an influence on the alpha parameter such as process conditions, type of catalyst, and chemical promoters. [6] The ASF product distribution as a function of α is depicted in Figure 2.5 (Chapter 2).

According to ASF distribution, ideally, the molar fraction (Mn) of the hydrocarbon product with a carbon number of n is only dependent on the chain-growth probability (α), which is a function of the rates of chain growth and chain termination, by the following equation:

$$Mn = (1-\alpha)\alpha^{n-1} \qquad (38)$$

In other words, the product selectivity is determined by α value in an ideal case. A smaller α value leads to lighter (C_1–C_4) hydrocarbons, while larger α value results in the formation of heavier (C_{21+}) hydrocarbons. However, the ASF distribution is unselective for the middle-distillate products, which are usually the target products. For examples, the maximum selectivity to gasoline-range (C_5–C_{11}) hydrocarbons is ∼45% and that to diesel-range (C_{10}–C_{20}) hydrocarbons is ∼35%. The development of selective FT catalysts, which can tune the

selectivities to desired products, is one of the most challenging targets in the field of FT synthesis [7].

The probability α is defined as the speed of growth (rg) divided by the sum of the speeds of all the possible reactions for the species in growth.

The probability to form a product P_n with n carbon atoms is the product of the probabilities that the adsorbed species are formed in 1, 2 ...., n-1 carbon atoms (precursors of the species P_n) and the probability that the adsorbed species an carbon atoms desorb. Writing a mathematical model leads to the ASF:

$$log\left(\frac{W_n}{n}\right) = n \cdot log\,\alpha + log\left(\frac{(1-\alpha)^2}{\alpha}\right) \qquad (39)$$

where Wn is the mass fraction of the product with n carbon atoms.

To get the equation of Anderson-Schulz-Flory.
We define:

- α as the probability of growth;
- r_t as the rate of chain terminations;
- r_p the speed of chain propagation.

For a chain of n carbon atoms is defined another parameter β_n given by:

$$\beta_n = \frac{r_t}{r_p} = \frac{1-\alpha_n}{\alpha_n} = \frac{\phi_n}{\sum_{n+1}^{\infty}\phi_i} \qquad (40)$$

where α_n is the probability that a chain of n carbon atoms remains on the catalyst to continue the propagation of the chains, ϕ_n is the number of moles of product C_n. If α_n is constant throughout the range of products, it may simply indicate with α and therefore starting from n = 1 we can write:

$$\phi_2 = \phi_1 \cdot \alpha$$
$$\phi_3 = \phi_2 \cdot \alpha = \phi_1 \cdot \alpha^2$$
$$\phi_4 = \phi_3 \cdot \alpha = \phi_1 \cdot \alpha^3$$

So in general:

$$\phi_n = \phi_1 \cdot \alpha^{n-1}$$

Starting from a generic molecule with x carbon atoms we can write:

$$\phi_n = \phi_x \cdot \alpha^{n-x} \quad (41)$$

Assuming that the monomeric units have the same molecular weight without regard to their position in the growing chain (these monomer units are CH2 with PM = 14), we can obtain the weight fraction Wn multiplying the equation (1) by n and dividing it by $\sum_{n=1}^{\infty} n\phi_n$. If we set x = 1, equation (41) remains:

$$W_n = \frac{n\phi_n}{\sum_{n=1}^{\infty} n\phi_n} = \frac{n\phi_1 \cdot \alpha^{n-1}}{\sum_{n=1}^{\infty} n\phi_1 \cdot \alpha^{n-1}} = \frac{n\alpha^{n-1}}{\sum_{n=1}^{\infty} n\alpha^{n-1}} \quad (42)$$

The denominator of the last member of equation (42) can be written as:

$$\frac{\partial \sum_{n=0}^{\infty} \alpha^n}{\partial \alpha} \quad (43)$$

In fact, the operators $\frac{\partial}{\partial \alpha}$ can be reversed and therefore

$$\frac{\partial}{\partial \alpha} \sum_{n=0}^{\infty} \alpha^n = \sum_{n=0}^{\infty} \frac{\partial}{\partial \alpha} \cdot \alpha^n = \sum_{n=0}^{\infty} \alpha^{n-1}$$

The series $\sum_{n=0}^{\infty} \alpha^n$ for $\alpha \neq 1$ be equal to $\frac{1}{1-\alpha}$.

The series in question is of the type

$S = a + ar^2 + ar^3 + \ldots + ar^n$

and the solution is equal to:

$$S = a\frac{1-r^n}{1-r}$$

Equation (2) can therefore be rewritten as follows:

$$W_n = \frac{n\alpha^{n-1}}{\frac{\partial}{\partial\alpha}\sum_0^{\infty}\alpha^n} = \frac{n\alpha^{n-1}}{\frac{\partial}{\partial\alpha}\left(\frac{1}{1-\alpha}\right)} = \frac{n\alpha^{n-1}}{(1-\alpha)^{-2}}$$

or

$$W_n = n\alpha^{n-1}(1-\alpha)^2 \quad (44)$$

Bringing in logarithmic form the equation (44) we have:

$$\ln W_n = \ln n + (n-1)\ln\alpha + 2\ln(1-\alpha)$$

$$\ln\left(\frac{W_n}{n}\right) = (n-1)\ln\alpha + 2\ln(1-\alpha)$$

$$\ln\left(\frac{W_n}{n}\right) = n\ln\alpha - \ln\alpha + 2\ln(1-\alpha)$$

$$\ln\left(\frac{W_n}{n}\right) = n\ln\alpha + \ln\frac{(1-\alpha)^2}{\alpha}$$

α is identified by the slope of the straight line obtained by plotting the log (Wn/n) as a function of n. The quality and the defect of the ASF model is its simplicity: one is in fact arises because of its ease of use across the agreement with experimental data is not always fully satisfactory, in fact the equation provides undifferentiated products while in reality various species are summarized.

In this file are calculated different values of α depending on the range of carbon atoms: C_3-C_{12}, C_{13}-C_{30}, C_3-C_{30}. Furthermore, it was calculated an α value for the range C_1-C_6 because it is common to all the catalysts: in fact, the nature of the tests performed on the various samples kinetics do not guarantee the α of the other range.

Mathematically α is calculated from:

- the moles of carbon/min of the various components;
- from the moles of carbon/min it is possible to find the moles of each component with the formula:

$$mol \quad to \quad carbon_i = \frac{mol \quad C_i}{\min} \cdot 60\left(\frac{\min}{h}\right) \cdot time \quad reaction(h)$$

- From the moles it is possible to get the grams of each component:

$$g_i = mol \quad C_i(mol) \cdot PM\left(\frac{g}{mol}\right)$$

- Wn is calculated (weight fraction) for each component

$$W_{n_i} = \frac{g_i}{\sum_{i=1}^{n} g_i}$$

- calculating the value of Wn/n (where n is the number of carbon atoms) for each component;
- calculating the $\ln(W_n/n)$.

By plotting the logarithm of the value of Wn/n as a function of the number of carbon atoms (n) is obtained a straight line whose slope gives the value of α desired.

4.2.5 Hydrogen

Hydrogen balance (Fig. 4.33f):

This data page allows to calculate the conversion of hydrogen and also the% of H_2 in the gas mixture leaving from the reactor.

H_2 Conversion					
Area H2	Area N_2	Real Flow mix [Nml min^{-1}]	Flow H2 OUT [Nml min^{-1}]	CONV. H2 (%)	(%) H2

As for the CO, from the analysis at the micro-GC we get the chromatographic areas of H_2 and N_2 that are used to calculate the outlet flow from the Fischer-Tropsch plant of carbon monoxide by the formula:

$$flow \quad H_{2_{OUT}} = \frac{Area \quad H_2}{Area \quad N_2} \cdot \frac{flow \quad N_{2_{OUT}}}{7.001}$$

where 7.001 is the correction factor determined by the calibration of the micro-gas chromatograph. As the output flow of nitrogen is equal to that in the input will have:

$$flow \quad H_{2_{OUT}} = \frac{Area \quad H_2}{Area \quad N_2} \cdot \frac{5{,}02}{7{,}001}$$

At this point we can calculate the conversion of H_2 by the formula

$$Conversion \quad H_2 = \frac{flow \quad H_{2_{IN}} - flow \quad H_{2_{OUT}}}{flow \quad H_{2_{IN}}}$$

The% H_2 is necessary to obtain the number of moles of hydrogen present in the gaseous stream leaving from the reactor, it is calculated through the formula:

$$\%H_2 = \frac{flow \quad H_{2_{OUT}}}{flow_{TOT}} \cdot 100$$

Hydrogen Balance

Also the balance of the hydrogen is performed at the end of the kinetic and it is calculated with the following formula:

$$\frac{moles \quad H_{2_{IN_{from\_H2}}} - moles \quad H_{2OUT_{from\_Mix}} - moles \quad H_{2OUT_{light}} - moles \quad H_{2OUT_{heavy}} - moli \quad H_{2OUT_{water}}}{moles \quad H_{2_{IN_{from\_H2}}}}$$

where:

1. $moles \quad H_{2OUT} \quad water = \frac{weight \quad _{aqueous \quad phase}}{18}$

2. $moles \quad H_2 \quad fom \quad organic \quad phase = \frac{weight \quad organic \quad phase}{PM_{CH_2}}$

The use of the molecular weight of methylene is because the CH_2 is the segment that grow joining to other segment of CH_2 to give the different hydrocarbons.

3. moles of H_{2OUT} light are the moles obtained by the summation of moles of H_{2OUT} of light hydrocarbons through the formula:

$$moles \quad H_{2OUT} \quad light = \frac{ml \quad gas_{OUT} \cdot n°H_i \cdot \% \quad compound_j \cdot 0{,}01}{22{,}4 \cdot 2}$$

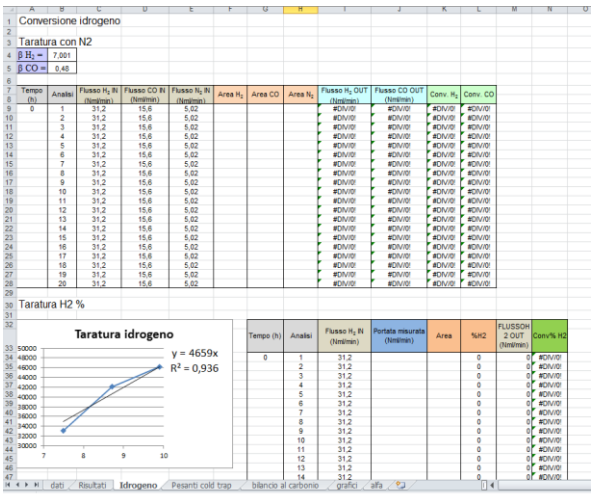

Fig. 4.33f. Example of "hydrogen balance" in FT data elaboration excel file

4.2.7 Oxygen Balance

As for the other two balances also the oxygen balance is carried out at the end of the kinetic run and it is calculated using the formula:

$$\frac{moles \quad O_{IN_{from\_CO}} - moles \quad O_{OUT_{from\_CO}} - moles \quad O_{OUT_{from\_CO_2}} - moles \quad O_{OUT_{fom\_H_2O}}}{moles \quad O_{IN_{from\_CO}}}$$

Where:

1. $moles \quad O_{OUT} \quad water = \dfrac{weight_{aqueous \ \ phase}}{18}$

2. $moles \quad O_{OUT} \quad CO_2 = \dfrac{ml \quad gas_{OUT} \cdot \% \quad CO_2 \cdot 0{,}01 \cdot 2}{22{,}4}$

In the calculation of the oxygen balance are not considered the oxygenated products while the moles of O_{IN} from CO and the moles of O_{OUT} from CO are respectively equal to the moles of CO_{IN} and CO_{OUT} from CO.

b) Seconf FTS unit (Unit 2)

The shape of the file excel is presented in a different way, but the equations are the same equations presented before (See First FTS unit in this chapter). The file is split in eleven pages: XCO, %CH4, %CO2, TCD, data, media, paraffins, fractions (1-4). As example the pages of one FT run (made with a Co based hydrotalcites catalyst Co35_2d) are reported in Fig. 4.34a-d:

TCD: In Fig. 4.34a-b are shown the conditions related to the number of tests carried out by the gas chromatograph, the time at which the analysis were made and the outside temperature at the time of sampling; the CO Conversion, that is referred to the quantity of gas reacted or converted referred to the gas entering inn the plant. From the gas chromatograph are taken the chromatographic areas of CO, CH_4, CO_2 and N_2 and used to calculate the selectivity.

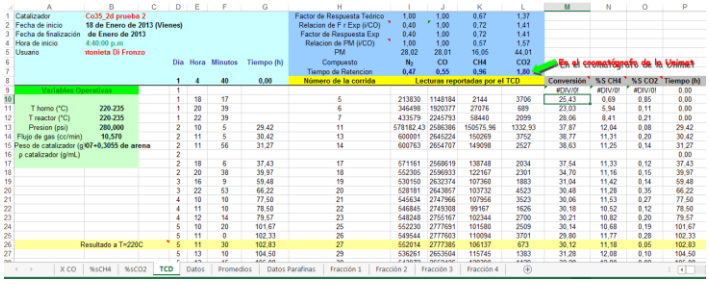

Fig. 4.34a Example of "data page _ TCD" in FT data elaboration excel file

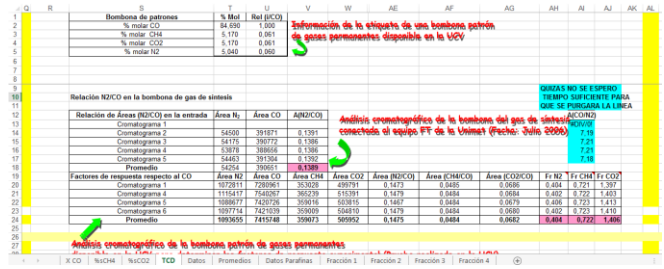

Fig. 4.34b Example of "data page _ TCD" in FT data elaboration excel file

Datos: In Fig.4.34 c is shown the information related to the selectivity of light hydrocarbons

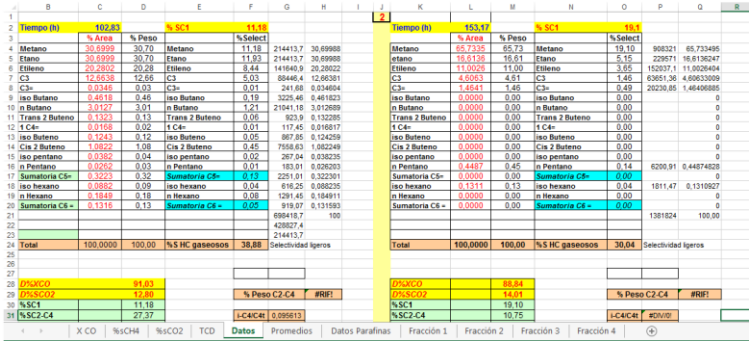

Fig. 4.34 c Example of "light hydrocarbons analysis page" in FT data elaboration excel file

In Fig. 4.34d the calculation of α is then performed making a diagram in which the $\log\left(\frac{W_n}{n}\right)$ is reported vs the carbon atom number.

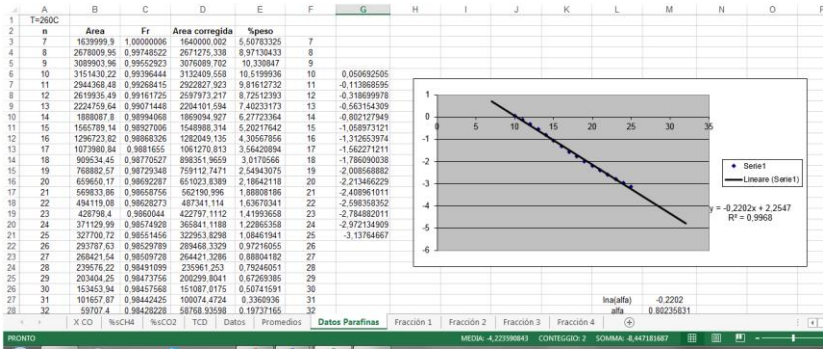

Fig. 4.34 d Example of "α calculation page" in FT data elaboration excel file

4.3 Novelties on the FT plant made in this PhD work

In the second year of the PhD, the reactor used in the laboratory at the "Università degli Studi di Milano", was brought in "Brignole" Company (Legnano – MI) for a general control and revision.

In this long revision, some fundamentals improvements have been made on the FT plant:

all the analytical procedures were optimized, verified and calibrated.

A new flowmeter was included in the feed, verified and calibrate

References

[1] C.L.Bianchi, C. Pirola, V. Ragaini, Cat Comm. 7 (2006) 669

[2] M.L. Cubeiro. López, A. Colmenares, L. Texeira, M. Goldwasser, M. J. Pérez, F. Machado, F. González, Applied Catalysis A: General 167 (1998) 183-193

[3] C. Pirola, C. L. Bianchi, A. Di Michele, P. Diodati, S. Vitali, V. Ragaini, Catal. Lett. 131 (2009) 294–304

[4] C. Pirola, C.L. Bianchi, A. Di Michele, S. Vitali, V. Ragaini, Catal. Comm. 10 (2009) 823–827

[5] C. Pirola, PhD 2007-2008, Novel supported iron based Fischer-Tropsch catalysts: Preparation, characterization and applications. Chapter 5

[6] Abelló, S; Montané, D. ChemSusChem 2011, 4, 1538−1556]

[7] Qinghong Z, Weiping D, Ye W. Review. Recent advances in understanding the key catalyst factors for Fischer-Tropsch synthesis. J Ener Chem 2013; 22:27–38

Chapter 5. Catalysts preparation and characterization

A serious of catalysts were prepared according different method of synthesis and using cobalt and iron depending on the kind of the study.

The catalysts reported in Table 5.1 are divided in two classes:

1) Catalysts of cobalt based, divided into two more groups
    a. Co based hydrotalcites with different amount of cobalt (5-35% wt.), prepared with an innovative method of synthesis (urea method).
    b. Co based catalysts with 8%wt of cobalt with different supports (SiO_2, Al_2O_3 or TiO_2) and the same samples with the addition of 0.1% of ruthenium carbonyl, all of them synthesized with the help of ultrasound.
2) Catalysts of iron (30% wt) with fixed (optimized) loading of promoters (K=2.0%; Cu=3.75%) and different method of synthesis;

The catalysts of the first series (Co), subdivided in two more groups (HTlc and bimetallic with the help of ultrasound), were studied to verify the activity of this new kind of catalysts in the CO hydrogenation.

More specifically, the hydrotalcites, were proposed as a new kind of catalysts, in which the active metal is part of the structural core of the HTlc, has been synthesized and tested. Activity tests conducted in a fixed bed reactor resulted in satisfactory catalytic performances as we will discuss later. Moreover, the structural and catalytic properties of these materials were verified at FTS operating conditions and correlations between catalyst features and efficiency

towards light and heavy hydrocarbons selectivities were achieved. And the cobalt based catalysts synthesized with the help of ultrasound (US) were studied to test the effects of sonochemical synthesis to prepare novel supported materials with particular properties as nanostructured catalysts [1]. The chemical effect of ultrasound arises from acoustic cavitation, i.e. the formation, growth and implosive collapse of bubbles in a liquid. Some of the interesting features resulting from the application of sonication as a synthetic method are the nanoparticles preparation, showing a more uniform size distribution, higher surface area and a more controlled phase composition. The use of high power ultrasound for long time is a difficult procedure because it is a critical point the control of the thermal stability of the ultrasound horn. In this PhD's work the possibility to use an ultrasound assisted synthesis of Co-based catalysts, by high power ultrasound for a long time, has been investigated using an innovative experimental apparatus equipped with a new cooling system, able to maintain stable the temperature US emitting horn.

The catalysts of the second series (Fe) were studied to verify the effect of the different methods of synthesis and the variation of the H_2 /CO ratio in order to simulate a feed with biosyngas and for an ulterior study about the develop of a kinetic model. The selection of this specific amount of Fe (30% wt.) and promoters (Cu and K with 2.0% wt. and 3.75%wt. respectively) was taken from a previous research [2] in which the effect of these amounts was extensively studied.

Promoters influence the bond strength of hydrogen and carbon oxide to metal. Addition of alkali metals (K in particular) to iron catalysts promotes electron transfer to the iron and inhibits hydrogen adsorption, because adsorption of hydrogen induces electron donation to the iron surface. Moreover K promotion

increases the electron density in iron and will result in an increase of CO adsorption. On Fe stronger metal-carbon bonds will lead to C_{2+} formation, and then to a low methane selectivity [3]. Copper promotes the reduction of iron oxide phases: from hematite (Fe_2O_3) to magnetite (Fe_3O_4), and then from magnetite to iron metal. A suggested mechanism for this promotion effect is the migration of atomic hydrogen from reduced Cu sites to the iron oxide. The copper needs to be very well mixed with iron oxide to provide the most favourable promoter effect [4].

An innovative preparation procedure with the use of Ultrasound and Microwave has been used with the iron based catalysts.

In Table 5.1 a general summary of all the prepared catalyst is reported.

Table 5.1. Summary of the catalysts synthesized and tested.

Metal	Catalysts	Samples
Co	HTlc	Co5
		Co 10
		Co 15
		Co 35
	Bimetallic US	Co/TiO_2
		Co/SiO_2
		Co/Al_2O_3
		$Co\text{-}Ru/TiO_2$
		$Co\text{-}Ru/SiO_2$
		$Co\text{-}Ru/Al_2O_3$
Fe	Traditional	$Fe_{30}K_{2.0}Cu_{3.75}/ SiO_2$ At different temperature and H_2/CO ratio: 2/1; 1.5/1;1/1
	Traditional + MW	MW1
		MW2
	Traditional + US	US1
		US2
	Co-precipitation*	Fe/SiO_2-TEOS.

The catalysts were characterized by TPR, BET, SEM, TEM, ICP, FT-IR, micro-RAMAN techniques in their fresh form (before the use in FT reactor) and in some cases after different activation procedure or after FT runs.

The physical properties of the catalysts (surface area and morphology) were investigated by BET, SEM and TEM analyses. The theoretic catalysts composition has been investigated and verified both qualitatively, using SEM-EDS, FT-IR and micro-RAMAN techniques, and quantitatively, using ICP characterization. The reduction behaviour of metal phase has been investigated by TPR analyses.

5.1 Catalysts preparation

5.1.1 Catalyst preparation procedure

5.1.1.1 Cobalt based catalysts

Two different types of cobalt based catalysts were prepared during this research. The synthesis is presented in the next paragraphs.

Co based Hydrotalcites by a modified urea method:

A series of ternary HTlc, with general formula $[Co_xZn_{(1-x-y)}Al_y(OH)_2](NO_3)_y \cdot 0.5H_2O$, was synthesized by a modified-urea method [5]. Different volumes of the solutions of the metal nitrates, all at a concentration of 0.5 M, were mixed to obtained either a Al/(Co+Al) or Al/(Co+Al+Zn) molar ratio of 0.3.

Solid urea was added to the solutions, in a molar ratio of 4 vs. Al. The obtained solutions were maintained at the reflux temperature in an open flask for 48 h. The precipitates were separated by centrifugation, washed with water, and then dried at 80°C.

Co based catalysts with the help of ultrasound

All the catalysts were prepared by a modified impregnation method. The metal precursors (cobalt and ruthenium carbonyl) were dissolved in n-decane together with the different support (SiO_2, Al_2O_3 or TiO_2). The solution was irradiated by an US horn (Fig. 5.1) for 3 h at 20 kHz at 300 W, and then put into a rotating vacuum oven at 40°C at 36 rpm for 24 h (impregnation step). Samples have been calcinated at 350 °C for 4 h.

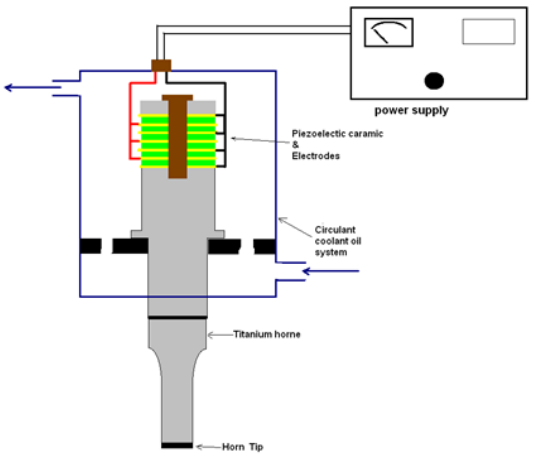

Fig. 5.1 Ultrasound horn with a cooling jacket where the coolant has two main characteristics: low viscosity at low temperature and dielectric liquid

5.1.1.2 Iron based catalysts

Four different types of iron based catalysts were prepared during this research. The methods used were the traditional impregnation method, the co-precipitation method and the traditional impregnation method with the help of microwave and ultrasounds.

Fe based catalysts by the Traditional Impregnation method:

The iron based supported on silica catalysts were prepared according to the traditional impregnation method, completely described in a previous work [6], starting from an aqueous solution of precursors and adding in a second time

the support (silica). The reagents used for the samples preparation are reported in Table 5.2

Table 5.2. Reagents used in the catalysts preparation $Fe_{30}K_{2.0}Cu_{3.75}/ SiO_2$

	Reagent	Main characteristics
Support	SiO_2	Company: Fluka (cod. 60740) Mesh: 70-230, 60 Å Molecular weight: 60,086 g/mol Purity: > 99% Superficial area: 500 m^2/g
Precursors	$Fe(NO_3)_3 \cdot 9H_2O$	Company: Riedel de Hean Molecular weight: 403,85 g/mol Purity: 98%
	KNO_3	Company: Merk Molecular weight: 101,11 g/mol Purity: > 99%
	$Cu(CH_3COO)_2 \cdot H_2O$	Company: Fluka Molecular weight: 199,65 g/mol Purity: 99%
Solvent	Extra pure water	

The standard methodology for the catalysts preparation is the following:

- Drying of silica in oven (T=120°C) for a night;
- Weigh of the calculated amount of iron, potassium and copper precursors
- In a pyrex vessel (250 ml) the weighed precursors, the water (25 ml) and silica (5 g) are added
- The vessel is put on a rotavapor (36 rpm, T=40°C, P = 1 bar) for 24 hours (Fig. 5.2)
- The solvent is evaporated (T = 80°C)
- The powder is dried in oven (T=120°C) for 4 hours
- Calcination (T = 500°C) in air for 4 hours

* The catalyst is sieved to obtain a powder mesh between 100 and 140

Fig. 5.2. Rotavapor used for catalyst preparation

The amount of precursors is calculated starting from the equation (1) to have the requested iron percentage in the not promoted catalysts:

$$\frac{gFe}{gFe + gSiO_2} = \%Fe \tag{1}$$

Then the moles of iron are equal as the moles of his precursor (moles Fe = moles $Fe(NO_3)_3.9H_2O$). The grams of precursors are calculated multiplying the moles for the molecular weight of $Fe(NO_3)_3.9H_2O$. This quantity must be divided for the purity grade of precursor.

For the promoted catalysts the amount of precursors is calculated using the following equations:

$$\frac{gFe}{gFe + gK + gCu + gSiO_2} = \%Fe \tag{2}$$

$$\frac{gK}{gFe + gK + gCu + gSiO_2} = \%K \tag{3}$$

$$\frac{gCu}{gFe + gK + gCu + gSiO_2} = \%Cu \tag{4}$$

The equation (2), (3) and (4) must be solved as equations system. The moles of Fe, K and Cu are equal as the moles of respective precursors. The grams of precursors are calculated multiplying the moles for the molecular weight of $Fe(NO_3)_3.9H_2O$, KNO_3 and $Cu(CH_3COO)_2H_2O$ respectively. This quantity must be divided for the purity grade of each precursors.

Specifically for the preparation of a catalyst having 30% wt. of iron, 2%wt. of potassium and 3,75%wt. of copper on silica:

$$\frac{gFe}{gFe+gK+gCu+5g}=0{,}30 \Rightarrow gFe=2{,}335$$

$$\frac{gK}{gFe+gK+gCu+5g}=0{,}02 \Rightarrow gK=0{,}156$$

$$\frac{gCu}{gFe+gK+gCu+5g}=0{,}0375 \Rightarrow gCu=0{,}292$$

moles Fe = $\frac{2{,}335g}{55{,}847g/moles}$ *=0,0418 moles*

moles K = $\frac{0{,}156g}{39{,}0983g/moles}$ *= 0,00398 moles*

moles Cu = $\frac{0{,}292g}{63{,}546g/moles}$ *= 0,0046 moles*

g $Fe(NO_3)_3 \cdot 9H_2O$ *= 0,0418 moles·403,85 g/moles = 16,882 g*

g KNO_3 *= 0,00398 moles·101,11g/moles = 0,4024 g*

g $Cu(CH_3COO)_2 \cdot H_2O$ *= 0,0046 moles·199,65 g/moles = 0,9168 g*

and the grams required to prepare the catalysts are:

$\frac{16{,}882g}{0{,}98}$ *=17,227 g* $Fe(NO_3)_3 \cdot 9H_2O$

$\frac{0{,}4024g}{1}$ = *0,4024 g* KNO_3

$\frac{0{,}9168g}{0{,}99}$ = *0,9261 g* $Cu(CH_3COO)_2 \cdot H_2O$

Fe based catalysts by the Traditional Impregnation method with the help of microwave (MW)**:**

For the synthesis of the catalysts with the aid of microwave (MW) a final step where the powder of catalyst, already calcined, is subjected to a MW irradiation was added. Two different methods for the MW irradiation were used. In the first one (MW1), a sample of catalyst was put into a beaker and then into a classical microwave oven (Moulinex, Micro-Chef 1305E, 600W) for 30 min.

In the second method (MW2), the catalyst (2 g) was suspended in hexane (400 ml), put into a microwave chemical reactor (ordinary 400 mL round bottom glass flask, filled with the liquid to be heated and activated) and treated for 1 h at 60W. MW were produced by a MW generator, and sent to the MW applicator by an insulated coaxial antenna. Details of the MW applicator and of the associated experimental techniques can be found in [7].

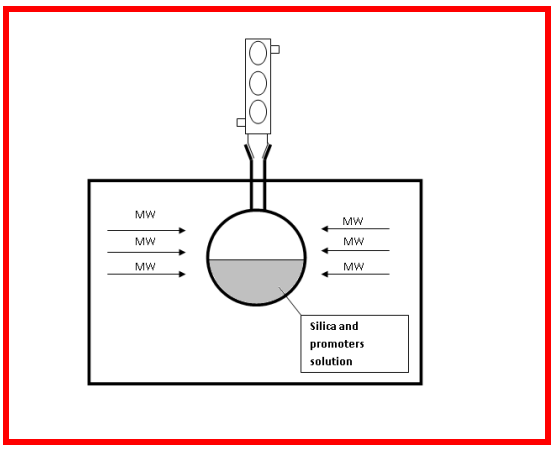

Fig. 5.3. Microwave (MW) Power (35-300 W). Treatment duration. (60 min). Atmosphere (air)

Fe based catalysts by Traditional Impregnation method with the help of ultrasound (US)**:**

In this particular preparation method a step using ultrasound (US) has been added. Ultrasound is simply sound pitched above the frequency bond of human hearing. It is a part of sonic spectrum that ranges from 20 kHz to 10 MHz and corresponds to the wavelengths from 10 to 10^{-3} cm [8]. The application of ultrasound, in connection to chemical reactions, is called sonochemistry. The range from 20 kHz to around 1 MHz is used in sonochemistry, since acoustic cavitation in liquids can be efficiently generated within this frequency range [9]. However, common laboratory equipment utilizes the range between 20 and 40 kHz. The Ultrasound are often used in the preparation of supported catalysts (some examples are reported in ref [10]), and their useful contribution concerns for example the dispersion of metal, the size of particles, the surface area and the advantage is evident in the performance of catalyst in many cases, both in term of conversion and of process selectivity [11].

The use of ultrasound may be very efficient to optimize the dispersion of high metal charge, as already verified in our laboratory in the past [2, 12-13]

US treatment has been performed between the impregnation and the evaporation step by irradiating the silica-precursors solution using a Sonicator (W-385 Heat Systems Ultrasonics) with an effective input power of 60 W and a tip diameter of 13 mm (Fig.5.4 and Fig. 5.5). Silica solution, promoters and water have been sonicated by the US horn for 0.5 h in air (US1). The same sample was successively sonicated in a suspension of hexane in argon for 3h (US2).

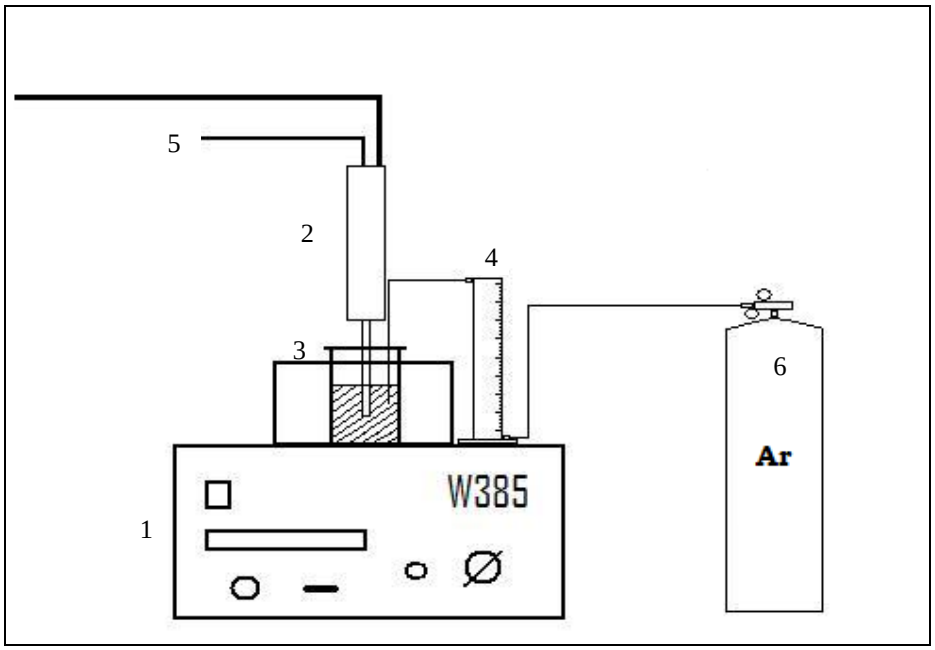

Figura 5.4: Diagram of sonication step

1. Sonicator US (W-385 of Heat Systems Ultrasonics),
2. Emitter head of US equipped with a titanium tip of 13 mm;
3. Beaker with the solution immerse in a bath of water/ice;
4. Flow meter of Ar ;
5. Connection with air;
6. Argon Cylinder.

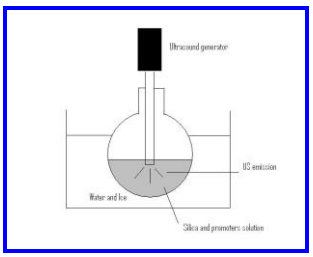

Fig. 5.5 Detail of the US treatment step: 20 kHz; 60 W; tip diameter of 13 mm; US switched on and off alternatively for 0.5 seconds (pulsed US), t =30 min.

Fe based catalyst by the co-precipitation method with TEOS:

Acidic silica sol (ASS) and tetraethoxysilane (TEOS) are widely used as silica sources of Fe/SiO2 catalysts [14-15], which can be incorporated into iron catalyst matrix during the precipitation of catalyst precursors and have an obviously dispersive effect on the iron oxide phase. It is well known that the tetraethoxysilane (TEOS) is insolvable in aqueous solutions but can slowly hydrolyze to hydrophilic silica sol/gel [16]

In the TEOS- water system, acid or basic can catalyze the hydrolysis of TEOS [17]. In the process of the co-precipitation, TEOS hydrolyzes into silica accompanied by the precipitation of ferric ions, whereas the silica particles in ASS may directly interact with ferric ions. The different properties of two silica sources should lead to a great diversity in both the structures and the physicochemical properties of catalysts, such as morphology, dispersion, phases, chemisorption, Fe-SiO_2 interactions and so on.

As a Fe/SiO_2 catalyst was prepared by a co-precipitation method using TEOS. The detailed process of the co-precipitation method has been described elsewhere [18]. In brief, an alcoholic solution of TEOS was mixed with an aqueous solution of iron nitrate with a Fe/Si atomic ratio of 100/25. The mixed solution was precipitated using an ammonium solution at 80 °C and a pH value of 8.5-9.0. After precipitation, the precipitates were aged for 2 h, washed and filtered. Then, the filtered cakes were dried at 120 °C overnight and calcined at 500 °C for 5 h. The catalyst was denoted as Fe/SiO_2-TEOS.

Some calculations have been made to prepare the catalyst.

To prepare 50ml 1M of solution of TEOS

$$ml\ TEOS = 1\frac{mol\ TEOS}{l} \cdot 0.05l \cdot \frac{208.33g\ TEOS}{1mol\ TEOS} \cdot \frac{1\ ml\ TEOS}{0.94\ g\ TEOS} \cdot \frac{1}{0.99} = 11.20\ ml\ TEOS$$

To prepare a catalyst with a Fe/TEOS= 4/1 ratio and using 1g of Fe are required:

To prepare the catalysts is required a ratio Fe/TEOS=4/1, that's mean 1g of Fe correspond with 0,25g of TEOS.

$$molFe = \frac{1gFe}{55{,}847\,g/molFe} = 0{,}0179molFe$$

$$gFe(NO_3)_3 \cdot 9H_2O = 0{,}0179molFe \cdot \frac{1molFe(NO_3)_3 \cdot 9H_2O}{1molFe} \frac{403{,}52gFe(NO_3)_3 \cdot 9H_2O}{molFe(NO_3)_3 \cdot 9H_2O} \cdot \frac{1}{0{,}98} = 7{,}38gFe(NO_3)_3 \cdot 9H_2O$$

$$mlTEOS = 0{,}25gTEOS \frac{1molTEOS}{208{,}33gTEOS} \cdot \frac{1lsol1M}{1mol} \cdot \frac{1000ml}{1l} = 1{,}20ml$$

- 700ml of distillate water was put into a beaker and heated at 77°C.
- $7{,}38gFe(NO_3)_3 \cdot 9H_2O$ and 1.20ml of TEOS were added
- Measurements of pH was taken until the solution acquired a pH between 8 and 9.
- Let stand for 2 hours
- The solvent is evaporated (T = 80°C)
- The powder is dried in oven (T=120°C) for 4 hours
- Calcination (T = 500°C) in air for 4 hours
- The catalyst is sieved to obtain a powder mesh between 100 and 140

5.2 Catalysts characterization:

5.2.1 Catalysis characterization: introduction and theory

According to [19] the basic catalyst characterization involves two main steps: the investigation on the porous nature of the catalyst support (physical properties) and on the properties of the active sites that are dispersed on the support surface (table 5.3).

The complete and accurate knowledge of the properties of a catalyst is fundamental for evaluating its performance. In this work there were used several techniques to investigate their physical and chemical properties.

The characterization has been made for the fresh catalysts, (after the calcination at 500°C and before their loading and activation or use in FT reactor) and in some cases after the activation and the FT reaction.

Table 5.3. General scheme of catalysts characterization [19]

Catalyst texture			
Physical properties		**Chemical properties**	
Result	**Technique**	**Result**	**Technique**
Geometry and shape	- Optical microscopy	Chemical composition	-Electron spectroscopy -Atomic adsorption
Total specific surface area	-Gas physisorption -Mercury porosimetry	Degree of dispersion	-Selective chemisorption -X-ray -Electron microscopy -Magnetisation analysis
True density	-X-ray analysis -Neutron diffraction	Degree of dispersion	-Selective chemisorption -X-Ray -Electron microscopy -Magnetisation analysis
Bulk and apparent density	-Helium pycnometry -Mercury porosimetry -Liquid displacement	Surface Energy	-Thermal analysis test -Temperature programmed desorption and reaction calorimetry
-Pore specific volume -Porosity	-Mercury porosimetry -Gas adsorption	Acid-base sites	-Selective chemisorption -Temperature programmed desorption
Pore size and mean pore size	-Mercury porosimetry -Gas Adsorption	Redox sites	-Spectroscopic methods -Temp. programmed reduction -Temp. Programmed oxidation
Particle size	-Sieves -Laser scattering -Sedimentation -Electrical sensing zone -Etc.	-Catalytic properties -Activity -Selectivity	Reactor tests and simulation
Surface structure	-Optical microscopy -Electron microscopy -X-Ray analysis		
Surface change	Z potential		

A brief description of the different techniques used in this work will be presented as follow:

- BET (adsorption method for surface area evaluation),
- SEM
- TEM (electron microscopy),
- FT-IR and RAMAN (vibrational spectroscopy for chemistry of surface groups),
- TPR (study of catalyst reduction vs. temperature),
- TPD
- ICP (quantification of element inside the catalyst).
- XRD

5.2.1.1 BET analysis (adsorption method for surface area evaluation)

According to [20] the most widely used method for determining surface area involves measuring the amount of gas adsorbed on a solid surface at a temperature close to the boiling point of the gas. Nitrogen is most commonly used as the adsorbate.

The interaction between the adsorbate and the adsorbent may be chemical (chemisorption) or physical (physisorption) in nature and ideally should be a surface-specific interaction. If the adsorption is measured at several gas pressures, the Brunauer- Emmett-Teller (BET) [21] equation can be used to calculate the amount of adsorbate required to form a monolayer [22]. This technique of characterization of solid has the particular equation that allows to determine a parameter of great importance in the study of the solid ones that is the superficial specific area. Such parameter expresses the relationship between the total surface of the catalyst and the weight of the same one and usually is expressed in m^2/g. Technique BET uses the principle of the physical inert gas adsorption (nitrogen) to varying of the relationship between the

partial pressure of nitrogen and its vapor pressure to the temperature of liquid nitrogen. The technique can be carried in static or dynamic conditions. Opportune procedures of calculation allow also to determine the distribution of the pores in the field of mesoporosity. BET theory is a well-known rule for the physical adsorption of gas molecules on a solid surface, that is basis for an important analysis technique for the measurement of the specific surface area of a material. The concept of the theory is an extension of the Langmuir theory, which is a theory for monolayer molecular adsorption, to multilayer adsorption with the following hypotheses: (a) gas molecules physically adsorb on a solid in layers infinitely; (b) there is no interaction between each adsorption layer; and (c) the Langmuir theory can be applied to each layer. The resulting BET equation is the following:

$$\frac{V}{V_m} = \frac{c\frac{p}{p^\circ}}{\left[1-\left(\frac{p}{p^\circ}\right)\right]\left[1+(c-1)\frac{p}{p^\circ}\right]} \qquad (5)$$

Where:

V = volume of adsorbed gas at pressure P

p° = gas saturation pressure, at temperature T

p/p° = relative pressure

C = BET constant, expressed by the following:

$$C = \exp\left((q_1 - q_L)/RT\right) \qquad (6)$$

Where

q_1 = heat of adsorption of the first layer

q_L = heat of adsorption of the second and higher layers

For the V_m calculation the (6) must be linearized and the linear relationship of this equation is maintained only in the range of $0.05 < P / P_0 < 0.35$:

$$\frac{\frac{p}{p^\circ}}{V\left[1-\left(\frac{p}{p^\circ}\right)\right]} = \frac{1}{CV_m} + \frac{(c-1)\frac{p}{p^\circ}}{cV_m} \qquad (7)$$

Equation (7) is an adsorption isotherm and can be plotted as a straight line with 1 / V[(*P*° / *P*) − 1] on the y-axis and *P* / P_0 on the x-axis according to experimental results. The specific surface area is determined on the V_m basis:

$$S.A. = \frac{V_m . N_{AV} . A_{mol}}{V_{mol}} \qquad (8)$$

Where:

N_{AV} = Avogrado's number

A_{mol}= adsorption cross section (for N_2 = 16.2 $Å^2$)

V_{mol}= molar volume of gas (22414 ml/mol)

Experimental: The samples have been analyzed using a Costech Sorptometer 1042 "KELVIN", using liquid nitrogen. Before the analysis, the catalyst is put in oven (T = 110°C for 16 h) to remove the adsorbed water. Then a quantity between 0.08 g and 0.2 g in analyzed in the instrument. The sample is pre-treated for 2 h at T = 200°C in a N_2 flow to remove all the impurity, then a check with helium is made to calibrate the interspatial volume.

5.2.1.2 Temperature programmed reduction. TPR analysis [19]

Some aspects related to catalysts characteristic and behaviour will be treated as determination of metal surface area and dispersion, spillover effect and synterisation. A description of the available techniques will follow, taking in consideration some aspects of the gas-solid interactions mechanisms (associative/dissociative adsorption, acid-base interactions, etc.).

The thermal analysis methods may be used with different objectives: the reaction or desorption profile may be used qualitatively to fingerprint a given system and then it is possible to make a quantitative considerations about the nature of chemical processes, the amount of gas involved in the chemical reaction and finally to calculate the number of the active sites, the reducibility degree of the sample related to the catalytic activity. All the methods relating some characteristic properties of a catalyst to its temperature during a programmable heating ramp are named commonly in the field of the thermal analysis.

The thermal analyses are often used to investigate surface modifications and bulk reactivity by varying the surface composition, the catalyst preparation method, the pre-treatment for catalyst activation and the analytical conditions. The TPR/O involve a bulk reaction.

The objectives of the programmed reduction (TPR) are essentially the following: 1) to find the most efficient reduction conditions; 2) to identify the supported precursor phases and their interactions with the support, 3) to characterize complex systems, as bimetallic or doped catalyst, to determine the role of the second component ant to establish alloy formation or promotion effects. There are several interesting studies about this technique: Robertson et al. [23] first reported TPR profile of nickel and nickel-copper catalysts and since then many catalysts have been investigated. In the TPR technique an oxided catalyst precursor is submitted to a programmed temperature rise, while a reducing gas mixture is flowed over it (usually, hydrogen diluted in some inert gas as nitrogen or argon). An interesting application of this technique is that the TPR/O analysis may be used to obtain evidence for the interaction between the atoms of two metallic components, in the case of bimetallic system or alloy as already cited. In general, TPR/TPO studies are

carried out under low partial pressure of the reactive gas. In this way it is possible to observe the intermediate reactions, depending from analytical conditions as temperature rate, flow rate and concentration of reactive gas.

Experimental:

- Conventional temperature-programmed reduction experiments (TPR) were performed on the calcined catalysts using a TPR/D/O110 instrument (Thermoquest). The samples were initially pre-treated in flowing argon at 200°C for 0.5 h. After being cooled to 50°C, the H_2/Ar (5.1% v/v) reducing mixture flowed through the sample at 30 ml/min while the temperature was increased from 50 to 900°C at constant rate of 8 °C/min.

5.2.1.3 SEM and TEM analysis

In electron microscopy as in any field of optics the overall contrast is due to differential absorption of photons or particles (amplitude contrast) or diffraction phenomena (phase contrast). The method provides identification of phases and structural information on crystals, direct images of surfaces and elemental composition and distribution. Routine applications, however, may be hampered by complexities of image interpretation and by constraints on the type and preparation of specimens and on the environment within the microscope.

The scanning electron microscope (SEM) is a type of electron microscope that creates various images by focusing a high energy beam of electrons onto the surface of a sample and detecting signals from the interaction of the incident electrons with the sample's surface. The type of signals gathered in a SEM varies and can include secondary electrons, characteristic x-rays, and back scattered electrons. In a SEM, these signals come not only from the primary

beam impinging upon the sample, but from other interactions within the sample near the surface. The SEM is capable of producing high-resolution images of a sample surface in its primary use mode, secondary electron imaging. Due to the manner in which this image is created, SEM images have great depth of field yielding a characteristic three-dimensional appearance useful for understanding the surface structure of a sample. This great depth of field and the wide range of magnifications are the most familiar imaging mode for specimens in the SEM. Characteristic x-rays are emitted when the primary beam causes the ejection of inner shell electrons from the sample and are used to tell the elemental composition of the sample. The back-scattered electrons emitted from the sample may be used alone to form an image or in conjunction with the characteristic x-rays as atomic number contrast clues to the elemental composition of the sample. The SEM was pioneered by Manfred von Ardenne in 1937 [24] and [25]. The instrument was further developed by Charles Oatley and first commercialized by Cambridge Instruments. The spatial resolution of the SEM depends on the size of the electron spot, which in turn depends on both the wavelength of the electrons and the magnetic electron-optical system which produces the scanning beam. The resolution is also limited by the size of the interaction volume, or the extent to which the material interacts with the electron beam. The spot size and the interaction volume both might be large compared to the distances between atoms, so the resolution of the SEM is not high enough to image individual atoms, as is possible in the shorter wavelength (i.e. higher energy) transmission electron microscope (TEM). The SEM has compensating advantages, though, including the ability to image a comparatively large area of the specimen; the ability to image bulk materials (not just thin films or foils); and the variety of analytical mode available for measuring the composition and nature of the specimen. Depending on the

instrument, the resolution can fall somewhere between less than 1 nm and 20 nm. In general, SEM images are easier to interpret than TEM images.

According to [22] topographical images in a SEM are formed from back-scattered primary or low-energy secondary electrons. The best resolution is about 2-5 nm but many routine studies are satisfied with a lower value and exploit the case of image interpretation and the extraordinary depth of field to obtain a comprehensive view of the specimen. With non-crystalline catalysts, SEM is especially useful for examining the distribution and sizes of mesopores. An energy dispersive X-ray spectroscopy device is a frequent attachment in the instrument.

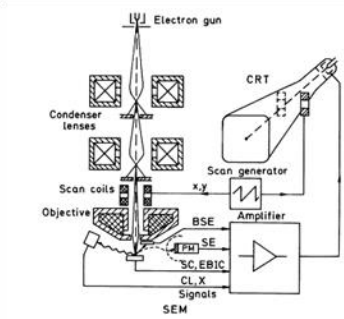

Fig. 5.6 Schematic ray path for a scanning electron microscope (SEM) [26]

Transmission electron microscopy (TEM) is a microscopy technique whereby a beam of electrons is transmitted through an ultra-thin specimen, interacting with the specimen as it passes through it. An image is formed from the electrons transmitted through the specimen, magnified and focused by an objective lens and appears on an imaging screen, a fluorescent screen in most TEMs, plus a monitor, or on a layer of photographic film, or to be detected by a sensor such as a CCD camera. The first practical transmission electron microscope was built by Albert Prebus and James Hillier at the University of

Toronto in 1938 using concepts developed earlier by Max Knoll and Ernst Ruska.

Theoretically the maximum resolution that one can obtain with a light microscope has been limited by the wavelength of the photons that are being used to probe the sample and the numerical aperture of the system. Early twentieth century scientists theorized ways of getting around the limitations of the relatively large wavelength of visible light (wavelengths of 400–700 nanometers) by using electrons. Like all matter, electrons have both wave and particle properties (as theorized by Louis-Victor de Broglie), and their wave-like properties mean that a beam of electrons can be made to behave like a beam of electromagnetic radiation. Electrons are usually generated in an electron microscope by a process known as thermionic emission from a filament, usually tungsten, in the same manner as a light bulb, or by field emission. The electrons are then accelerated by an electric potential (measured in V, or volts) and focused by electrostatic and electromagnetic lenses onto the sample. The beam interacts variously with the sample due to differences in density or chemistry. The beam that is transmitted through the sample contains information about these differences, and this information in the beam of electrons is used to form an image of the sample. The contrast in a TEM image is not like the contrast in a light microscope image. A crystalline material interacts with the electron beam mostly by diffraction rather than absorption, although the intensity of the transmitted beam is still affected by the volume and density of the material through which it passes. The intensity of the diffraction depends on the orientation of the planes of atoms in a crystal relative to the electron beam; at certain angles the electron beam is diffracted strongly from the axis of the incoming beam, while at other angles the beam is largely transmitted.

Just as details of a light microscope sample can be enhanced by the use of stains, staining can be used to enhance differences in a sample for electron microscopy. Compounds of heavy metals such as osmium, lead or uranium can be used to selectively deposit heavy atoms in areas of the sample and to enhance structural detail by the dense nuclei of the heavy atoms scattering the electrons out of the optical path. The electrons that remain in the beam can be detected using a photographic film, or fluorescent screen among other technologies. So areas where electrons have been scattered in the sample can appear dark on the screen, or on a positive image due to this scattering. TEM is suitable for examination of supported catalysts with particle sizes down to 2-3 nm, giving information on particle location over the support, on particle-size distributions in favourable cases, on particle and support morphology and on the nature and distribution of deposits having a thickness of the order of 2-3 nm. Surface topography can be examined using replication techniques. [22]

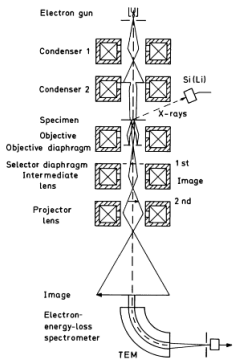

Fig.5.7 Schematic ray path for a transmission electron microscope (TEM) [26]

Experimental:

The **SEM analysis** have been made in collaboration with Perugia University. SEM images were measured using an electron microscopy Philips XL-30CP with RBS detector of back-scattered electrons and EDS analyzer was used to describe the surface and elemental composition of catalysts.

The **TEM analysis** have been made in collaboration with Perugia University. The morphology of the samples was investigated by a transmission electron microscope Philips 208 Transmission Electron Microscope (TEM), a drop of the dispersion was deposited on a copper grid covered with a polymeric film Formvar, subsequently evaporated in air at room temperature.

In order to obtain more accurate information concerning the atomic percentage of the elements on the surface, EDX measurements were made using the high-resolution TEM instrument, at the Department of Chemical Science and Technology and Biosystems studies at the University of Siena. This instrumentation allows to obtain with high precision information on the atomic percentage in different areas of the sample, going to select individual points or individual areas

5.2.1.4 FT-IR analysis

This vibrational spectroscopy is used for characterization of high area supported or unsupported catalysts. Information is available, either directly or by study of 'probe' adsorbates, on the chemistry of surface groups (particularly on oxides). It is also used for the study of the behavior of precursor compounds during catalyst preparation.

Infrared spectroscopy is the subset of spectroscopy that deals with the infrared region of the electromagnetic spectrum. It covers a range of techniques, the most common being a form of absorption spectroscopy. As with all spectroscopic techniques, it can be used to identify compounds or investigate sample composition. Infrared spectroscopy correlation tables are tabulated in the literature.

The infrared portion of the electromagnetic spectrum is divided into three regions; the near-, mid- and far- infrared, named for their relation to the visible spectrum. The far-infrared, approximately 400-10 cm^{-1} (1000–30 μm), lying

adjacent to the microwave region, has low energy and may be used for rotational spectroscopy. The mid-infrared, approximately 4000-400 cm^{-1} (30–1.4 μm) may be used to study the fundamental vibrations and associated rotational-vibrational structure. The higher energy near-IR, approximately 14000-4000 cm^{-1} (1.4–0.8 μm) can excite overtone or harmonic vibrations. The names and classifications of these sub regions are merely conventions. They are neither strict divisions nor based on exact molecular or electromagnetic properties.

Infrared spectroscopy exploits the fact that molecules have specific frequencies at which they rotate or vibrate corresponding to discrete energy levels. These resonant frequencies are determined by the shape of the molecular potential energy surfaces, the masses of the atoms and by the associated vibronic coupling. In order for a vibrational mode in a molecule to be IR active, it must be associated with changes in the permanent dipole. In particular, in the Born-Oppenheimer and harmonic approximations, i.e. when the molecular Hamiltonian corresponding to the electronic ground state can be approximated by a harmonic oscillator in the neighbourhood of the equilibrium molecular geometry, the resonant frequencies are determined by the normal modes corresponding to the molecular electronic ground state potential energy surface. Nevertheless, the resonant frequencies can be in a first approach related to the strength of the bond, and the mass of the atoms at either end of it. Thus, the frequency of the vibrations can be associated with a particular bond type.

Simple diatomic molecules have only one bond, which may stretch. More complex molecules have many bonds, and vibrations can be conjugated, leading to infrared absorptions at characteristic frequencies that may be related to chemical groups. For example, the atoms in a CH_2 group, commonly

found in organic compounds can vibrate in six different ways: symmetrical and antisymmetrical stretching, scissoring, rocking, wagging and twisting.

The infrared spectra of a sample are collected by passing a beam of infrared light through the sample. Examination of the transmitted light reveals how much energy was absorbed at each wavelength. This can be done with a monochromatic beam, which changes in wavelength over time, or by using a Fourier transform instrument to measure all wavelengths at once. From this, a transmittance or absorbance spectrum can be produced, showing at which IR wavelengths the sample absorbs. Analysis of these absorption characteristics reveals details about the molecular structure of the sample.

This technique works almost exclusively on samples with covalent bonds. Simple spectra are obtained from samples with few IR active bonds and high levels of purity. More complex molecular structures lead to more absorption bands and more complex spectra. The technique has been used for the characterization of very complex mixtures.

According to [10] problems in vibrational spectroscopy include low transmission at high metal loadings and strong oxide scattering. Absorption at lower wavenumbers often prevents observation of modes such as adsorbate-metal stretching. Fourier Transform (FI-IR) spectrometers offer two pronounced advantages over dispersive instruments: higher energy throughput and faster data acquisition or higher signal-to-noise ratio. Data processing is easy. These features are significant when examining very strongly absorbing and scattering solids and when following dynamic processes. Much IR transmission work, however, requires examination of only limited frequency ranges at medium resolution and computerised dispersive spectrometers may then be preferable.

Experimental: The FT-IR analysis have been made in collaboration with Perugia University. Infrared spectra were measured with a FTIR model IFS113V Bruker spectrometer, resolution of 1 cm^{-1} in the spectral region 370-5000 cm^{-1}.

Fig. 5.8 FTIR model IFS113V Bruker spectrometer

5.2.1.5 micro-Raman analysis

Raman spectroscopy is more versatile for catalysts characterization and in comparison with IR spectroscopy it presents at least two important advantages: there is no need of sample preparation and the spectra of water-metal interfaces are obtained easily and quickly.

Raman spectroscopy is a spectroscopic technique used in condensed matter physics and chemistry to study vibrational, rotational, and other low-frequency modes in a system [27]. It relies on inelastic scattering, or Raman scattering of monochromatic light, usually from a laser in the visible, near infrared, or near ultraviolet range. The laser light interacts with photons or other excitations in the system, resulting in the energy of the laser photons being shifted up or down. The shift in energy gives information about the phonon modes in the system. Infrared spectroscopy yields similar, but complementary information. Typically, a sample is illuminated with a laser beam. Light from the illuminated spot is collected with a lens and sent through a monochromator. Wavelengths close to the laser line, due to elastic Rayleigh scattering, are filtered out while

the rest of the collected light is dispersed onto a detector. Spontaneous Raman scattering is typically very weak, and as a result the main difficulty of Raman spectroscopy is separating the weak inelastically scattered light from the intense Rayleigh scattered laser light. Raman spectrometers typically use holographic diffraction gratings and multiple dispersion stages to achieve a high degree of laser rejection. In the past, PMTs were the detectors of choice for dispersive Raman setups, which resulted in long acquisition times. However, the recent uses of CCD detectors have made dispersive Raman spectral acquisition much more rapid. Raman spectroscopy has a stimulated version, analogous to stimulated emission, called stimulated Raman scattering. The Raman effect occurs when light impinges upon a molecule and interacts with the electron cloud of the bonds of that molecule. The incident photon excites one of the electrons into a virtual state. For the spontaneous Raman effect, the molecule will be excited from the ground state to a virtual energy state, and relax into a vibrational excited state, which generates Stokes Raman scattering. If the molecule was already in an elevated vibrational energy state, the Raman scattering is then called anti-Stokes Raman scattering. A molecular polarizability change, or amount of deformation of the electron cloud, with respect to the vibrational coordinate is required for the molecule to exhibit the Raman effect. The amount of the polarizability change will determine the intensity, whereas the Raman shift is equal to the vibrational level that is involved. This technique is widely applicable. The large frequency range (50-4000 cm^{-1}) makes adsorbate-adsorbent stretching modes accessible. Problems include specimen heating, high background fluorescence and low signal strengths. Surface enhanced Raman scattering (SERS), however, can give greatly increased signals in favorable cases, e.g., with rough surfaces or small

particles of certain compounds. It is particularly useful in the studies of supported monolayer catalysts and adsorbed layers [22].

Experimental: The Micro-Raman analysis have been made in collaboration with Perugia University. Micro-Raman spectra were made by an Olympus microscope mod. BX40 connected to an ISA Jobin-Yvon model TRIAX320 single monochromator, resolution 1 cm^{-1}. The exciting source was a Melles Griot 25LHP925 He-Ne laser used in single line excitation mode at 632.8 nm. The power focused on the samples was always less than 2 mW. The scattered Raman photons were detected by a liquid-nitrogen cooled CCD, Jobin Yvon Mod. Spectrum One. Samples were not pre-treated but measured as a power placed on a microscope slide: in this way it is possible to analyse the few microns grain size and not to focus on those regions where the presence of the support (silica) was predominant. The reproducibility of the spectra was always controlled sampling different points of the catalyst. Through the optical microscope analysis we also verified that no local degradation occur during laser irradiation.

5.2.1.6 ICP-MS analysis

ICP-MS (Inductively coupled plasma mass spectrometry) is a type of mass spectrometry that is highly sensitive and capable of the determination of a range of metals and several non-metals at very low concentrations. It is based on coupling together an inductively coupled plasma as a method of producing ions (ionization) with a mass spectrometer as a method of separating and detecting the ions. ICP-MS is also capable of monitoring isotopic speciation for the ions of choice. A plasma is a gas that contains a sufficient concentration of ions and electrons to make the gas electrically conductive. The plasmas used in

spectrochemical analysis are essentially electrically neutral, with each positive charge on an ion balanced by a free electron. In these plasmas the positive ions are almost all singly-charged and there are few negative ions, so there are nearly equal numbers of ions and electrons in each unit volume of plasma.

ICP for spectrometry is sustained in a torch that consists of three concentric tubes, usually made of quartz. The end of this torch is placed inside an induction coil supplied with a radio-frequency electric current. A flow of argon gas (usually 14 to 18 l/min) is introduced between the two outermost tubes of the torch and an electrical spark is applied for a short time to introduce free electrons into the gas stream. These electrons interact with the radio-frequency magnetic field of the induction coil and are accelerated first in one direction, then the other, as the field changes at high frequency (usually 27.12 million cycles per second). The accelerated electrons collide with argon atoms, and sometimes a collision causes an argon atom to part with one of its electrons. The released electron is in turn accelerated by the rapidly-changing magnetic field. The process continues until the rate of release of new electrons in collisions is balanced by the rate of recombination of electrons with argon ions (atoms that have lost an electron). This produces a 'fireball' that consists mostly of argon atoms with a rather small fraction of free electrons and argon ions. The temperature of the plasma is very high, of the order of 10,000 K. The ICP can be retained in the quartz torch because the flow of gas between the two outermost tubes keeps the plasma away from the walls of the torch. A second flow of argon (around 1 l/min) is usually introduced between the central tube and the intermediate tube to keep the plasma away from the end of the central tube. A third flow (again usually around 1 l/min) of gas is introduced into the central tube of the torch. This gas flow passes through the centre of the plasma, where it forms a channel that is cooler than the

surrounding plasma but still much hotter than a chemical flame. Samples to be analyzed are introduced into this central channel, usually as a mist of liquid formed by passing the liquid sample into a nebulizer. As a droplet of nebulised sample enters the central channel of the ICP, it evaporates and any solids that were dissolved in the liquid vaporize and then break down into atoms. At the temperatures prevailing in the plasma a significant proportion of the atoms of many chemical elements are ionized, each atom losing its most loosely-bound electron to form a singly charged ion.

The ions from the plasma are extracted through a series of cones into a mass spectrometer, usually a quadrupole. The ions are separated on the basis of their mass-to-charge ratio and a detector receives an ion signal proportional to the concentration.

The concentration of a sample can be determined through calibration with elemental standards. ICP-MS also lends itself to quantitative determinations through Isotope Dilution, a single point method based on an isotopically enriched standard.

Experimental: ICP measurements were determined by Inductively Coupled Plasma-Optical Emission Spectrometers (ICP-OES) Varian 700-ES.

Fig 5.9: Instrument Varian Liberty ICP-OES.

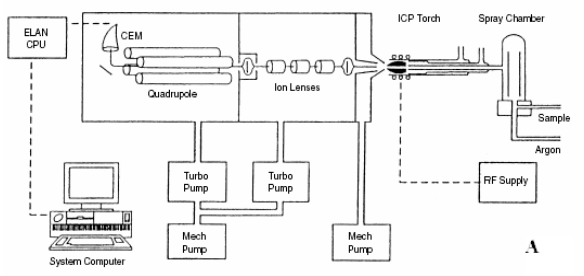

Fig. 5.10: scheme of instrument Varian Liberty ICP-OES.

5.2.1.7 XRD

The XRD analysis have been made in collaboration with Perugia University.

The obtained materials were characterized by X-ray powder diffraction (XRD: PANalytical X'Pert Pro, CuKα radiation) operating at 40 kV and 40 mA, step scan 1 min^{-1} and 1 s counting time in the 2–40° range at room temperature.

Fig 5.11 Instrument XRD: PANalytical X'Pert Pro, CuKα radiation

5.2.2 Catalysts characterization: results

The characterization analyses were performed on the fresh, and in some cases on used catalysts. "Fresh catalysts" indicate the samples as prepared. "Activated catalysts" indicate the samples charged in the FTS reactor and reduced using the activation procedure and removed from the reactor. "Used

catalysts" indicate the samples after their use in the Fischer-Tropsch synthesis reaction.

5.2.2.1 BET characterization results

The BET results are reported in Table 5.4

Table 5.4. BET characterization results

CATALYST		**Specific Surface area (m^2/g)**
Co-based HTlc	Co5	17.46
	Co10	11.47
	Co15	7.20
	Co35	5.84
Co synthesized with US	Co/SiO_2	360.0
	Co/Al_2O_3	116.0
	Co/TiO_2	55.0
	$Co\text{-}Ru/SiO_2$	346.0
	$Co\text{-}Ru/Al_2O_3$	108.0
	$Co\text{-}Ru/TiO_2$	13.0
Fe-based	$Fe_{30}K_{2.0}Cu_{3.75}$ TR	160
	$Fe_{30}K_{2.0}Cu_{3.75}$-MW1	180
	$Fe_{30}K_{2.0}Cu_{3.75}$-MW2	224
	$Fe_{30}K_{2.0}Cu_{3.75}$-US1	201
	$Fe_{30}K_{2.0}Cu_{3.75}$-US2	210

MW1= Catalyst put it into a kitchen MW and processed in powder, MW2= Catalyst put it into MW and suspended in hexane, US1= Catalyst suspended in aqueous solution in air atmosphere for 0.5 h, US2= Catalyst sonicated and suspended in hexane in Argon atmosphere for 3h

- The composition and specific surface area (SSA) of the HTlc are reported in Table 5.4. Note that the SSA decreases with the increase of the amount of cobalt. The relatively large dimensions and high crystallinity of particles reflect a low specific surface area [28]. The surface area of Co15 and Co35 after the reduction procedure was determined by BET

method. The values obtained are 73.4 m^2 g^{-1} for the sample Co15 and 78.3 m^2 g^{-1} for the sample Co35, both higher than the untreated materials.

- For the Co and Co-Ru based catalysts synthesized with the help of ultrasound, it is clear how the addition of the promoter show a diminution of the SSA in every case (Co/SiO_2 360.0, higher than the co-respective Co-Ru/SiO_2 with 346.0 55.0 and 13.0 for Co and Co-Ru/TiO_2 and 116.0 and 108.0 for Co and Co-Ru/Al_2O_3). The SiO_2 acts as the best support even in presence of the promoter. The TiO_2 tends to keep lower the SSA of the catalyst and the Al_2O_3 represents an intermediate way of the supports used in this group of catalysts.
- The surface area of catalysts is influenced by the method of synthesis, as shown in Table 5.5 and in Fig. 5.12. Fe-based catalysts treated with MW and US have higher values of SSA than the traditional ones; the effect of MW and US on SSA increases increasing the US or MW emitting power.

  According to [1]. The samples sonicated in argon (US2) present the highest SSA, indicating that the US effects in argon atmosphere are more remarkable. The use of this gas enhances cavitation effects because increases the temperatures of the collapsing bubbles generated by US [29]. The change of catalysts morphology due to US treatment (SEM analyses) could explain the increase of SSA in these samples. Catalysts prepared by MW show a higher SSA than the traditional ones: 180 and 224 m^2 g^{-1} for the samples Fe30-MW1 and Fe30-MW2, respectively, with a similar increase of about 25% respect the traditional prepared sample. Moreover, the surface area of these

samples seems not to be dependent on the power of the MW treatment.

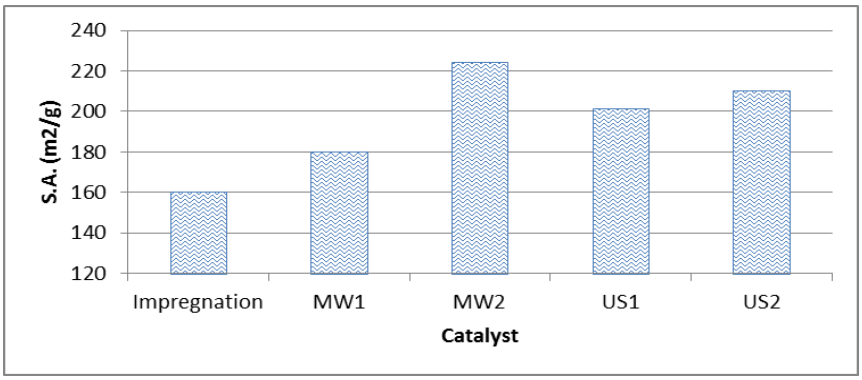

Fig 5.12. $Fe_{30}K_{2.0}Cu_{3.75}$ surface area vs. different methods of synthesis

5.2.2.2 TPR characterization results

- Co-based catalysts HTLc

As discussed previously, the active phase in the FTS is the metallic cobalt, while the HTlc materials contain Co(II) ions randomly dispersed inside the brucitic layers. Therefore, in order to have an active catalyst, a reduction procedure is required to form the cobalt particles. TPR analyses were performed to study the reduction process and select the best conditions for the catalyst activation. Fig. 5.13 shows the TPR profile of the samples Co5, Co15, Co35, while Table 5.5 reports the reduction temperature and the percentage of reduced Co. All the profiles exhibit two regions of reduction; the first at lower temperatures (below 400°C), which is due to the reduction of Co_3O_4 while the second peak, above 700 °C, indicates the presence of hardly reducible species. These species are probably spinel-type mixed oxides formed during the thermal treatment. TPR profiles of CoO_x mixed oxides is well described in the literature [30-36]. The reduction profile of Co_3O_4 in the low temperature region consists in two peaks, corresponding to the reduction of Co^{3+} to Co^{2+} and Co^{2+} to Co^0.

According to Alvarez et al [37], these two peaks are well separated for samples with small particle size, while an intermediate particle size causes the overlapping of the two reduction steps resulting in a complete reduction with only one maximum at an intermediate temperature (328 °C). The TPR profiles of our HTlc (Fig. 5.13) are consistent with the latter case. Based on the TPR results (Table 5.5), the tested catalysts were activated at 350°C for 4 hours under hydrogen atmosphere, in order to reduce the Co ions to metallic Co.

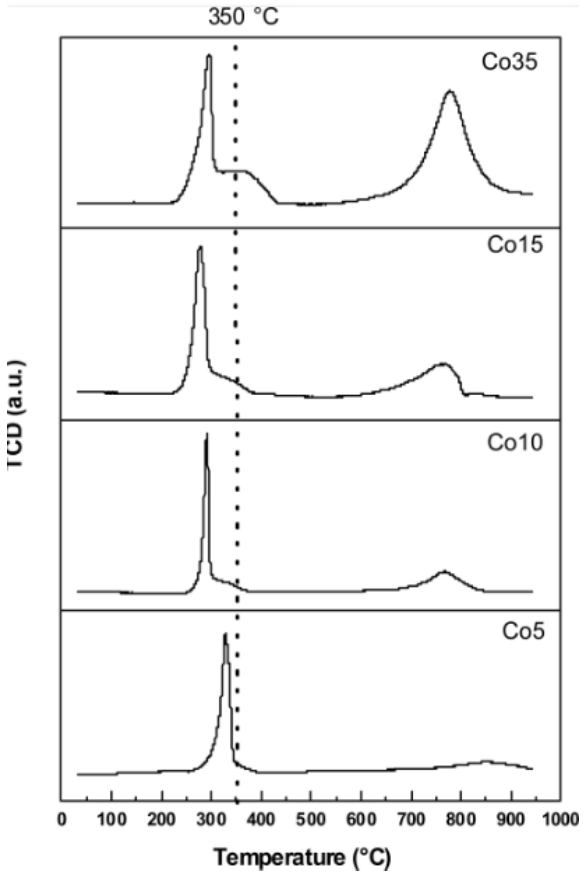

Fig. 5.13: TPR profile of the fresh samples Co5, Co10, Co15, Co35. The activation temperature used in the FTS reactor before the catalytic test is indicated with the dashed line.

Note that the sample Co15 exhibit the lowest reduction temperature that is significantly lower than the activation temperature adopted in the FT process (350°C). A low reduction temperature may favour the presence of catalyst in its reduced state during the catalytic process. The % of reduced Co evaluated by TPR is generally high. However, these values strongly depend on reduction conditions (pressure, temperature ramp, gas flow, etc.) that are different from those used in the FT reactor, as detailed in the experimental section.

Table 5.5: Reduction temperature and % of cobalt reduction of the fresh samples Co5, Co15, Co35.

Sample	TPR	
	T_{max} (°C)	% Co Red
Co5	328	58
Co15	278	54
Co35	295	83

- Co and Co-Ru catalysts synthesized with US

Table 5.6 shows the TPR profiles of the samples Co/Al_2O_3, Co/SiO2, Co/TiO2 and $Co\text{-}Ru/Al_2O_3$, Co-Ru /SiO2, Co-Ru /TiO2

Table 5.6. TPR diagrams and values summary for Co and Co-Ru catalysts with US

Catalyst	TPR Profile
Co/Al_2O_3	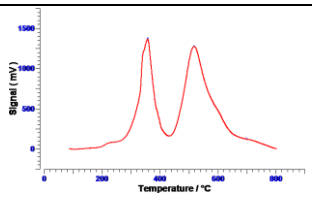
Co/SiO_2	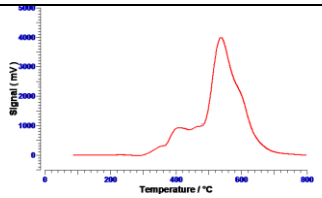
Co/TiO_2	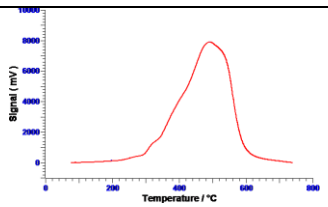
$Co\text{-}Ru/SiO_2$	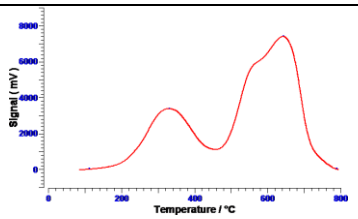
$Co\text{-}Ru/Al_2O_3$	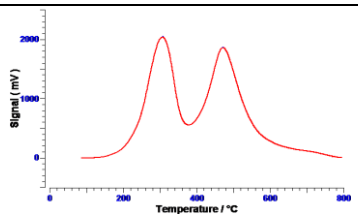
$Co\text{-}Ru/TiO_2$	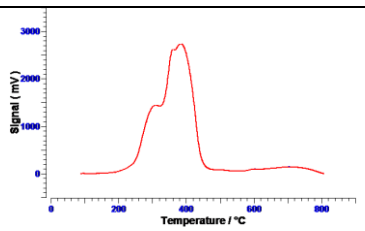

- Iron catalysts:

For the supported iron based catalysts, three stage of phase transformation could be identified, starting from oxidised form of iron: hematite (Fe_2O_3) to magnetite (Fe_3O_4), magnetite to metallic iron (α-Fe) [39]. It is known [39-40] that copper promotes the reduction to hematite to magnetite, and also the reduction of magnetite to α-Fe to a lesser extent, but it needs to be very well mixed with iron to provide the most favourable promoter effect on the hematite → magnetite phase transformation. For what concerns the support (silica), Jin and Datye [38] observed that the most important effect of silica is an improvement in the thermal stability of the catalysts, in fact the silica support is very effective at inhibiting the sintering of the iron catalyst.

The results of TPR characterization for iron catalysts are reported in Table 5.7.

The number, the position and the shape of the peaks agree with literature [38]. In many cases the TPR peaks corresponding to transformations of CuO → Cu and Fe_2O_3 → Fe_3O_4 were found to overlap, and this is the first peaks at low temperature. The second broad peak at higher temperature on the TPR profile corresponds to the phase transformation of Fe_3O_4 → α-Fe. The large peak width for this last transformation indicates this is slow process.

TPR analyses show that the metal reduction starts at about 230°C for promoted catalysts. According to Pirola [2] it is clear therefore the role of Cu in the improvement of iron oxide phases reduction, as well known in literature: a suggested mechanism for this promotion effect is the migration of atomic hydrogen from reduced Cu sites to the iron oxide [38, 40].

Therefore, the different preparation methods do not influence the peaks temperature of the reduction steps of the catalytic samples in any case.

Table 5.7. TPR diagrams and values summary for $Fe_{30}K_{2.0}Cu_{3.75}$, catalysts with different methods of synthesis

Catalysts	Diagrams
$Fe_{30}K_2Cu_{3.75}/SiO_2$	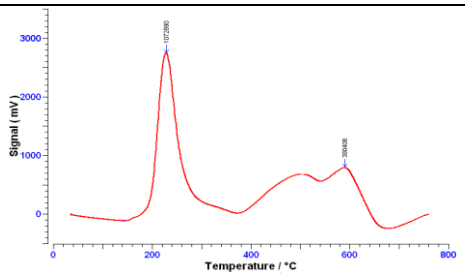
$Fe_{30}K_2Cu_{3.75}/SiO_2$ (MW2)	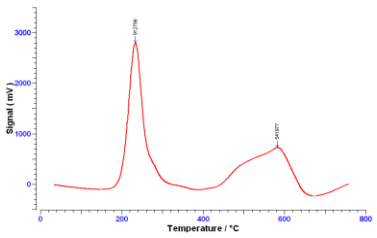
$Fe_{30}K_2Cu_{3.75}/SiO_2$ (MW1)	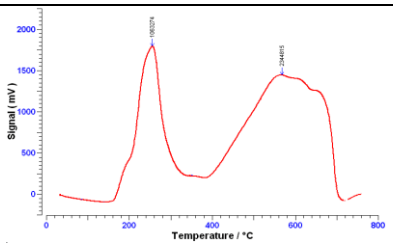
$Fe_{30}K_{2.0}Cu_{3.75}/ SiO_2$ (US1)	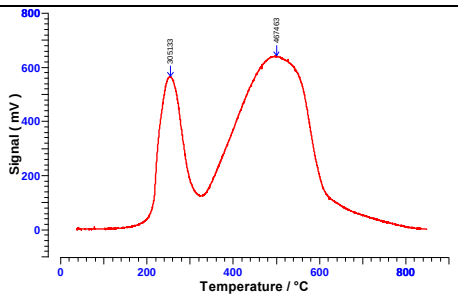

5.2.2.3 SEM – TEM characterization results

SEM analyses are reported in Fig. 5.14 (for HTlc), Fig. 5.15 (for Co and Co-Ru with US) and in Fig 5.16 (for Fe catalysts)

- Cobalt Catalysts
    - HTlc

The morphology of the synthesized HTlc was investigated by SEM and TEM. Images of Co15 and Co35, selected as representative samples (Fig. 5.14 a-d), show that they are constituted by homogeneous aggregates of hexagonal and platy particles of few hundreds nanometers of thickness and with a dimensional range between 2-5 µm. In TEM micrographs the hexagonal morphology of HTlc microcrystals is clearer. The relatively large dimensions and high crystallinity of particles reflect a low specific surface area, in the range of 6-18 m^2g^{-1} (Table 5.4). Composition maps of Co15 (Fig. 5.15), obtained with coupled SEM-EDS analysis, highlight the homogeneous Co, Zn and Al dispersion over the entire analyzed spot area, without creating single-metal domains indicating good metal distributions in the samples. Similar dispersion characteristics were obtained for all the samples studied, although not reported here for the sake of brevity.

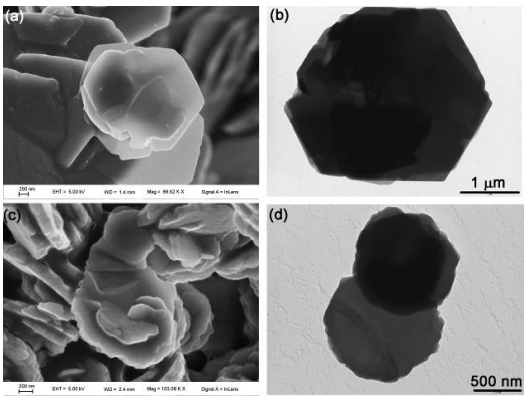

Fig.5. 14: SEM (left) and TEM (right) images of fresh samples Co15 (a,b) and Co35 (c,d).

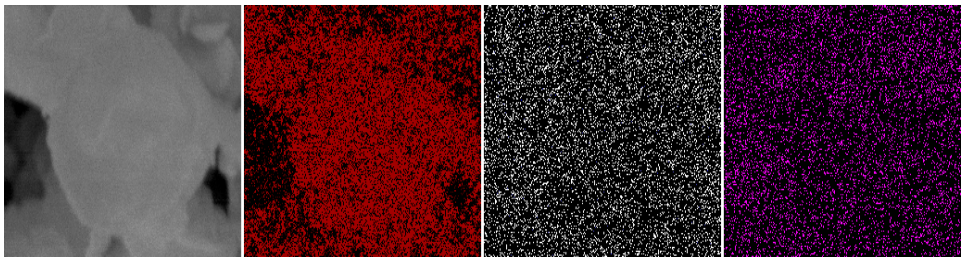

Fig.5. 15: SEM image of fresh sample Co15 and the corresponding EDS images of the metals: Al (red), Co (white) and Zn (pink).

SEM and TEM images of two activated samples are reported in Fig. 16a-d. The results indicate that the material keeps the original morphology with hexagonal crystals of micrometric dimensions. At higher magnification (TEM images) the segregation of dense particles homogeneously distributed on the surface and having dimensions of about 8 nm, probably due to metallic Co, was evident. [41].

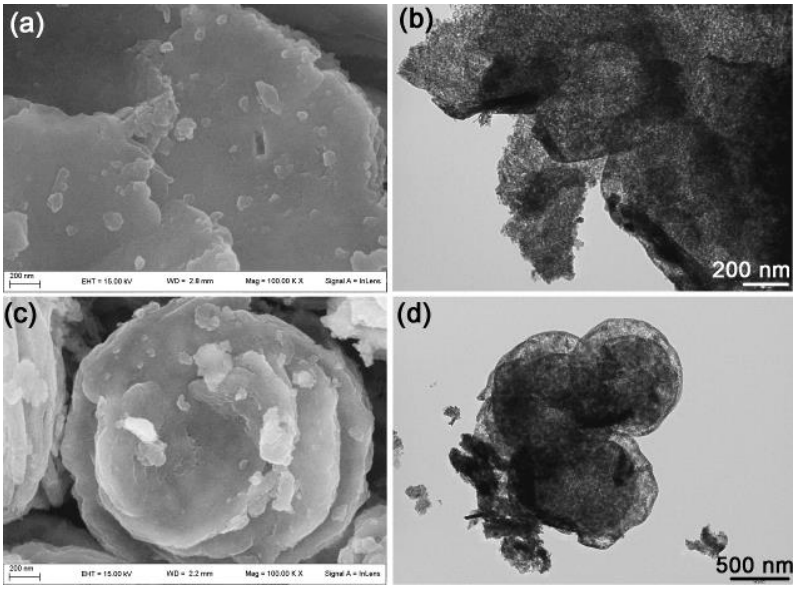

Fig. 5.16: SEM (left) and TEM (right) images of activated Co15 (a,b) and Co35 (c,d).

SEM images of Co5, Co15 and Co35 after the catalytic run at 260°C are shown in Fig. 5.17. Samples containing Zn (Co5 and Co15) reveal the presence of a

nanometric phase crystallized on the catalyst surfaces. The absence of this nanometric phase on Co35 surface (which does not contain Zn) may indicate the presence of ZnO, according to the XRD pattern (it will be show later).

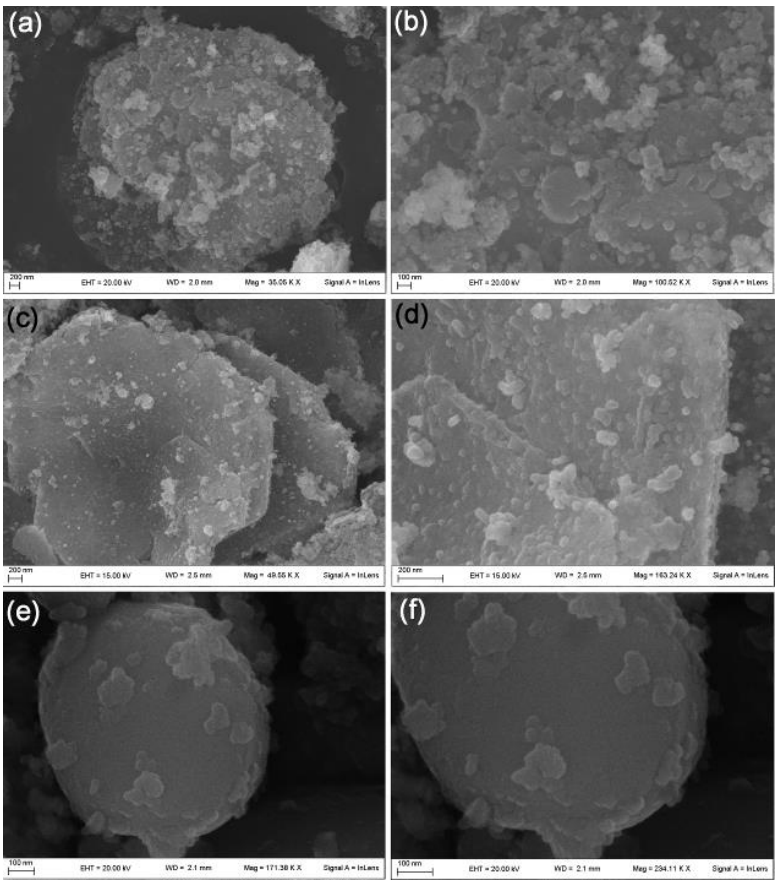

Fig.5.17 SEM images of Co5 (a,b); Co15 (c,d), Co35 (e,f) after catalytic run at 260°C and 20 bar and at different magnifications.

- Co and Co-Ru synthesized with US. The Fig. 5.18 show the SEM analyses of the samples with and without the presence of Ru. The chemical effect of US arises from acoustic cavitation, i.e. the formation, growth and implosive collapse of bubbles in a liquid. Some of the interesting features resulting from the application of sonication as a synthetic method are the nanoparticles

preparation, showing a more uniform size distribution, higher surface area and a more controlled phase composition (Fig.5.18).

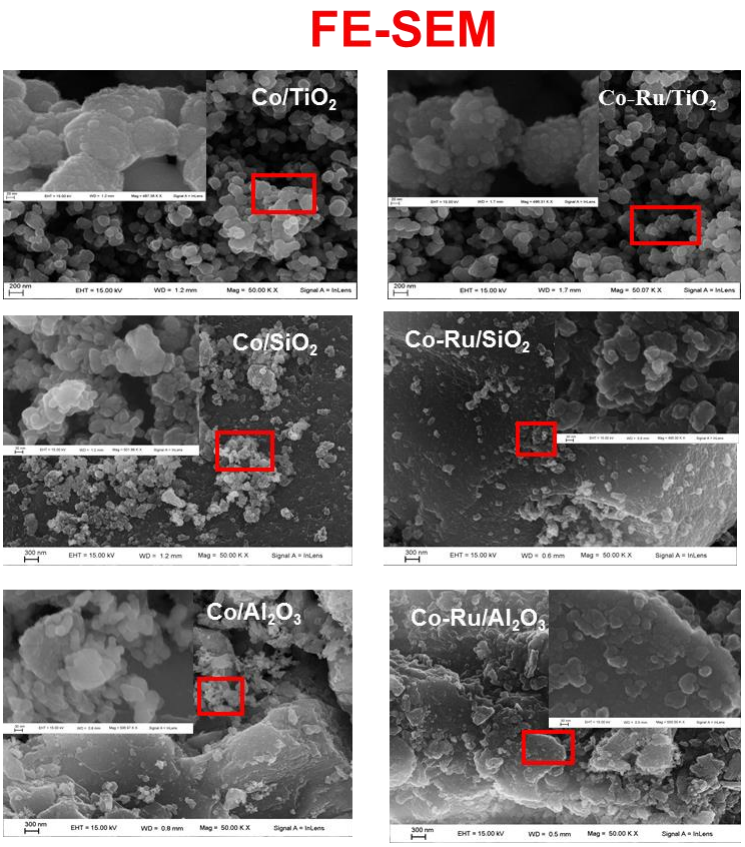

Fig. 5.18. SEM analyses for Co based catalysts with US. Magnification: 2000X.

- Iron Catalysts

SEM analyses are essential to evaluate the morphology of catalysts with high loading of iron and to control the metal dispersion. The iron covers the surface of silica in a progressive level with its increase, and it is well distributed in the more loaded catalyst too [40].

The aggregates of iron with spherical shape are regularly distributed on the support. In the case of the catalysts prepared with the step of ultrasound, it can be seen an uniform layer of iron on SiO_2. The spherical shape aggregates are substituted by this iron layer. The catalyst morphology and the metal dispersion are similar for the two US samples [43].

SEM analyses (Fig. 5.19) have been the key to both evaluate the morphology of all the prepared catalysts and observe their metal distribution (using EDX analysis). Notwithstanding this general trend, both the morphology and the shape of iron aggregates strongly depend on preparation method. In Fig. 5.19, SEM analysis of samples through different preparation methods are reported. In the traditional prepared sample (Fig. 5.19.a) it is possible to observe Fe spherical shape aggregates on the bare silica surface. Iron is present only in these particles and coverage of the support is not complete. The same morphology is present in the MW prepared sample (Fig. 5.19b). On the contrary, on US prepared ones (Fig. 5.19c (air) and 5.19d (argon)) there is a uniform layer of iron on SiO_2. The support, in fact, is not easily visible due to its complete coverage as confirmed by SEM–EDX analyses. The spherical shape aggregates are substituted by this iron layer; both the catalyst morphology and the metal dispersion are similar for the two US samples but completely different with both the traditional and the MW ones.

It is even more interesting the comparison between samples prepared by different sonication time, for example Fe30-US2 (Fig. 5.19c) and Fe30-US1 (Fig. 5.19d): when the US treatment is performed for 0.5 h the surface seems to be covered by Fe small leafs that are completely faded when sonication is prolonged for 3 h and in their place only crashed Fe clusters are present [1].

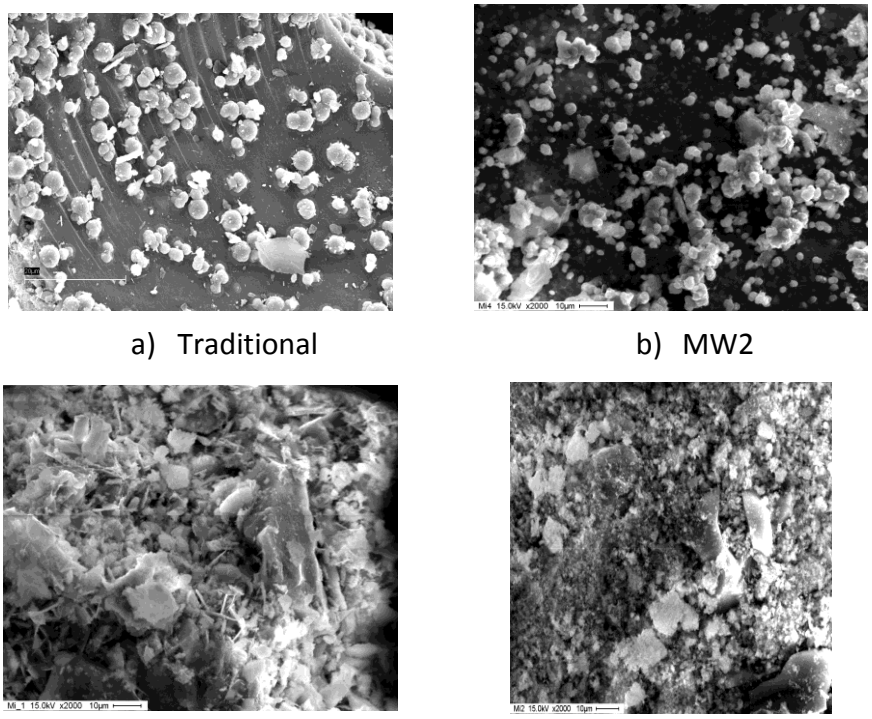

a) Traditional b) MW2

c) US1 d) US2

Fig. 5.19. SEM analyses for iron catalysts. Magnification: 2000X.

5.2.2.4 XRD and micro-RAMAN characterization results

- Cobalt Catalysts
  - For the HTlc the XRD and micro-RAMAN analyses Figure 5.20 shows the XRD patterns of the samples listed in Table 5.1. The interlayer distance of 8.9 Å, determined from the first XRD reflection, is compatible with the presence of nitrate between the sheets [43].

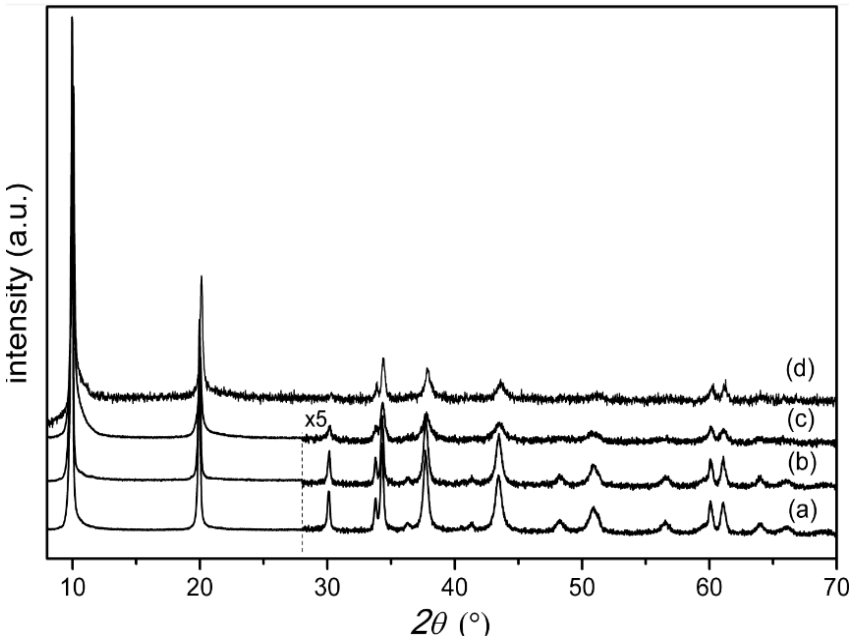

Fig. 5.20: XRD pattern of the fresh samples: (a) Co5, (b) Co10, (c) Co15 and (d) Co35.

Activated HTlc were first characterized by XRD. As an example, the XRD pattern of activated Co15 is reported in Fig. 5.21. The pattern shows the presence of very poorly crystalline ZnO and a spinel phase, such as Co_3O_4, $CoAl_2O_4$, and/or $ZnAl_2O_4$ (note that mixed-oxide spinel phases show very similar XRD patterns, irrespective of their composition). Moreover, the reflection at 43° 2θhas been assigned to a CoO phase with very low crystallinity and no metal aggregation is observed. The sample after the reduction treatment does not show metallic Co phases indicating the presence of active metal atoms homogeneously dispersed at the nanometer level [44]. According to Jong et al. [45] and Den Breejenet et al. [46] cobalt-based catalysts need large particle size of the active species to create optimal domains of active sites because the activity drops for particles smaller than 6 nm.

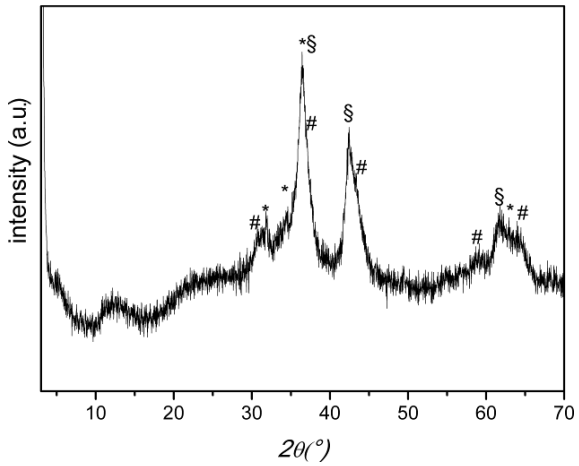

Fig. 5.21: XRD pattern of activated Co15. * ZnO, # Co_3O_4, $CoAl_2O_4$, $ZnAl_2O_4$, § CoO.

In order to better understand the stability of the materials, XRD patterns of sample Co15 after the catalytic tests at two different temperatures (235°C and 260°C) were collected (Fig. 5.22). At the lower temperature (Fig. 5.22 a) the pattern is close to that recorded just after the reduction process (Fig. 5.21). Therefore we can hypothesize that the catalyst does not change as a consequence of the FTS process. On the other hand, the XRD pattern of the catalyst recovered after the reaction at 260°C (Fig. 5.22b) shows more crystalline ZnO and spinel phase, and the strong reduction of the peak assigned to CoO. This may indicate that during the FTS process, at high temperatures, cobalt ions crystallized into a spinel phase.

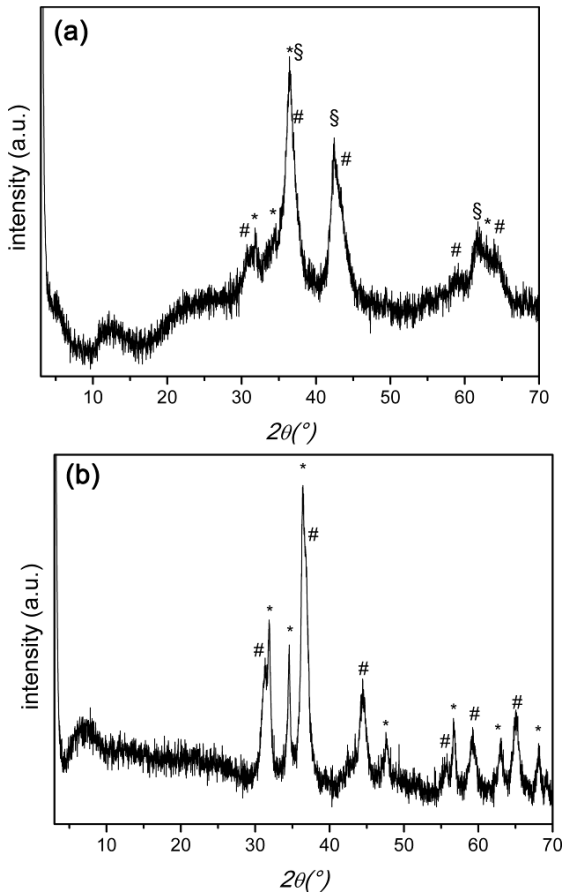

Fig.5.22 XRD pattern of used Co15 after catalytic runs a) at 235°C and 20 bar and b) at 260°C and 20 bar. * *ZnO*, # Co_3O_4, $CoAl_2O_4$, $ZnAl_2O_4$, § *CoO*.

- Iron catalysts.

The XRD and micro-RAMAN analyses were made to identify the iron phase after the calcination treatments. A Raman spectrum (Fig. 5.23a) and an XRD pattern (Fig. 5.23b) for $Fe_{30}K_2Cu_{3.75}/SiO_2$ are reported.

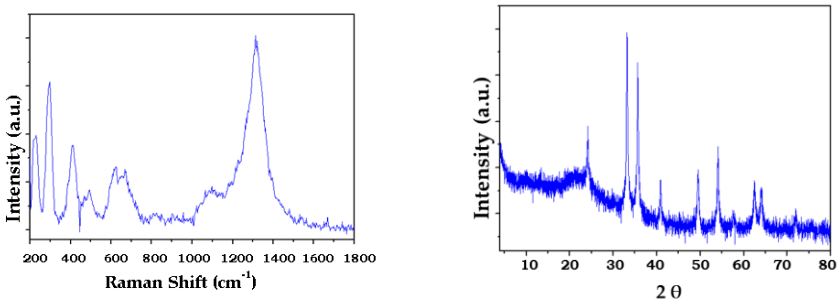

Fig. 5.23 a) Micro-Raman analysis and b) XRD for the $Fe_{30}K_2Cu_{3.75}/SiO_2$ catalyst

Comparing these results with the tables reported in literature [47-48] for the assignment of the peaks it is possible to conclude that the iron after calcination is present as hematite Fe_2O_3, as expected and as reported in literature [39].

5.2.5.5 ICP characterization results

ICP analysis was made to verify the catalysts composition.

- Cobalt based catalyst
  - HTlc: In Table 5.8 the results are reported.

Table 5.8. ICP characterization results for Co catalysts (HTlc)

HTlc	Atomic percentage in solution			Basic Formula
	Zn	Co	Al	
Co5	55	15	30	$[Zn_{0.57}Co_{0.10}Al_{0.33}(OH)_2](NO_3)_{0.33}\cdot 0.5\ H_2O$
Co10	45	25	30	$[Zn_{0.45}Co_{0.21}Al_{0.34}(OH)_2](NO_3)_{0.34}\cdot 0.5\ H_2O$
Co15	35	35	30	$[Zn_{0.39}Co_{0.32}Al_{0.29}(OH)_2](NO_3)_{0.29}\cdot 0.5\ H_2O$
Co35	-	70	30	$[Co_{0.67}Al_{0.33}(OH)_2](NO_3)_{0.33}\cdot 0.5H_2O$

- Co and Co-Ru with US: In Table 5.9 the results are reported.

Table 5.9. *ICP characterization results for Co catalysts*

Sample	Co $\%_{wt}$	Ru $\%_{wt}$
Co_{10}	8.0	-
$Co_{10}Ru_{0.1}$	8.0	0.08

In general, these results indicate the composition of catalysts is in good agreement with the theoretical values.

- Iron based catalysts: In Table 5.10 the results are reported.

Table 5.10 ICP characterization results for Fe catalysts

Sample	Fe $\%_{wt}$	K $\%_{wt}$	Cu $\%_{wt}$
$Fe_{30}K_{2.0}Cu_{3.75}$	31.4	1.9	4.0

5.2.2.6 XRD and micro-RAMAN characterization results

- Cobalt Catalysts
  - For the HTlc the XRD and micro-RAMAN analyses

In order to better understand the behaviour of the materials after activation, FT-IR spectra of the sample Co15 (as a representative sample), calcined and activated, and Co_3O_4 have been registered (Fig. 5.26). The spectrum of Co15 showed the typical absorption bands of the nitrate anion at 1377 cm^{-1} present in the interlayer region of HTlc. After calcination this band disappeared due to nitrate degradation and the spectrum presented the typical absorptions of Co_3O_4 spinel phase at 667 cm^{-1} and 566 cm^{-1}. The activation process leads to the formation of a material with very wide bands attributed to the Co_3O_4 phase.

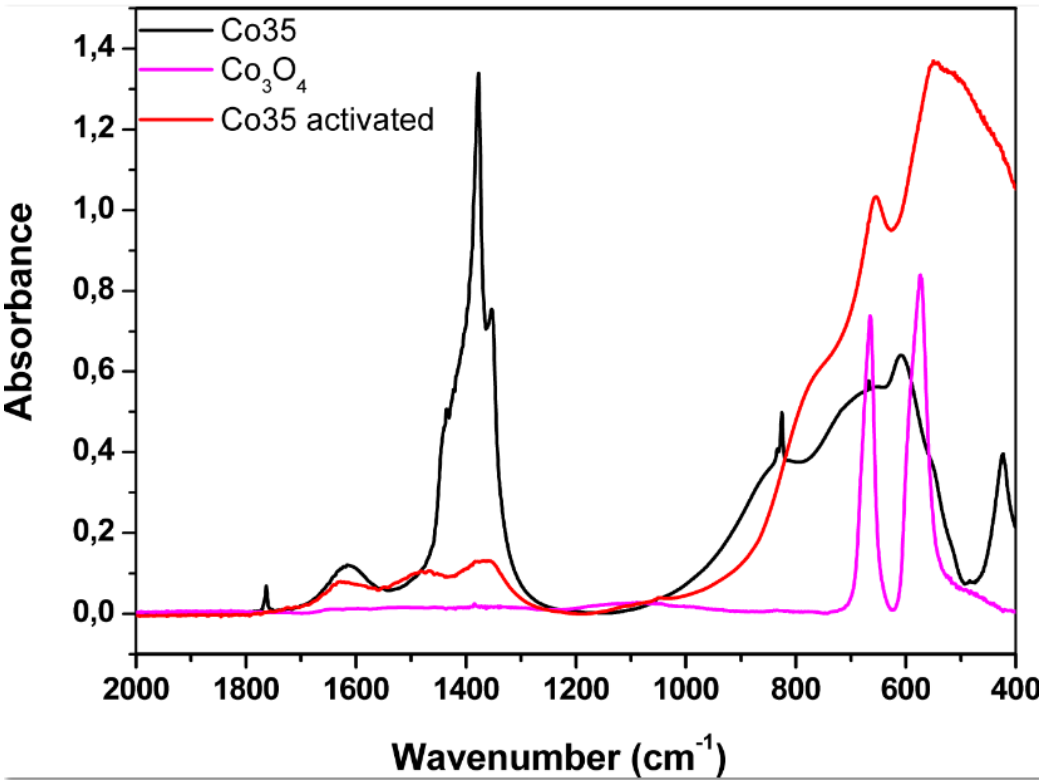

Fig. 5.24: FT-IR spectra of the fresh and activated Co15 and of the reference Co_3O_4.

References

[1] C. Pirola, C. L. Bianchi, A. Di Michele, P. Diodati, D. C. Boffito, V. Ragaini, *Ultrasonic Sonochem*. 17,610-616 (2010)

[2] C. Pirola, PhD 2007-2008, Novel supported iron based Fischer-Tropsch catalysts: Preparation, characterization and applications

[3] G.P.Vaan Deer Laan, A.A.C.M.Beenackers, Catal.Rev.-Sci.Eng.,41 (3&4) (1999) 255

[4] Y.Jin, A.K.Datye, Journal of catalysis 196 (2000) 8

[5] Costantino U, Marmottini F, Nocchetti M, Vivani R, Eur J Inorg Chem 1998; 10:1439 -1446

[6] C. Pirola, C.L. Bianchi, A. Di Michele, P. Diodati, S. Vitali, V. Ragaini, Catal Lett. 131 (2009):294-304

[7] G. Biffi Gentili, M. Linari, I. Longo, A. Ricci, A, IEEE Transactions on microwave theory and techniques. 57, (9-2009) 2268-2275
[8] B.Toukoniitty, J.P.Mikkola, D.Yu.Murzin, T.Salmi, Applied Catalysis A: General 279 (2005) 1
[9] K.S.Suslick, Sonocatalysis, Handbook of Heterogeneous Catalysis, VCH Verlagsgesellschaft mbH, Weinheim, Germany (1997), 1350
[10] B.Toukoniitty, J.P.Mikkola, D.Yu.Murzin, T.Salmi, Applied Catalysis A: General 279 (2005) 1
[11] W.Bonrath, Ultrasonics Sonochemistry 12 (2005) 103
[12] C.L.Bianchi, V.Ragaini, Catalysis Letters 95 (2004) 61
[13] C.L.Bianchi, F.Martini, V.Ragaini, Ultrasonics Sonochemistry 8/2 (2001) 131
[14] Zhao R, Goodwin JG Jr, Jothimurugesan K, Gangwal SK, Spivey JJ (2001) Ind Eng Chem Res 40:1065 10.
[15] Yang Y, Xiang HW, Tian L, Wang H, Zhang CH, Zhong B, Li YW (2005) Appl Catal A 284:105
[16] Suo, Haiyun; Zhang, Chenghua; Wu, Baoshan; Xu, Jian; Yang, Yong; Xiang, Hongwei; Li, Yongwang; Cat Today Volume 183-1 (2012) 88–95.
[17] Donatti DA, Ruiz AI, Vollet DR (2002) Ultrason Sonochem 9:133
[18] Yang Y, Xiang HW, Tian L, Wang H, Zhang CH, Zhong B, Li YW (2005) Appl Catal A 284:105
[19] Fadoni, M. and Lucarelli, University of Milan and CE Instruments (Thermoques S.p.A)
[20] F. M. NELSEN and F.f. EGGERTSEN Shell Development Co., Emeryville, Calif. ANALYTICAL CHEMISTRY VOL. 30, NO. 8, AUGUST 1958, 1387-1390
[21] 11 S. Brunauer, P. H. Emmett and E. Teller, J. Am. Chem. Soc. 60 (1938) 309
[22] J.Haber, J.H.Block and B.Delmon , Pure&appl. Chem. 67, Nos 8/9 (1995) 1257
[23] S.D.Robertson, B.D.McNicol, J.H.De Baas, S.C.Kloet, J.W.Jenkins, J.Catal 37 (1975) 424
[24] Von Ardenne, Manfred. "Das Elektronen-Rastermikroskop. Theoretische Grundlagen". Zeitschrift fur Physik 108 (1938) 553
[25] Von Ardenne, Manfred. "Das Elektronen-Rastermikroskop. Praktische Ausführung". Z. Techn. Phys. 108 (1938) 407
[26] Ludwig Reimer, Helmut Kohl; Springer Series in Optical Sciences 36, fifth edition, 2008. Transmission Electron Microscopy: Physics of Image Formation
[27] Gardiner, D.J. (1989). Practical Raman spectroscopy. Springer-Verlag. ISBN 978-0387502540
[28] A. Di Fronzo, C. Pirola, A. Comazzi, F. Galli, C.L. Bianchi, A. Di Michele, R. Vivani, M. Nocchetti, M. Bastianini, D.C. Boffito, Fuel 119 (2014) 62-69

[29] T.J. Mason, J.P. Lorimer, Sonochemistry, Ellis Horwood, Chichester, 1988, p. 58
[30] Bianchi CL, Catal Lett 2001; 76(3–4):155-159.
[31] Lin HY, Chen YW, Li C. Thermochim Acta 2003; 400:61–67.
[32] Lin HY, Chen YW. Mater Chem Phys 2004; 85:171–175.
[33] Sexton BA, Hughes AE, Turney TW. J Catal 1986; 97(2):390–406.
[34] Kumar N, Payzant EA, Jothimurugesan K, Spivey JJ. Phys Chem Chem Phys 2011; 13:14735–14741.
[35] Tsakoumis NE, Dehghan R, Johnsend RE, Voronov A, Van Beek W, Walmsley JC, Borg Ø, Rytter E, Chen D, Rønning M, Holmen A. Catal Today 2013; 205:86–93.
[36] Tsakoumis NE, Rønning M, Borg Ø, Rytter E, Holmen A. Catal Today 2010; 154:162–182.
[37] Alvarez A, Ivanova S, Centeno MA, Odriozola JA. Appl Catal A 2012; 431-432:9-17
[38] Y.Jin, A.K.Datye, Journal of catalysis 196 (2000) 8, 20
[39] D.B.Bukur, K.Okabe, M.P.Rosynek, C.P.Wang, D.J.Rao, K.R.P.M. and G.P.Huffman, J.Catal. 155 (1995)353
[40] Y.Yang, H.Xiang, Y.Xu, L.Bai, Y.Li, Appl.Catal.A 266 (2004) 181
[41] 32 Rudolf C, Dragoi B, Ungureanu A, Chirieac A, Royer S, Nastro A, Dumitriu E, Catal Sci. Technol DOI: 101.1039/C3CY00611E.
[42] C. Pirola, C.L Bianchi, A. Di Michele, S. Vitali, V. Ragaini, Catal Comm. 10 823 (2009)
[43] Iyi N, Fujii K, Okamoto K, Sasaki T. Appl Clay Sci 2007; 35:218-227
[44] C.L. Bianchi, C. Pirola, D.C. Boffito, A. Di Fronzo, A. Di Michele, R. Vivani, M. Nocchetti, M. Bastianini, S. Gatto, Co-Zn-Al based hydrotalcites as catalysts for Fischer-Tropsch process, Proceeding of DGMK Conference 2011, Catalysis:Innovative Applications in Petrochemistry and Refining, 4-6 October 2011, Dresden, Germany ISBN 978-3-941721-17-3.
[45] Leendert G, Bitter JH, Kuipers HPCE, Oosterbeek H, Holewijn JE, Xu X, Kapteijn F, Jos van Dillen A, Krijn P, J Am Chem Soc 2006; 128:3956-3964.
[46] 31 Den Breejen JP, Radstake PB, Bezemer GL, Bitter JH, Frøseth V, Holmen A, Krijn P., J Am Chem Soc 2009; 131:7197-7203.
[47] Thickett and Oldyha, J.Therm.Anal.Cal, 80 (2005)
[48] M.A.Legodi, D.de Waal/Dyes and Pigments 74 (2007) 161

Chapter 6. High Fe Loaded Supported Catalysts for Biosyngas Fischer – Tropsch Conversion: experimental and simulation results

6. Development of the kinetic model

One of the objectives of this research work was the development of a kinetic model for the synthesis of FT in collaboration with the Politecnico di Milano.

This model, based on experimental data obtained in the pilot plant using iron based catalyst ($Fe_{30}K_{2.0}Cu_{3.75}$) at different temperatures and different H_2/CO ratios allows to obtain and simulate the performance of these catalysts at temperatures and ratios of incoming flows feeding different.

The modeling work has not been limited to the laboratory scale, since it is possible to "predict" the trend of the reaction kinetics using these types of catalysts in reactors with much greater volumes and integrated in an entire industrial process such as the use of biosyngas for FT synthesis obtained from biomass.

6.1 Regression of kinetic constants

After obtaining the experimental data, it is necessary to regress them. With the regression we could obtain the respective kinetic constants.

The model is based on the fact that both reactions, the FT reactions and WGS are active, therefore we will need to regress the rate constants of both reactions which we call k_{FT} (kinetic constant of the FT reaction) and k_{WGS} (kinetic constant of the WGS reaction).

The equations that express the reaction rate of the two reactions are [1]:

For the FT reactions:

$$r_{FT} = k_{FT} \frac{P_{CO}\, P_{H_2}}{P_{CO} + a_{FT}\, P_{H_2O} + b_{FT}\, P_{CO_2}} \qquad k_{FT} = \left[\frac{mol}{Kg_{cat} \cdot Pa \cdot s}\right]$$

For the WGS reaction:

$$r_{WGS} = k_{WGS}\frac{P_{CO}\,P_{H_2O} - P_{H_2}P_{CO_2}/K_p}{P_{CO} + a_{WGS}\,P_{H_2O} + b_{WGS}\,P_{CO_2}} \qquad k_{WGS} = \left[\frac{mol}{Kg_{cat}\cdot Pa\cdot s}\right]$$

From these equations we note that the reaction rate, in both cases, is a function of the partial pressures of the reactants (CO and H_2), of the products (H_2O and CO_2), of the constants ($a_{FT/WGS}$ e $b_{FT/WGS}$) and the equilibrium constant Kp expressed as:

$$K_p = e^{(\frac{4578}{T} - 4.33)}$$

From the regression of the reaction rate constants is obtained the $K_{0,i.}$ These values are correlated to the $k_{FT/WGS}$ through the equation:

$$k_i = k_{0,i}e^{-E_i/(RT)}$$

The parameter values of the previous reports were obtained with a regression, using the MATLAB software, based on the method of least squares from the experimental data using the original coefficients $K_{0,FT}$, $k_{0,WGS}$, a_{FT}, a_{WGS}, b_{FT}, b_{WGS}, as values of the first iteration [2]. The software allows the regression of $k_{0,i}$ establishing an objective function that must be minimized as much as possible (10^{-6} tolerance basis of MATLAB):

$$Fobj = \sum_{i=1}^{N}(Xi,exp - Xi,model)^2$$

There was no regression of the activation energy of the two reactions, but kept constant as reported in literature [2].

The probability of growth of the hydrocarbon chain is instead given by the correlation developed by Lox and Froment [3-4] or iron based catalysts:

$$\alpha_{ASF} = \frac{k_1 P_{CO}}{k_1 P_{CO} + k_2 P_{H_2} + k_3}$$

For the regression of the data, there were not taken into account the energy balances because we consider an isothermal catalytic bed. The drop pressure is neglected since it can be assumed that in the whole catalytic bed the pressure is constant at 20 bar and the efficiency of the catalyst was considered unitary. On the contrary, these aspects must be taken into account if we are working with industrial volumes.

6.2 Mass Balance

In the kinetic model have been fully taken into account (even on lab-scale) the mass balances shown in the equations below:
Mass balance equations in the gas phase:

$$\frac{dW_i}{dV} = (1-\varepsilon) a\, K_{P_i}\left(P_{i,s} - P_{i,b}\right) + \varepsilon \sum_{k=1}^{NRom} \nu_{i,k}\, r_{om,k}$$

$$W_i = \left[\frac{Kg}{s}\right] \quad K_{P_i} = \left[\frac{Kg}{m^2 \cdot s \cdot Pa}\right] \quad a = \left[\frac{m^2}{m^3}\right]$$

Where, ε: degree of vacuum

a: catalyst surface per unit volume

($P_{i,s}$-$P_{i,b}$): pressure difference of the reactants between the bulk and the solid's surface.

v: stoichiometric coefficient

r: reaction in homogeneous phase

If it does not consider gas-phase reactions, but only on the surface of the catalyst:

$$\frac{dW_i}{dV} = (1-\varepsilon)a\,K_{P_i}\left(P_{i,s} - P_{i,b}\right)$$

Mass balance on the solid:

$$a\,K_{P_i}\left(P_{i,b} - P_{i,s}\right) + \varrho_{cat}\sum_{j=1}^{NR} \nu_{i,j}\; r_{eff,j}\; M_i = 0$$

$$r_{eff,j} = \left[\frac{Kmol}{Kg_{cat}\cdot s}\right] \qquad M = \left[\frac{Kg}{Kmol}\right]$$

Where, ρ: density of the catalyst

Mi : molecular weight

It gets:

$$\frac{dw_i}{dV} = \frac{R_i}{W}$$

$$R_i = (1-\varepsilon)\varrho_{cat}\sum_{j=1}^{NR} \nu_{i,j}\; r_{eff,j}\; M_i$$

Where W is the total mass flow and w_i is the mass fraction of *i* component.

6.3 Energy Balance

As previously mentioned, in the modeling of laboratory scale is not considered any heat balance in the catalytic bed because it is considered as isothermal one, however in the case of modeling a reactor in industrial volumes the energy balance will be addressed in this way:

Energy balance equation in the gas phase for a plug-flow reactor (PFR):

$$\left(\sum_{i=1}^{NC} W_i c_{p,i}\right)\frac{dT}{dV} = (1-\varepsilon)h\,a\,(T_s - T) + \varepsilon \sum_{k=1}^{NRom}\left(-\Delta H_{om,k}\right) r_{om,k} + U\frac{dA}{dV}(T_{cool} - T)$$

$$c_{p,i} = \left[\frac{KJ}{Kg \cdot K}\right] \quad h = \left[\frac{KW}{m^2 \cdot K}\right] \quad \Delta H_{om,k} = \left[\frac{KJ}{Kmol}\right] \quad r_{om,k} = \left[\frac{Kmol}{m^3 \cdot s}\right] \quad U = \left[\frac{W}{m^2 \cdot K}\right]$$

Where: $C_{p,i}$: Specific heat of the i species

h: Laminar coefficient

(Ts-T): the temperature difference between the surface and the bulk

ΔH_{om},k: entalphy of the K-esimo reaction in gas phase

U: overall heat transfer coefficient

If there are no gas-phase reactions:

$$\left(\sum_{i=1}^{NC} W_i c_{p,i}\right)\frac{dT}{dV} = (1-\varepsilon)h\,a\,(T_s - T) + U\frac{dA}{dV}(T_{cool} - T)$$

Energy balance on the solid:

$$h\,a\,(T - T_s) + \varrho_{cat}\sum_{j=1}^{NR}\left(-\Delta H_j\right)\, r_{eff,j} = 0$$

$$\Delta H_j = \left[\frac{KJ}{Kmol}\right]$$

6.4 Pressure variation

As for the energy balance, also the ΔP has not been taken into account in the modeling, however in the case of simulations of kinetic tests over PFR reactors in industrial volumes it will be necessary to take them into account because before and after the catalytic bed there will be a difference of pressure.

The equation that allows to calculate the pressure drop in a fixed bed reactor is the Ergun's equation:

$$\frac{dP}{dV} = -\left(1.75 + 150\left(\frac{1-\varepsilon}{Re}\right)\right)\left(\frac{u^2 \varrho_{gas}}{D_p}\left(\frac{1-\varepsilon}{\varepsilon^3}\right)\right) \Big/ A_i$$

With

$$Re = \frac{\varrho_{gas} u\, D_p}{\mu_{gas}}$$

Where, u: velocity surface

Re: Reynolds number

Dp: diffusion coefficient

Ai: inlet area of the tube

6.5 Catalyst Efficiency

The efficiency of the catalyst, considered unitary to simplify the model on laboratory scale, can not be considered as such in real systems and especially of large reactors where the problems of diffusion of the reactants on the catalyst surface are no longer negligible

The efficiency of the catalyst is expressed with the equation:

$$\eta_j = \frac{\int_0^{V_p} r_j(T, P_i)\varrho_{cat} dV}{V_p \cdot r_j(T_s, P_{i,s})\varrho_{cat}}$$

$$r_{eff,j} = \frac{\int_0^{V_p} r_j(T, P_i)\varrho_{cat}\, dV}{V_p\, \varrho_{cat}}$$

Where, T: Bulk temperature

Ts: surface temperature

Pi: pressure of *i* species in the bulk

Pi,s: pressure of the *i* species in the surface

Vp: volume of the particle catalyst

References

[1] W.H. Zimmerman, D.B. Bukur, Reaction kinetics over iron catalysts used for Fischer-Tropsch synthesis. The Canadian journal of chemical engineering (68) 1990, p. 292-301

[2] Ahmad Rafiee, Optimal design issues of a gas-to-liquid process, Thesis for the degree of Philosophy Doctor, Norwegian University of Science and Technology, Faculty of Natural Sciences and Technology Chemical Engineering Department,2012.

[3] E.S. Lox, G.F. Froment, Kinetics of the Fischer-Tropsch reaction on a precipitated promoted iron catalyst. 2. Kinetic modeling. Ind. Eng. Chem. Res. (32) 1993, p.71-82.

[4] E.S. Lox, G.F. Froment, Kinetics of the Fischer-Tropsch reaction on a precipitated promoted iron catalyst. 2. Kinetic modeling. Ind. Eng. Chem. Res. (32) 1993, p. 61-70

Chapter 7. Fischer Tropsch runs results and discussion

In this chapter the experimental results concerning the FT runs will be presented in term of CO conversion and of products selectivity toward CO_2, CH_4, light hydrocarbons (< C_7) and heavy hydrocarbons (> C_7). To join all these data the parameter "yield C_{2+}" will be reported too. This parameter is defined in the following equation:

$$\text{Yield } C_{2+} = \text{CO conversion \% x (selectivity } <C_7 + \text{selectivity } >C_7) \quad (1)$$

then, the selectivity to CO_2 and CH_4 (undelivered products) is not taken into account by this parameter. The data concerning all the products distribution, i.e. selectivity for each carbon atom number, have been collected in this PhD's research work, for all the catalysts and all the experimental conditions, but for practical space of reasons they are not here reported.

The results could be divided into two groups. The experimental runs with two kind of catalytical systems, it means: cobalt based catalysts and iron based catalyst (kinetic runs) and the development of a kinetic model for the sample $Fe_{30}K_2Cu_{3.75}$. The selection is related to the better performance in terms of stability.

More in detail,

Kinetic Runs:

Cobalt based catalysts

HTlc. The activated samples were tested at different temperatures in the FTS plant, following the procedure reported in the experimental section. In Fig. 7.1 the CO conversion vs. the reaction temperature is

reported for all the catalysts, while the products selectivity is displayed in Table 7.1.

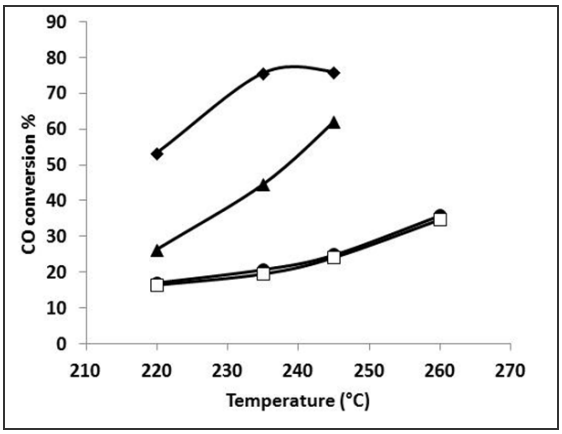

Fig. 7.1: %molar CO conversion to Co5 (●), Co10 (■), Co15 (♦), Co35 (▲), obtained at different reactor temperatures after 24 hours of reaction.

As expected, for each catalyst the activity is strongly influenced by the reaction temperature: the higher the temperature, the higher the CO conversion, but also the selectivity towards CO_2, CH_4 and light hydrocarbons is favored by a higher temperature. The CO conversion is similar for Co5 and Co10, while it is higher for the two samples with a larger amount of cobalt, i.e. Co15 and Co35. In particular, Co15 exhibits the highest CO conversion at all the selected temperatures. In FTS it is fundamental to obtain low quantities of CH_4 and CO_2 (undesired products) to favor the formation of higher hydrocarbons. For this reason, temperatures in the 220-235°C range are more suitable than the higher ones.

Moreover, Table 7.1 shows that Co15 exhibits the highest CO conversion and the highest C_2+ total yield (without considering CH_4 and CO_2, see note in Table 7.1) also at the lowest temperature (220°C) which is so important from an economical point of view. This result confirms that Co15 is the best performing catalyst obtained in this part of the study

Table 7.1: FTS products selectivity at different reactor temperatures.

Sample	Temperature (°C)	Products Selectivity %				C_2+ Yield
		CO_2	CH_4	$\leq C_7$	$>C_7$	
Co5	220	0.3	2.9	3.3	93.4	16.5
	235	0.3	5.9	10.4	83.4	19.4
	245	1.1	8.5	12.7	77.6	22.4
	260	1.9	14.1	16.0	67.9	30.0
Co10	220	3.2	2.6	9.8	84.4	15.5
	235	3.8	4.9	14.3	76.9	17.8
	245	3.3	6.0	15.4	75.3	21.8
	260	8.1	16.3	41.3	34.3	26.2
Co15	220	1.4	10.1	17	70.5	46.7
	235	8.1	26.2	47.3	18.5	49.8
	250	17.8	17.7	44.3	20.2	49.1
Co35	220	1.4	3.9	10.3	84.4	25.0
	235	1.8	9.6	23.4	65.1	39.5
	245	5.1	25.7	65.6	10.5	47.3

$\leq C_7$: all the hydrocarbons in the range C_2-C_7
$>C_7$: all the hydrocarbons greater than C_7
Product ‘‘i” selectivity = (moles C in product i) / (converted moles C) x 100.
C_2+ yield = CO conversion x (selectivity $\leq C_7$ + selectivity $>C_7$) $x10^{-2}$

.

The obtained data suggest the possibility of using synthetic hydrotalcites as Co-based catalysts for FTS and pursuing subsequent studies on the same subject. Similar trends were obtained in “Unit 2” at lower temperatures and lower amount of cobalt (Co10 and Co15) (Table 7.2).

The stability of these catalysts in the operating conditions adopted in the catalytic tests (P ≤ 2.0 MPa and T ≤ 350°C) was evaluated by comparative analysis between fresh samples and samples discharged from the reactor maintained at high pressures and temperatures.

Table 7.2: FTS products selectivities at different reactor temperatures. Two different pilot plants with the same flow sheet

Sample	Temp. (°C)	CO Conv (%)	Products Selectivity %				C_2+ Yield
			CO_2	CH_4	≤C_7	>C_7	
Co10 (Unit 1)	220	17.0	3.2	2.6	9.8	84.4	15.5
	235	20.7	3.8	4.9	14.3	76.9	17.8
	245	24.8	3.3	6.0	15.4	75.3	21.8
	260	35.8	8.1	16.3	41.3	34.3	26.2
Co10 (Unit 2)	220	14.7	0.1	1.2	5.3	93.5	14.5
	235	18.0	1.5	3.2	7.3	88.0	17.1
	245	89.1	14.0	29.1	39.3	17.6	50.6
Co35 (Unit 1)	220	26.4	1.4	3.9	10.3	84.4	25.0
	235	44.6	1.8	9.6	23.4	65.1	39.5
	245	62.1	5.1	25.7	65.6	10.5	47.3
Co35 (Unit 2)	220	47.3	5.0	22.4	29.6	43.1	34.3
	235	76.8	16.2	20.5	28.8	34.5	48.5
	245	99.8	15.4	24.1	32.2	28.2	60.4

*≤C_7: all the hydrocarbons in the range C_2-C_7.>C_7: all the hydrocarbons greater than C_7.*Product ‘‘i” selectivity = (moles C in product i) / (converted moles C) x 100. C_2+ yield = CO conversion x (selectivity ≤C_7 + selectivity >C_7) x10^{-2}

It is important to highlight that the aim of this work was the evaluation of the possibility to use HTlc as a new kind of catalyst for the Fischer-Tropsch process rather than a quantitative comparison with other kinds of traditional FTS catalysts. Moreover, a reliable comparison between HTlc and traditional cobalt

based FTS catalysts is very difficult, due to the different structural and morphological features (surface area, metal dispersion, morphological structure, reduction properties, porosity and so on), which are involved in the very complex catalytic systems for the FTS. Nevertheless, from a qualitative point of view, it is possible to conclude that this new kind of catalytic materials for FTS process give results fully comparable with those obtained by traditional supported cobalt. As general behaviour, it is possible to state that cobalt catalysts are characterized by high CO conversion, high heavy hydrocarbons selectivity and low light hydrocarbons, CH_4 and CO_2 selectivity. The wide literature concerning traditional Co-based catalysts is rich of different examples that, depending on several operative parameters and preparation procedure, give different FTS results, but always following the general trends reported by the previous papers. Some exhaustive examples are shown in a recent review of Qinghong et al [1] and Muthu et al. [2].

Co and Co-Ru

The use of ultrasound (US) might be very efficient to optimize the dispersion of a so high metal charge, as already verified in our laboratory in the past [3-4].

This special type of synthesis should give at the catalyst a particular structure with a high surface area and a high metal dispersion that improves its activity towards the synthesis of Fischer-Tropsch. In the case of cobalt supported catalysts a simple ultrasound step has been added in the catalyst preparation.
As regard the results presented in table 7.3, it can be seen how all the samples resulted active in FTS, in particular the bimetallic samples give high CO conversion with a noteworthy selectivity towards heavy hydrocarbons. The

support plays a crucial role and in particular TiO_2 based samples are the most active.

Moreover, Table 7.3 shows that Co-Ru/SiO_2 exhibits the highest selectivity towards heavy hydrocarbons and the highest C_2+ total yield (without considering CH_4 and CO_2, see note in Table 7.3). This result confirms that Co-Ru/SiO_2 is the best performing catalyst obtained in this part of the study.

Table 7.3: CO Conversion; C_{2+}total yield; CH_4, CO_2, light hydrocarbon and heavy hydrocarbon selectivity of Co/Co-Ru based catalyst at T=255°C.

Catalyst	CO Conv (%)	C_{2+} total yield	Selectivity (%)			
			CH_4	CO_2	$<C_7$	$> C_7$
Co/TiO_2	28	23	5	14	10	71
Co/SiO_2	6	5	19	6	23	52
Co/Al_2O_3	8	6	13	7	19	61
Co-Ru/TiO_2	98	73	18	8	14	60
Co-Ru/SiO_2	94	82	9	4	8	79
Co-Ru/Al_2O_3	84	73	11	2	12	75

As we have seen from the BET and TPR analysis, the support and the promoter play a key role in the performance of the catalyst because they are responsible for the modification of some key parameters such as surface area and the metal dispersion.

Iron based Catalysts

With regard to the treatment with the help of US (see table 7.4), it can be concluded that the sonication of an aqueous mixture, salts and precursors of support (US1), is preferable instead of to the calcined catalyst suspended in

non-polar solvent, such as hexane (US2). With regard to treatment with MW (see table 7.4) there were obtained better results in term of CO conversion, with the powder catalyst treated directly in the MW (MW1), while the test conducted by suspending the catalysts in hexane and then treated in a MW reactor (MW2) for an hour did not give valid results. The best FTS results in term of C_{2+} yield (41%) has been obtained using MW1, while in tem of CO conversion (58%), using US1. All of them gave FTS results better than the traditional one. It's evident that the use of US or MW optimizes the catalytic performance in accord with previous similar results [4].

In agreement with [5] the FTS results show that TEOS as silica source is favorable for the enhancement of the FTS activity.

Table 7.4: Catalytic Results of $Fe_{30}K_{2.0}Cu_{3.75}$. Different preparation techniques. Support: SiO_2, Diluting Material: α-Al_2O_3. T=220°C

Preparation	CO Conv (%)	C_{2+} Total yield	Selectivity (%)			
			CO_2	CH_4	$< C_7$	$> C_7$
TR	49	32	27	7	22	44
MW1	52	41	17	5	18	60
MW2	32	24	17	8	27	48
US1	58	38	29	6	22	43
US2	36	25	22	9	30	39
Co-precipitation*	38	32	2	13	28	57

$\leq C_7$: all the hydrocarbons in the range C_2-C_7

$> C_7$: all the hydrocarbons greater than C_7

Product ''i" selectivity = (moles C in product i) / (converted moles C) x 100.

C_{2+} yield = CO conversion x (selectivity $\leq C_7$ + selectivity $> C_7$) $x10^{-2}$

* *The co-precipitation test was made at T=250°C and TEOS as a support*

Iron based Catalysts

To work with this part it is important to know the effect of the H_2 /CO ratio in the feeding gas. The FTS for the production of liquid hydrocarbons from synthesis gas has become important as the planet faces exhaustion of its petroleum reserves in the near future. The use of coal or biomass to manufacture synthesis gas is attractive in view of its vast reserves. However, synthesis gas manufactured from coal or biomass typically has a low H_2/CO ratio (about 0.7) while the stoichiometry of the reaction requires an H_2/CO ratio of about 2.0. Iron catalysts can make up this deficit with their high WGS activity [6].

This important characteristic of iron based catalysts is essential for their applications.

Fig. 7.2 show that the activity of catalyst is good enough using also feeding ratio between 1.0 and 2.0.

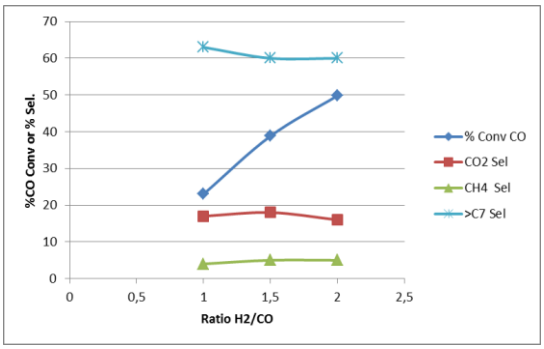

Fig. 7.2. % CO conversion or % selectivity vs H_2/CO feeding ratio for $Fe_{30}K_{2.0}Cu_{3.75}$ catalyst at T=250°C

Higher the H_2 / CO ratio is, higher the CO conversion becomes, but the heavy hydrocarbons is the highest for the stoichiometric ratio.

In the present work there were made some tests with $Fe_{30}K_{2.0}Cu_{3.75}$ catalyst, by feeding mixtures with a ratio H_2/CO between 0.5 and 2.0 in order to optimize

the activity, selectivity and the lifetime of this kind of FT catalyst in work conditions of biosyngas feeding.

On the basis of the collected data, a rigorous simulation of the FT synthesis reactor has been developed for different purposes: (i) to support the experimentations and their planning; (ii) to predict the reactor yield and conversion; (iii) to optimize the performance of the reactor system with different operating conditions; and (iv) to calculate novel reliable kinetic parameters based on the experimental data fitting by means of model-based nonlinear regression techniques. To do so, the FT reactor is modeled as a catalytic plug-flow reactor using mass and energy balances and reaction kinetics for Fe-based catalyst defined by Zimmerman and Bukur, as explained in chapter 6 [7] leading to an ordinary differential equation system with structured Jacobian. Lumping techniques have been used to model heavy hydrocarbons. The system is solved by means of dedicated solvers to handle stiffness and nonlinearities of heterogeneous reactive systems [8].

Typical H_2/CO ratio of syngas manufactured from coal or biomass are between 0.7-1.2 and the Fig. 7.2 show that the activity of catalyst is good enough using also feeding ratio between 1.0 and 2.0.

In the table 7.5 there is the data concerning the carbon monoxide conversion (%), and the selectivity towards undesired products (CO_2 and CH_4) and lighter and heavy hydrocarbons of Fe-based catalyst. The CO conversion increase with the increase of the H_2/CO ratio, because of the proximity of the stoichiometric required of the reaction. The selectivities are constant with the variations of H_2/CO ratio. Instead of that the C_2^+ yield increase with the variations of H_2/CO ratio. A comparison at T=250°C, show that the best performance in terms of CO conversion, C_2^+ and selectivity towards heavy hydrocarbons is given by working with a H_2/CO ratio of 2 (stoichiometric required of the reaction).

These data were used to propose a suitable kinetic model for the FTS using a math program in collaboration with the *Politecnico di Milano*. Some hypothesis were taken into account to prepare the kinetic model (FT reactor is modeled as a catalytic plug-flow reactor using mass and energy balances and reaction kinetics for Fe-based catalyst defined by Zimmerman and Bukur [7-8]; $\Delta P = 0$; isothermic catalytic bed; FT reaction and WGS are both active on the catalyst). The kinetic parameters were calculated and compared with the experimental data. The first results show a good fitness of the experimental data.

Table 7.5: FTS products selectivities at different H_2/CO ratio and reactor temperatures of $Fe_{30}K_2Cu_{3,75}$.

				Selectivity (%)			
H_2/CO	T(°C)	CO Conversion (%)	C_{2+} total yield	CO_2	CH_4	<C7	>C7
2/1	220	8,5	6,9	11	8	22	59
2/1	235	21,1	17,5	11	6	20	63
2/1	250	49,8	39,3	16	5	19	60
2/1	260	56,7	42,5	19	6	20	55
1.5/1	250	38,8	29,9	18	5	17	60
1.5/1	260	46,3	33,8	22	5	17	56
1/1	250	23	18,2	17	4	16	63
1/1	260	38,9	27,2	26	4	16	54

$\leq C_7$: all the hydrocarbons in the range C_2-C_7
$>C_7$: all the hydrocarbons greater than C_7
Product ‘‘i” selectivity = (moles C in product i) / (converted moles C) x 100.
C_2+ yield = CO conversion x (selectivity $\leq C_7$ + selectivity $>C_7$) $x10^{-2}$

In Fig. 7.3 is presented a comparison between the experimental data obtained in the laboratory and the data obtained using the kinetic model. The first two

columns represent the conversion of hydrogen and carbon monoxide, while in the other columns are represented the molar fraction of hydrogen, carbon monoxide, water, methane, and lump C_2, C_{3-4}, C_{5-10}, C_{11+}. As a first approximation, it can be seen that the kinetic model present a good fitness regard to the experimental data.

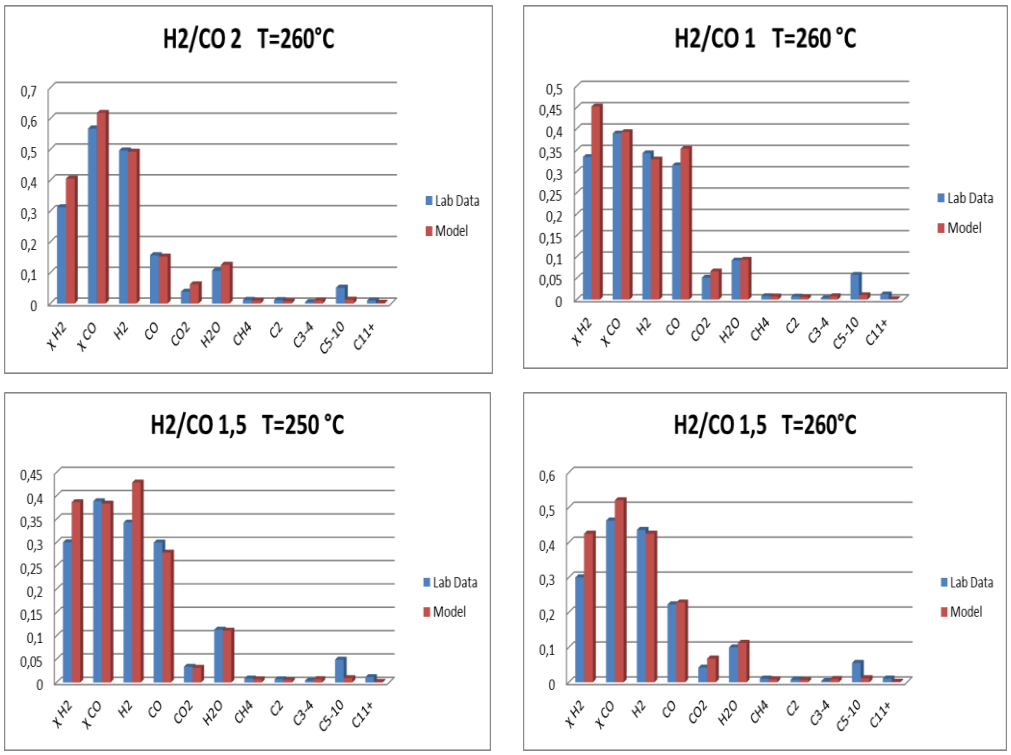

Fig. 7.3. Comparison between experimental data and kinetic model.

References:

[1] Qinghong Z, Weiping D, Ye W. Review. Recent advances in understanding the key catalyst factors for Fischer-Tropsch synthesis. J Ener Chem 2013; 22:27–38

[2] Muthu KG, Gary J, Wilson DS, Burtron HD. Fischer–Tropsch synthesis: Activity of metallic phases of cobalt supported on silica. Catal Today 2013; 215:13– 17
[3] C.L.Bianchi, V.Ragaini, Catalysis Letters 95 (2004) 61-65.
[4] C. Pirola, C. L. Bianchi, A. Di Michele, P. Diodati, D. C. Boffito, V. Ragaini, Ultrasonic Sonochem. 17, (2010) 610
[5] Suo, Haiyun; Zhang, Chenghua; Wu, Baoshan; Xu, Jian; Yang, Yong; Xiang, Hongwei; Li, Yongwang; A comparative study of Fe/SiO2 Fischer–Tropsch synthesis catalysts using tetraethoxysilane and acidic silica sol as silica sources. Catalysis Today Volume 183, Issue 1, 20 March 2012, Pages 88–95
[6] M.D.Shroff, A.K.Datye, Catalysis Letters 37 (1996) 101
[7] W.H. Zimmerman, D.B. Bukur Can. J. Chem. Eng., 68, (1990) 292-301
[8] F. Manenti, I. Dones, G. Buzzi-Ferraris, H.A. Preisig, Ind. Eng. Chem. Res. 48, (2009) 9979-9984

Chapter 8. Final remarks and Conclusions

New kind of cobalt and iron based catalysts were synthetized and used in the Fischer-Tropsch synthesis. Different methods of synthesis, different amounts of cobalt and different process temperatures were investigated. All the catalysts under study were active in the FTS. The catalytic activity of the samples strictly depends on the temperature, as expected.

Cobalt based hydrotalcites, cobalt and cobalt-ruthenium synthesized with the help of ultrasound and iron supported catalysts with a high loading of iron (30% wt), have been prepared and characterized, and both the preparation procedure and the working conditions were fully optimized.

For each catalytic system it can be summarized the following aspects:

Cobalt based catalysts

HTLC: In the case of Co-based hydrotalcites, CO conversion and process selectivity towards light and heavy hydrocarbons are closely related to the cobalt amount in the catalysts, but not in a linear way.

The reduction behavior under a H_2 flow of the Co-based hydrotalcites is achieved in one step at lower temperature and it is not related to its morphology but is strictly correlated to the particle size. In addition, the relatively large dimensions and high cristallinity of these catalysts favor the creation of optimal domains of active sites that make them more efficient.

The obtained data suggest the possibility of using synthetic hydrotalcite as Co-based catalysts for FTS and open the possibility for subsequent studies on the same subject.

Future studies may involve the investigation of the effects of various parameters such as morphology/size of crystallites, or the addition of small amounts of promoters such as Ru in the composition of Co based hydrotalcites. Temperatures in the 220-235°C range are more suitable than the higher ones.

Cobalt based bimetallic: The catalysts show a low selectivity to methane and carbon dioxide and formation of higher hydrocarbons. The more interesting results are the highest CO conversion, at lower temperatures measured with a catalysts promoted with a Ru. Even the support, although it is inert, it is very important because it radically alters the surface area of the catalyst.

Iron catalysts: The samples appears to be highly dependent on the method of preparation used. The catalysts treated with US and MW seem to show significant improvements over traditional catalysts and the reason is a more homogeneous and uniform distribution of Fe in the media.

The catalyst $Fe_{30}K_2Cu_{3,75}$ is active with a H_2/CO ratio ≤2.

Develop of a kinetic model: On the basis of the collected data, a rigorous simulation of the FT synthesis reactor has been developed to support the experimentations and their planning; to predict the reactor yield and conversion; to optimize the performance of the reactor system with different operating conditions; and to calculate novel reliable kinetic parameters based on the experimental data fitting by means of model-based nonlinear regression techniques. For this, lumping techniques have been used to model heavy hydrocarbons, the system is solved by means of dedicated solvers to handle stiffness and nonlinearities of heterogeneous reactive systems and finally, the

model made in collaboration with the *Politecnico di Milano* show a good fit of the experimental data

Concerning the results obtained in this PhD's research work, it is clear that all the samples tested have given good results. The Co-based catalysts, synthesized using the traditional impregnation method, with an additional step of ultrasound have given good results in comparison with the results in the current literature. The hydrotalcites have given lower results, if compared with the Co-based catalysts synthesized with the help of ultrasound, but they have opened an alternative and innovative way, that has never been tried before. Iron based catalysts allow a direct conversion of the biosyngas, and the results have shown how our catalysts are active with an H_2/CO ratio ≤2. Furthermore, trends have been modeled with success. In conclusion, the PhD's research work, has given a serious contribution to the current state of the art on catalysis in the Fischer-Tropsch synthesis either with cobalt and iron based catalysts. With cobalt has been optimized a traditional synthesis procedure with the introduction of ultrasound, furthermore has been created a completely new kind of catalyst. With iron has continued an optimization's work of iron supported with high loading metals, so to develop a suitable kinetic model able to work not only with syngas, but also with biosyngas.

List of publications

Publications

- C. Pirola, D.C. Boffito, G. Carvoli, **A. Di Fronzo**, V. Ragaini and C.L. Bianchi (2011). Soybean Oil De-Acidification as a First Step Towards Biodiesel Production, Recent Trends for Enhancing the Diversity and Quality of Soybean Products, Prof. Dora Krezhova (Ed.), ISBN: 978-953-307-533-4, InTech, DOI: 10.5772/17812. Available from: http://www.intechopen.com/books/recent-trends-for-enhancing-the-diversity-and-quality-of-soybean-products/soybean-oil-de-acidification-as-a-first-step-towards-biodiesel-production

- C.L. Bianchi, C. Pirola, D.C. Boffito, **A. Di Fronzo**, G. Carvoli, D. Barnabè, R. Bucchi and A. Rispoli (2011). Non Edible Oils: Raw Materials for Sustainable Biodiesel, Biodiesel - Feedstocks and Processing Technologies, Dr. Margarita Stoytcheva (Ed.), ISBN: 978-953-307-713-0, InTech, DOI: 10.5772/25397. Available from: http://www.intechopen.com/books/biodiesel-feedstocks-and-processing-technologies/non-edible-oils-raw-materials-for-sustainable-biodiesel

- **A. Di Fronzo**, C. Pirola, A. Comazzi, F. Galli, C.L. Bianchi, A. Di Michele, R. Vivani, M. Nocchetti, M. Bastianini, DC Boffito, **Co-based Hydrotalcites as new Catalysts for the Fischer-Tropsch Synthesis Process**. Fuel, 119 (2014) 62–69

Publications in Conference Proceedings (peer reviewed)

- C.L. Bianchi, C. Pirola, D.C. Boffito, **A. Di Fronzo**, A. Di Michele, R. Vivani, M. Nocchetti, M. Bastianini, S. Gatto, Co-Zn-Al based hydrotalcites as catalysts for Fischer-Tropsch process, Proceeding of DGMK Conference 2011, Catalysis: Innovative Applications in Petrochemistry and Refining, 4-6 October 2011, Dresden, Germany ISBN 978-3-941721-17-3.
- C. Pirola, **A. Di Fronzo**, D.C. Boffito, C.L. Bianchi, A. Di Michele, Biosyngas Fischer – Tropsch Conversion by High Fe Loaded Supported

Catalysts Prepared with ultrasound and Microwave, Proceeding of DGMK Conference 2012, Reducing Carbon Footprint of Fuels and Petrochemicals October 8 – 10, 2012, Berlin, Germany ISBN 978-3-941721-26-5

Communications at congress

- **A. Di Fronzo**, C. Pirola, D.C. Boffito, C.L. Bianchi, A. Di Michele, R. Vivani, M. Nocchetti, M. Bastianini, Synthetic Hydrotalcites as suitable Co-based catalysts for Fischer-Tropsch Process, XVIII Congresso Nazionale della Divisione di Chimica Industriale della SCI. *LE SFIDE DELLA CHIMICA INDUSTRIALE PER UN'INNOVAZIONE SOSTENIBILE, 11-14 giugno 2012 (Oral presentation)*
- **A. Di Fronzo,** D.C. Boffito, C.Pirola, G. Carvoli, S. Vitali, C.L. Bianchi, Scalable free fatty acids esterification for methyl esters production, XVIII Congresso Nazionale della Divisione di Chimica Industriale della SCI. *LE SFIDE DELLA CHIMICA INDUSTRIALE PER UN'INNOVAZIONE SOSTENIBILE, 11-14 giugno 2012 (Poster presentation)*
- **A.Di Fronzo**, C. Pirola, D.C. Boffito, C.L. Bianchi, A. Di Michele, R. Vivani, M. Nocchetti, M. Bastianini, Synthetic Hydrotalcites as suitable Co-based catalysts for Fischer-Tropsch Process, Cat4bio conference. Advances in catalysys for biomass valorization. Tesalónica Grecia 2012 (Poster)
- C.L. Bianchi, **A. Di Fronzo**, C. Pirola, D.C. Boffito, A. Di Michele, R. Vivani, M. Nocchetti, M. Bastianini, Synthetic Hydrotalcites as suitable Co-based catalysts for Fischer-Tropsch Process**,** 7th edition of the International Conference on Environmental Catalysis Lion-Francia (Poster)
- **A. Di Fronzo**, C. Pirola, C.L. Bianchi, A. Di Michele, Ultrasonidos y microondas en la preparaciòn de catalizadores soportados para la sìntesis de Fischer-Tropsch, JIFI-EAI 2012 Jornadas de Investigaciòn Ecuentro acadèmico industrial, Universidad Central de Venezuela, Facultad de Ingenierìa, 26-30 noviembre.
- C. Pirola, C.L. Bianchi, **A. Di Fronzo**, D. Boffito, A. Di Michele, G. S. Patience. Ultrasound and microwave assisted preparation of high Fe

loaded supported catalysts for biosyngas Fischer-Tropsch conversion. Intervento presentato al 245. convegno ACS National Meeting & Exposition tenutosi a New Orleans, Louisiana nel 2013.

- C. Pirola, C. L. Bianchi, **A. Di Fronzo**, F. Manenti, M. Hillestad, High Fe Loaded Supported Catalysts for Biosyngas Fischer – Tropsch Conversion: experimental results and detailed simulation**,** XVII National Congress of Catalysis GIC 2013 and XI National Congress of Zeolites Science and Technology 15-18/09/2013
- F. Galli, C. Pirola, **A. Di Fronzo**, A. Comazzi, C.L.Bianchi , Di Michele, Co Based Bimetallic Catalysts for Fischer-Tropsch Synthesis Prepared by High Power Ultrasound**,** XVII National Congress of Catalysis GIC 2013 and XI National Congress of Zeolites Science and Technology 15-18/09/2013
- Di Michele, C. Pirola, **A. Di Fronzo**, A. Comazzi, F. Galli and C.L.Bianchi**,** Co Based Bimetallic Catalysts for Fischer-Tropsch Synthesis Prepared by High Power Ultrasound, AOSS Melbourne 10-12/07/2013.
- C. Pirola, **A. Di Fronzo**, A. Comazzi, F. Galli, A. Di Michele, C.L.Bianchi, Co based bimetallic catalysts for Fischer-Tropsch synthesis prepared by high power ultrasound, 11^{th} European Congress on Catalysis – EuropaCat-XI, Lyon, France, September 1^{st}-6^{th}, 2013
- Workshop Clausthal Germany 22-23/11/2013. Fischer-Tropsch Synthesis from syngas and biomass using Fe or Co based catalysts: Experimental and simulation results. (Oral Presentation)